FLOW CHARACTERISATION OF AN ON–LINE ELECTROCHEMICAL ANALYSER

Mohammed Nadim Shaik

A dissertation submitted to the Faculty of Engineering and the Built Environment, University of the Witwatersrand, Johannesburg, in fulfilment of the requirements for the degree of Master of Science in Engineering.

Johannesburg, 2005

DECLARATION

I declare that this dissertation is my own, unaided work except where indicated. It is being submitted for the degree of Master of Science in Engineering in the University of the Witwatersrand, Johannesburg. It has not been submitted before for any degree or examination in any other university.

_____

_____ day of _____ _____

ABSTRACT

The flow characteristics of an on-line analyser were measured using a stimulus – response technique. The analyser was developed for monitoring homogeneous catalyst concentrations in a non-aqueous solution and it was considered important to limit dispersion effects between sample injection and measuring points. Various tube lengths between these points were used and the system was operated over a range of flow rates. The detectors employed were electrochemical in nature and of two different designs.

The residence time distributions of the system were determined experimentally and analysed by the method of moments and frequency techniques. As expected dispersion of the sample decreased as tube length decreased and flow rate increased.

An attempt was made to fit the experimental results to the axially dispersed plug flow model. This was only successful over a limited range of the variables.

In loving memory of my late mother

Zarina Bibi Shaik

ACKNOWLEDGEMENTS

In the name of God, the most beneficial and the most merciful. I would like to express my appreciation and gratitude to Professor A.W. Bryson, Professor I. Cukrowski, Professor D. Glasser and Professor D. Hildebrandt for their advice, assistance, and supervision during the course of this study. I am truly indebted to them. I would like to thank Mrs. W.K. Maboya for her assistance and for the preparation of the chemical compounds. I would like to thank the gentlemen at the workshop for the fabrication of certain components and the gentlemen at the chemical stores for their assistance. I would also like to thank Mr. B. Chassoulas for his assistance. I would like to thank the National Research Foundation and Sasol Technology for providing financial assistance. Lastly I would like to thank my wife and family for their support and patience.

TABLE OF CONTENTS

LIST OF FIGURES

LIST OF SYMBOLS

A,A_n	Amplitude Ratio
a_n	System response n^{th} Fourier coefficient
b_n	System response n^{th} Fourier coefficient
$\mathbf{b}$	Vector of parameters
$\mathbf{b^m}$	Vector of parameters evaluated at m^{th} iteration
$C(t)$	Tracer concentration
$C'(t)$	Dimensionless tracer concentration
$C'_{ave}(t)$	Tracer concentration if evenly distributed throughout vessel
$C_i(t)$	Inlet tracer concentration
$C_o(t)$	Outlet tracer concentration
D,D_z	Axial dispersion coefficient
D_r	Radial dispersion coefficient
$\bar{\mathbf{E}}(s)$	Laplace transform of $\boldsymbol{E}(t)$, system transfer function
$\boldsymbol{E}(t)$	System residence time distribution function
$\bar{\mathbf{f}}(s)$	Laplace transform of $f(t)$
$f(t)$	Arbitrary function of time
$f(x)$	Arbitrary function of x
g	Complex number
i	Imaginary variable, $\sqrt{-1}$
$\mathbf{J}$	Jacobian matrix
$\mathbf{J}_j$	j^{th} Jacobian matrix
j	Integer
K_i	Input signal proportionality factor

K_o	Output signal proportionality factor
k	Number of parameters
L	Length of tubing between injection and detection points
m	Integer
n	Integer
p_n	Input function n^{th} Fourier coefficient
q_n	Output function n^{th} Fourier coefficient
$R_i(t)$	Recorded input signal
$R_o(t)$	Recorded output signal
r	Radial direction
s	Laplace transform variable
T	Half period of any arbitrary function
t	Time
u	Mean velocity
u_n	Input function n^{th} Fourier coefficient
v_n	Output function n^{th} Fourier coefficient
v	Number of dependent variables
w_j	j^{th} weighting factor
$\boldsymbol{Y}$	Dependent variable
$\boldsymbol{Y}_j$	j^{th} dependent variable
$\boldsymbol{Y}^*$	Vector of experimental observations of dependent variable
$\boldsymbol{Y}_j^*$	Vector of experimental observations of j^{th} dependent variable
x	Independent variable
z	Axial direction

α_n	n^{th} moment about origin of $\boldsymbol{E(t)}$
α_{ni}	n^{th} moment about origin of $\theta_i(t)$
α_{no}	n^{th} moment about origin of $\theta_o(t)$
$\alpha_n^{/}$	cumulant, n^{th} moment about mean of $\boldsymbol{E(t)}$
$\alpha_{ni}^{/}$	cumulant, n^{th} moment about mean of $\theta_i(t)$
$\alpha_{no}^{/}$	cumulant, n^{th} moment about mean of $\theta_o(t)$
Φ , Φ_n	Phase lag
φ	Sum of squared residuals
$\bar{\theta}_i(s)$	Laplace transform of $\theta_i(t)$
$\bar{\theta}_o(s)$	Laplace transform of $\theta_o(t)$
$\theta_i(t)$	Input function
$\theta_o(t)$	Output function
σ^2	Variance of system residence time distribution function
σ_i^2	Variance of input function
σ_o^2	Variance of output function
σ_j^2	Variance of vector of experimental observations of j^{th} dependent variable
τ	System mean residence time
τ_i	Input function mean residence time
τ_i	Output function mean residence time
ω	Frequency
$\zeta(C(t))$	Reaction rate or source term

1 INTRODUCTION

Sasol is the largest petrochemical company in South Africa, and was founded in 1950 by the South African government. South Africa has abundant coal reserves and Sasol is the world leader in converting coal and gas into fuels and valuable chemicals using proprietary Fischer-Tropsch technology.

Sasol are currently developing a process to convert olefins to linear alcohols. The process employs a homogeneous catalyst usually consisting of cobalt or rhodium compounds.

Sasol have commissioned pilot facilities for the development of this process, and require some means of monitoring catalyst concentrations in non – aqueous media.

Monitoring of the catalyst concentration on – line will be both time and money saving, and will enable Sasol to control and optimise their process. Furthermore, Sasol require an analytical system that is capable of providing results every 30 to 60 minutes, capable of sampling from more than just one location, be robust and should require infrequent maintenance.

The initial period of this study was devoted to the development of an analyser capable of satisfying the requirements of Sasol. Apart from other activities the development phase included drafting a design for the analyser, surveying commercial literature (catalogues, brochures and user manuals), acquisition of the necessary components for the analyser, development of software to control components of the analyser (and the analyser as a whole) and lastly assembly and testing of the analyser system.

The analyser developed for monitoring of the Sasol catalyst was a flow injection analyser with an electrochemical detector. Flow injection analysers operate on the principle where a sample volume is injected into a continuously flowing stream, called a carrier stream or carrier solution.

The carrier stream transmits the injected sample towards the detector. On route to the detector, the injected sample disperses into the carrier stream by means of molecular diffusion and convection [1].

The electrochemical detector or cell was a block of a certain polymer material with nut threads for the attachment of electrodes and tubing. Two different types of electrochemical detectors were employed in this study. The first design was termed the wall jet cell and the second, the flow by cell. In both these designs, three electrodes were attached to each cell block. The differences between the two types of electrochemical detectors will be highlighted in Section 2.

The electrochemical technique employed was chronoamperometry. In this technique, the working electrode is held at a fixed potential with respect to the reference electrode. The background electrolyte or the carrier solution is pumped through the detector. The current is monitored as a function of time as the solution flows through the detector. Thereafter a small volume of sample is injected and is carried with the carrier stream towards the detector. If the injected sample present in the solution flowing past the working electrode is electroactive, then the electroactive species is either reduced or oxidised, depending on the working electrode potential. If the species is oxidised or reduced, then an oxidation or reduction current is observed, which is the recorded signal.

The focus of this dissertation, however, is not on the development of the analyser itself, but rather on the methods and techniques used in describing the dispersion of sample and the flow within the analyser system. The extent of sample dispersion within the analyser system affects the detector reading and hence the analytical signal quality. The dispersion of sample in a flow injection analyser can be varied depending on the type of analytical procedure being followed [2, 3]. For example, in determining the pH of a sample using a flow injection analyser, the sample has to be transported to the detector without being mixed with the carrier fluid. For analytical procedures like spectrophotometry the sample

has to be mixed with the carrier solution, allowing a certain reaction to take place in order to form a compound, which is detectable. Similarly for electrochemical detectors, a certain degree of mixing or homogeneity is required between the background electrolyte and injected sample. Should the background electrolyte and injected sample flow through the electrochemical detector without any mixing as discrete volumes, then distorted or irregular signals would be observed. On the contrary, the dispersion of sample in the background electrolyte should be limited, such that significant dilution of the sample does not occur. Dilution of the sample results in peak broadening, which is unwanted. Dilution of the injected sample leads to excessive tailing, which results in computational errors.

The dispersion of sample within the analyser system is a function of the flow rate of carrier solution within the analyser system, the length of tubing between the injection point and detector, the diameter of the tubing situated between the injection and detection points and the volume of sample injected [2, 4-11]. In this study the effect of varying the flow rate of carrier solution and the length of tubing between the injection and detection points on sample dispersion was investigated. Tests were also conducted using two different types of electrochemical detectors in order to qualitatively determine the dispersion caused by the detector itself, and to compare the analytical signal quality obtained using the different detector designs.

In trying to understand the effect of varying these two parameters on sample dispersion, it is useful to attempt to formulate a flow model to represent the flow pattern and mixing behaviour within the analyser system. This requires a knowledge of the flow pattern of fluid elements within the system which may be obtained if the velocity distribution of fluid elements within the system is known. However in many circumstances the velocity distribution is not known or cannot be derived from the solution of the Navier-Stokes equation. Valuable information regarding the flow pattern and mixing behaviour can be obtained from the exit age

distribution (residence time distribution) of fluid elements leaving the system. The residence time distribution is obtained experimentally by a technique termed the stimulus – response technique. In this technique a tracer or sample is injected at the inlet to the system and the response at the system exit is observed. The shape of the experimentally determined residence time distribution can be used to draw conclusions regarding the flow pattern and mixing behaviour within the system. The flow model is then chosen on the basis of matching the experimentally determined residence time distribution with that obtained from the theoretical or mathematical model. However in order to perform quantitative comparisons between them other methods may be used. The methods employed in this work were moment analysis and frequency analysis. A major advantage of the method of moments is that both the experimental and theoretical moments may easily be determined [12-14]. This means that less computational time is required when using this method. Not only are the theoretical moments easily obtained, but also the expressions derived for the theoretical moments are simple and compact [12-14]. The method of moments does, however, suffer from certain disadvantages, which include uneven weighting of the tail of the signal, large errors due to noisy data, errors due to baseline drifting and lastly this method provides no information on how well a model fits the data [12-15]. Classical work on frequency analysis involved exciting the flow system with a sinusoidal input, and measuring the output when the system has reached steady state. The classical form of frequency analysis has disadvantages. This method is time consuming since the duration of the experiments will be lengthy for two reasons. Firstly time must be allowed for the system transients to disappear and secondly in order to obtain data for a wide frequency range a large number of experiments must be performed. Building and operating an instrument to generate a sinusoidal tracer input is difficult [13, 15]. To overcome the disadvantages associated with sinusoidal tracer testing, many workers have used the pulse testing method. This method involves injecting a pulse input signal and recording

the output signal. The shape of the pulse is not critical, as long as a closed pulse is injected at the input [15]. A closed pulse is a pulse, which starts and ends at zero (concentration), and has a finite value for a finite time period [15]. A single pulse experiment yields the same amount of information as a series of sinusoidal tracer input experiments [13, 15]. Unlike the method of moments, it is possible to test the validity of a certain model using frequency analysis. This was demonstrated by a number of workers [13, 16, 17]. Some workers [18-22] have applied the stimulus – response technique for the evaluation of dispersion in flow analysis systems or components of flow analysis systems. Some of these workers have used moment analysis to characterize or describe the dispersion. It is known that the method of moments suffers from shortcomings [12-15] and only moments up to the second moment can be estimated with reasonable accuracy. In cases where excessive tailing is present in signals, the accuracy of even the second moment is doubtful. In order to determine the response or residence time distribution function of the flow system, these workers have utilised either some numerical inversion technique or deconvolution. Frequency analysis is a much simpler alternative to both of these techniques for the determination of the system response. Frequency analysis is also less sensitive to the tail portion of signals, and hence more accurate than moment analysis [13].

Essentially the tasks performed in this work included:

- determining the residence time distribution of fluid elements in the analyser system by pulse testing
- obtaining the experimental system response or system residence time distribution by frequency analysis, which included plotting the experimentally determined amplitude ratio and phase lag against frequency
- drawing conclusions regarding the flow pattern and mixing behaviour within the analyser system from the shape of the experimentally determined system residence time distribution.

- determining the moments of the experimental system residence time distribution
- proposing a flow model based on the shape of the experimental system response curve
- testing the validity of the of the proposed flow model using frequency analysis.

2 EXPERIMENTAL

In the experimental work conducted two analyser systems were studied. The difference between the analyser systems was the type of electrochemical detectors used. The aim of these experiments was to determine the effect on the dispersion of the injected sample by varying the flow rate of carrier solution and the length of tubing between the injection and detection points for both systems. The flow rates that were tested were 0.5, 0.75, 1.0, 1.5 and 2.0 ml/min. The lengths of tubing between the injection and detection points that were used were 0.25, 0.5, 0.8 and 1 m. All of the flow rates were tested for each of the lengths for both analyser systems. A detailed description of the experimental apparatus, analyser systems and reagents follows below.

2.1 Apparatus

The apparatus used in these experiments consisted of two pumps, a six port loop valve, two electrochemical flow-through detectors (cells) with three electrodes each, narrow bore tubing, fittings (nuts and ferrules), two potentiostats, a data acquisition system and a personal computer. A diagram of the experimental apparatus, a description of the analyser systems and each component are presented below.

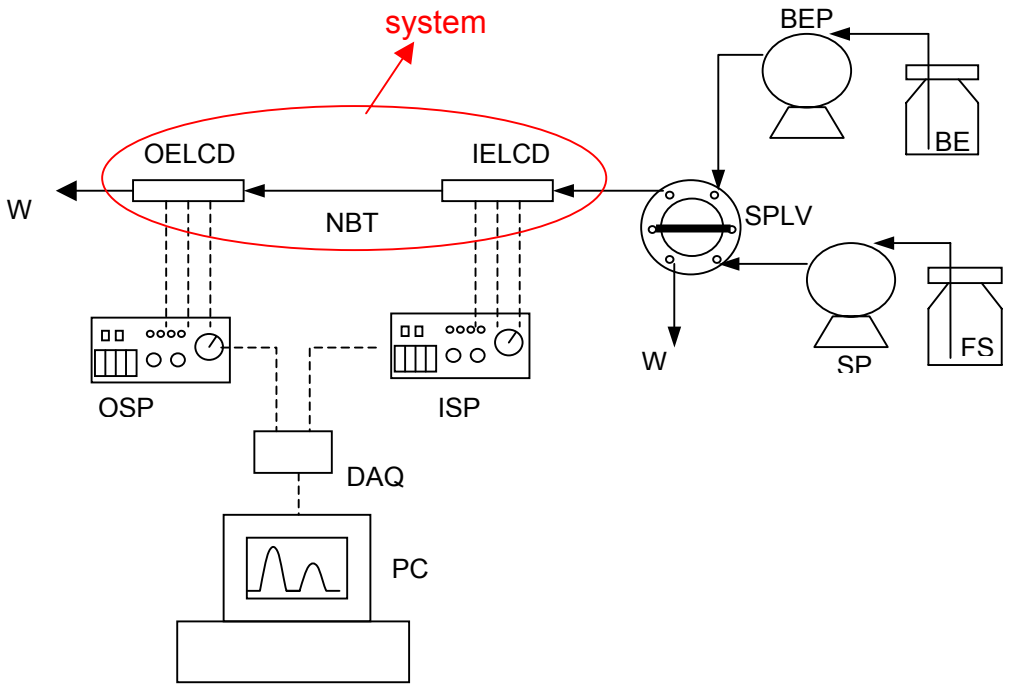

Figure 2.1: Diagram of experimental apparatus. BE – background electrolyte, BEP – background electrolyte pump, DAQ – data acquisition system, FS – ferrocene stock solution (tracer), SP – sample pump, SPLV – six port loop valve, IELCD – input electrochemical cell detector, OELCD – output electrochemical cell detector, ISP – input signal potentiostat, OSP – output signal potentiostat, PC – personal computer, NBT – narrow bore tubing and W – waste. For details see text below.

In the first analyser system (analyser system A) both the input and the output electrochemical cell detectors were of the same type, called the wall jet cell. In the second analyser system (analyser system B) the input and the output electrochemical cell detectors were of different types. For analyser system B the input electrochemical cell detector was based on a design termed the flow by detector, whilst the output electrochemical cell detector was a wall jet cell. The wall jet cell and flow by cell detectors had different geometric configurations, and as a result the flow configurations in the analyser systems differed. Representations of analyser systems A and B are shown below in Figures 2.2 and 2.3 from which the flow configurations can be clearly seen. The red arrows indicate the direction

of the solution flow. As an example the tubing length between the injection and detection points is shown as 0.25 m. In analyser system A shown in Figure 2.2 both the input and output detectors were wall jet cell detectors. A detailed representation of the wall jet cell detector is shown in Figures 2.6, 2.7 and 2.8. In analyser system B shown in Figure 2.3, the input detector was a flow by cell detector. A detailed representation of the flow by cell detector is shown in Figures 2.9, 2.10 and 2.11. The output detector for analyser system B which was a wall jet cell detector is represented in detail in Figures 2.6, 2.7 and 2.8.

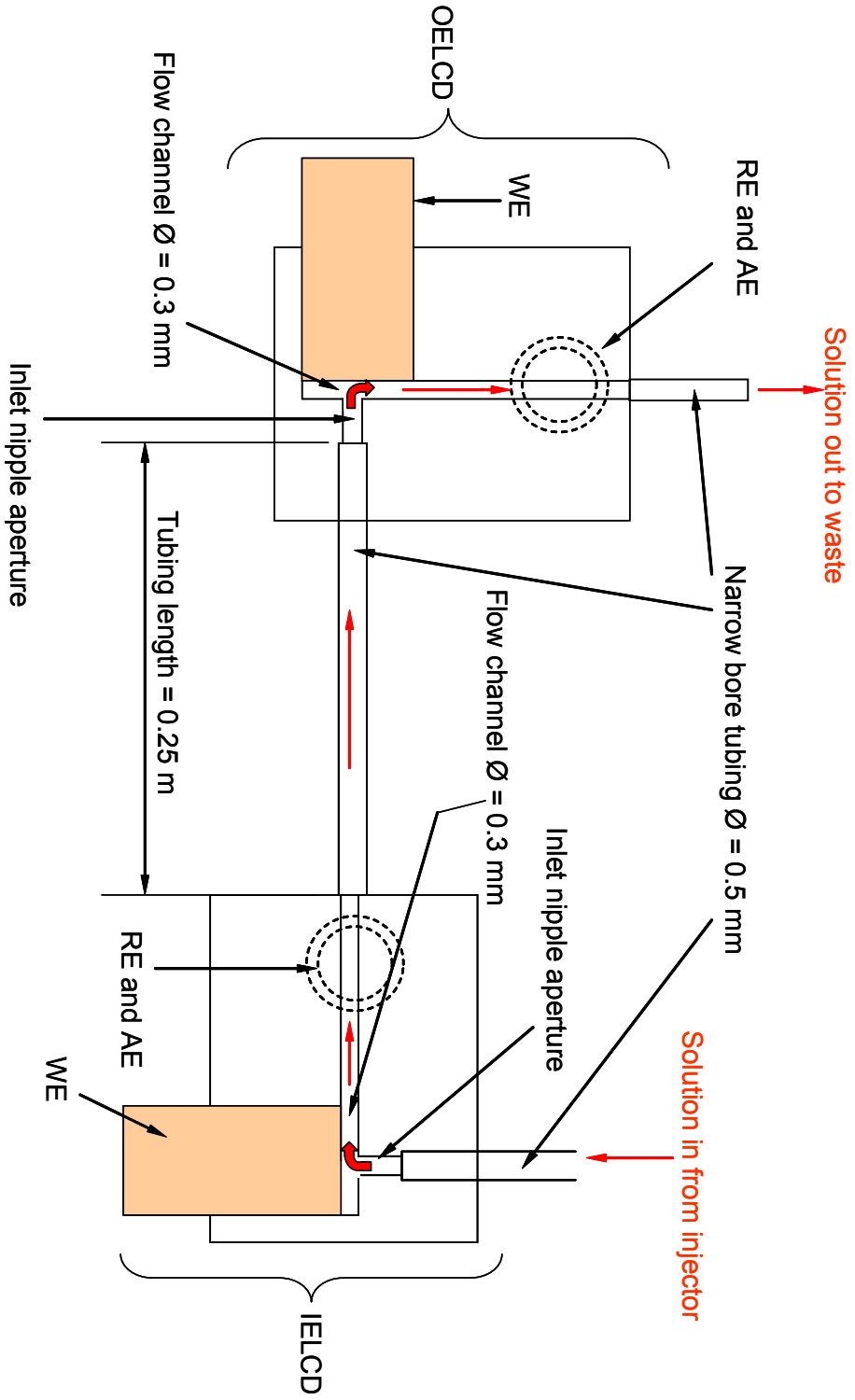

Figure 2.2: Representation of analyser system A. IELCD – input electrochemical cell detector, OELCD – output electrochemical cell detector, AE – auxiliary electrode, RE – reference electrode and WE – working electrode.

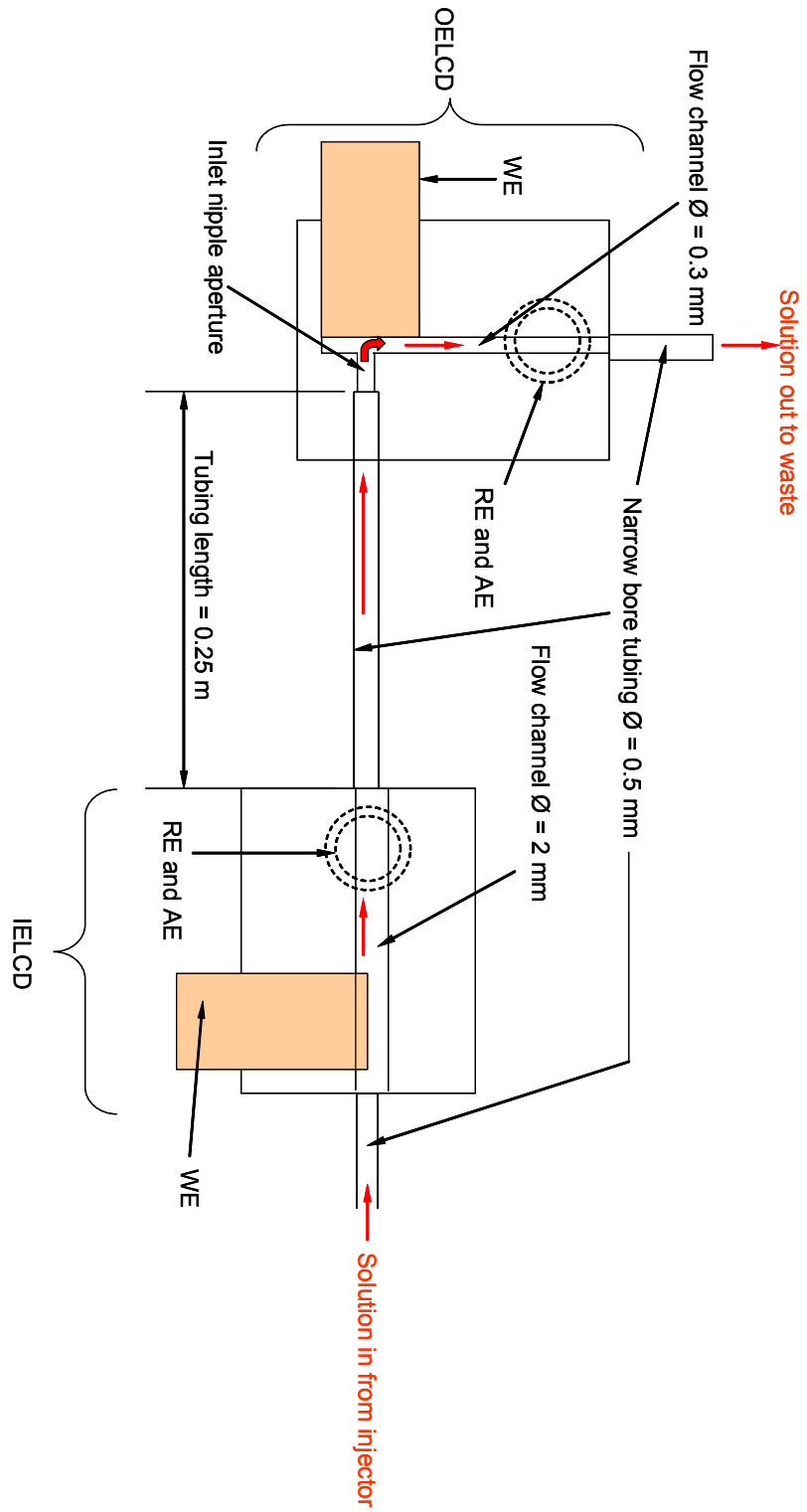

Figure 2.3: Representation of analyser system B. IELCD – input electrochemical cell detector, OELCD – output electrochemical cell detector, AE – auxiliary electrode, RE – reference electrode and WE – working electrode.

2.1.1 Electrochemical cell detectors

The electrochemical detectors were based on two different designs. The first design is termed the wall jet cell and the second design termed the flow by cell. In both these designs three electrodes were employed in each detector. These electrodes are called the working electrode, auxiliary electrode and reference electrode. In either cell designs, the working electrode was a platinum disc with a diameter of 2 mm encased in a cylindrical PEEK (polyether – ether ketone) shaft. The outer diameter of the PEEK shaft was 6 mm. For the wall jet design the auxiliary electrode was a gold rod with a 2 mm diameter, which was embedded in the cell. For the flow by cell the auxiliary electrode was a gold disc with a diameter of 2 mm encased in a PEEK shaft also with a diameter of 6 mm. For both cell designs, the reference electrode was a silver rod, with a diameter of 4 mm, immersed in silver nitrate reference electrolyte contained in an electrolyte vessel. Apart from the auxiliary electrode design the difference between the two cell designs was in the configuration of the flow channel. The wall jet cell that was used in the experiments is commercially available, model 6.5303.030 (Metrohm, Herisau, Switzerland), whilst the flow by cell was custom built. Shown below in Figure 2.4 is a representation of the working electrodes for both the wall jet and flow by cells and a representation of the auxiliary electrode for the flow by cell. These electrodes were attached to the cell blocks by means of locking screws. In order to ensure leak tight seals, PTFE (polytetrafluoroethylene) sealing gaskets were employed. The electrodes, locking screws and PTFE sealing gaskets are all commercially available. Shown in Figure 2.5 is a representation of the reference electrodes for both detector types. For the reference electrode a silver rod was encased in a locking screw. The locking screw was inserted into the reference electrolyte storage vessel, which was filled with reference electrolyte. To ensure no leaks from the top of the reference electrolyte storage vessel (where the silver rod locking screw was attached), a PTFE sealing gasket was used. The reference electrolyte storage vessel with

the attached silver rod was screwed into the body of the detector cell. To ensure no leaks from the cell block, once again PTFE sealing gaskets were utilised. The tip of the reference electrolyte storage vessel was embedded with a ceramic frit. The ceramic frit did not allow for reference electrolyte to leak out of the storage vessel or for other solutions to flow into the storage vessel, but did allow for diffusion of ions. The reference electrolyte storage vessels used in these experiments are commercially available. However the locking screws embedded with silver rods were custom made.

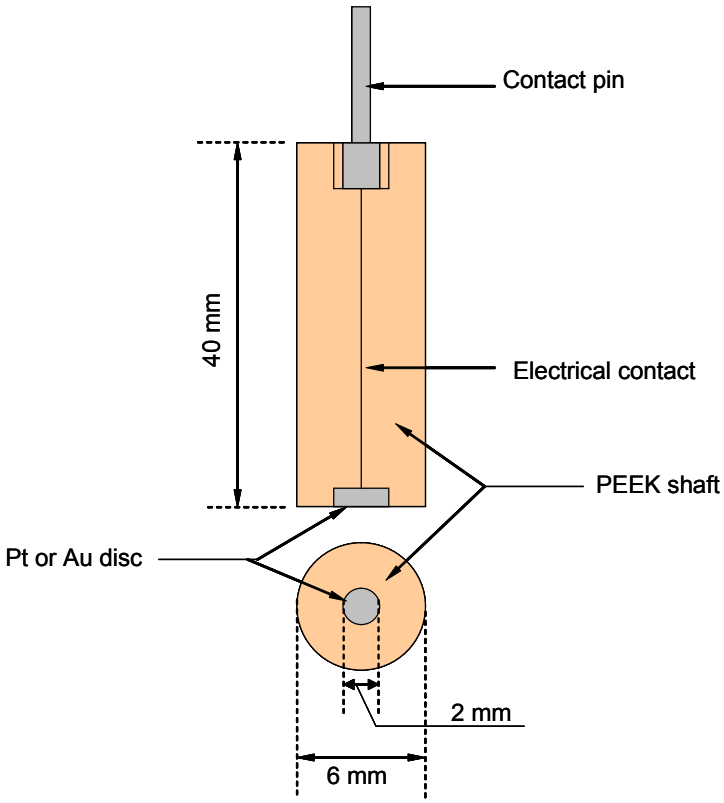

Figure 2.4: Representation of working electrode for wall jet and flow by cells and representation of auxiliary electrode for flow by cell.

In the wall jet design, the auxiliary and reference electrodes were situated directly opposite each other. A very small space existed between the

reference and auxiliary electrode, which was the flow channel. The diameter of the flow channel was approximately 0.3 mm.

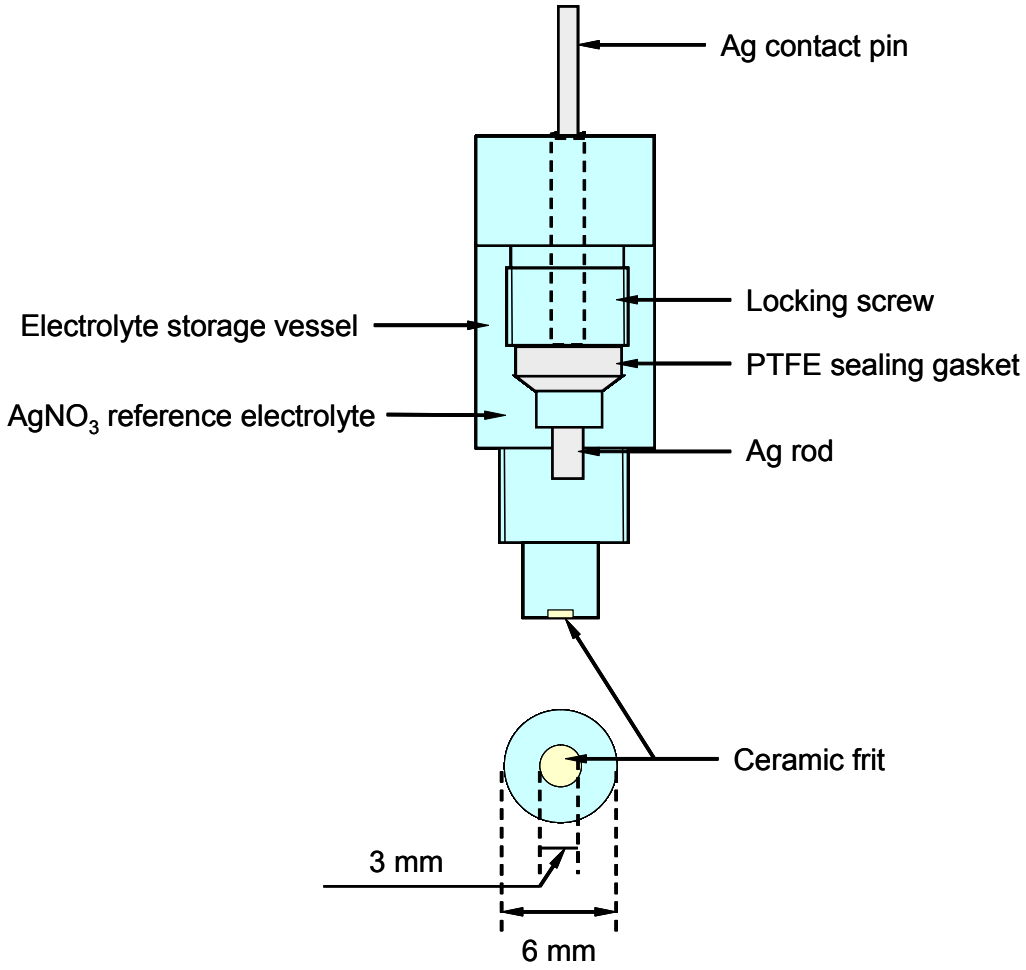

Figure 2.5: Representation of reference electrode.

Both the auxiliary and reference electrodes were situated close to the solution exit. This is illustrated in Figure 2.6.

The solution inlet tubing was screwed into a nipple, which in turn was screwed into the cell body. The working electrode and solution inlet nipple were situated directly opposite each other. A very small spacing existed between the working electrode surface and solution inlet nipple. The solution flowing into the cell therefore impinged perpendicularly onto the

working electrode surface creating a jet of liquid. This liquid then flowed through the flow channel towards the exit. The working electrode and solution inlet nipple were situated in a plane perpendicular to the reference and auxiliary electrode. Figure 2.7 below is representation of the wall jet cell, showing the position of the working electrode and solution inlet. Figure 2.8 below is a representation of the wall jet cell, which clearly illustrates the flow path. The dimensions of the wall jet cell block are shown on Figures 2.6 and 2.7.

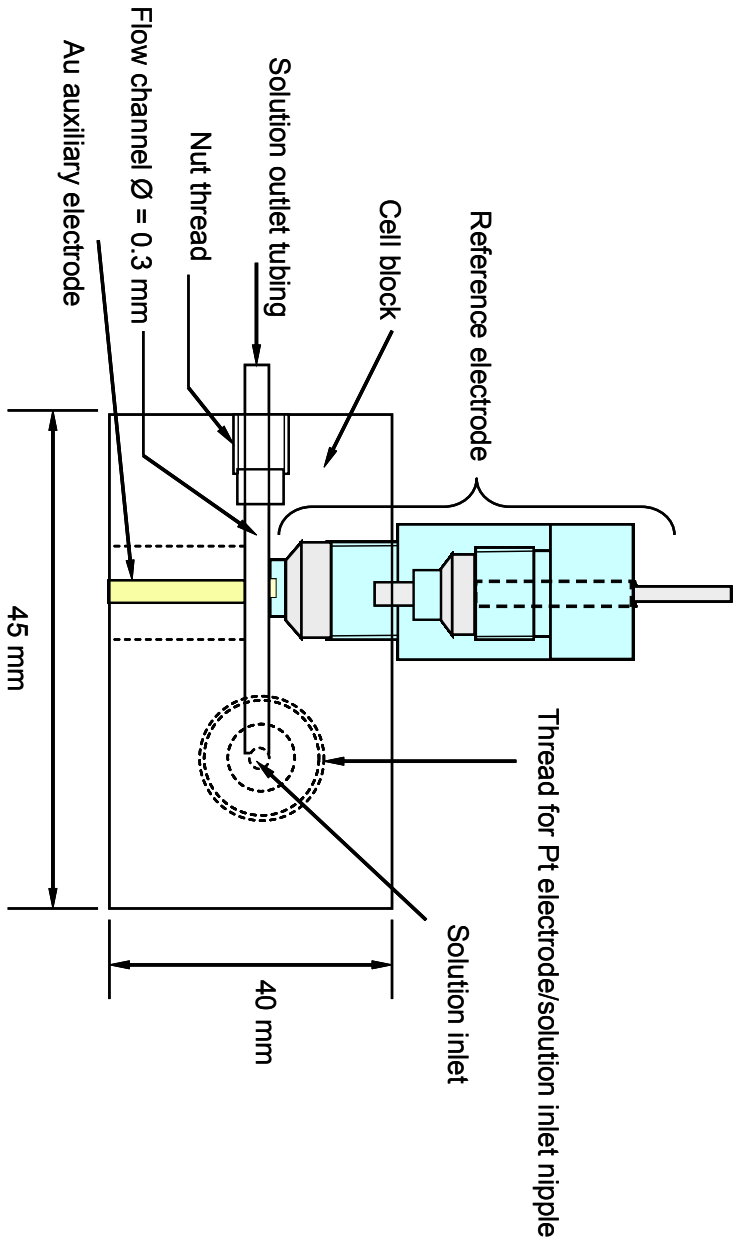

Figure 2.6: Illustration of wall jet cell and components – side view.

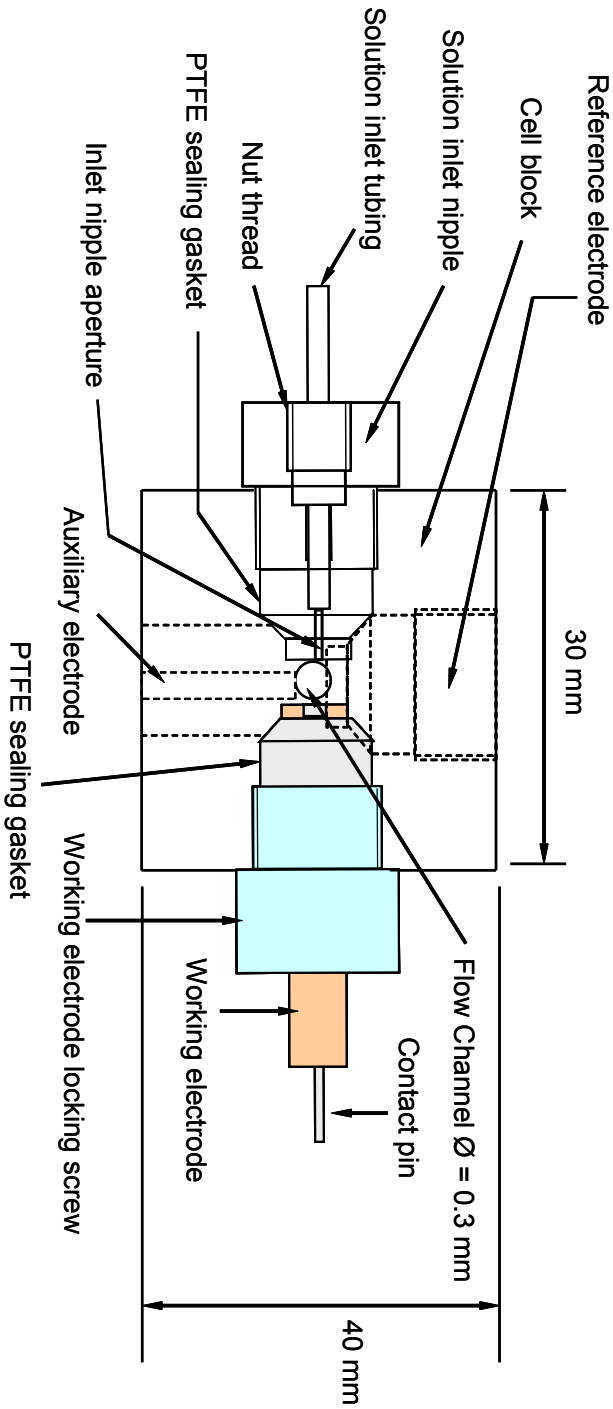

Figure 2.7: Illustration of wall jet cell and components – front view.

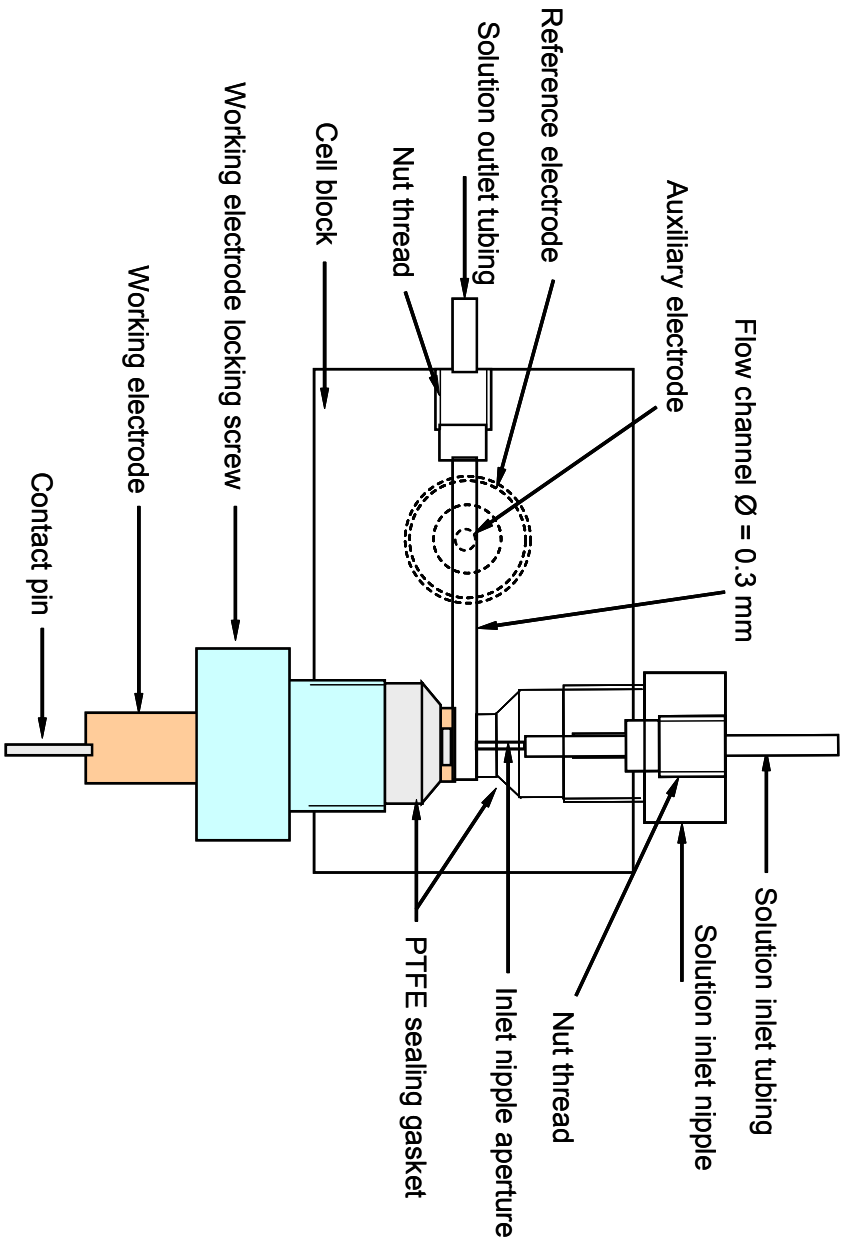

Figure 2.8: Illustration of wall jet cell and components – top view.

The design of the flow by cell is illustrated in Figures 2.9, 2.10 and 2.11 below. In this design, the auxiliary and reference electrode were situated directly opposite each other, as was the case for the wall jet design. The spacing between the auxiliary electrode surface and the ceramic frit of the reference electrode was the flow channel, which had a diameter of 2 mm. The flow by cell therefore had a flow channel that had a greater diameter than the wall jet cell. In the flow by cell design, the auxiliary and reference

electrodes protruded slightly into the flow channel. This is illustrated in Figure 2.9. The working electrode was situated in a plane perpendicular to the reference and auxiliary electrodes, as was the case for the wall jet cell detector. In the flow by cell design there was no solution inlet nipple. The flow channel extended through the length of the flow by cell. On either ends of the flow channel were nut threads for the attachment of inlet and outlet solution tubing. The working electrode also protruded slightly into the flow channel. Therefore for the flow by cell design, the flow of solution was parallel to the working electrode surface. This is clearly illustrated in both Figures 2.9 and 2.11. The dimensions of the flow by cell block were the same as the wall jet cell block.

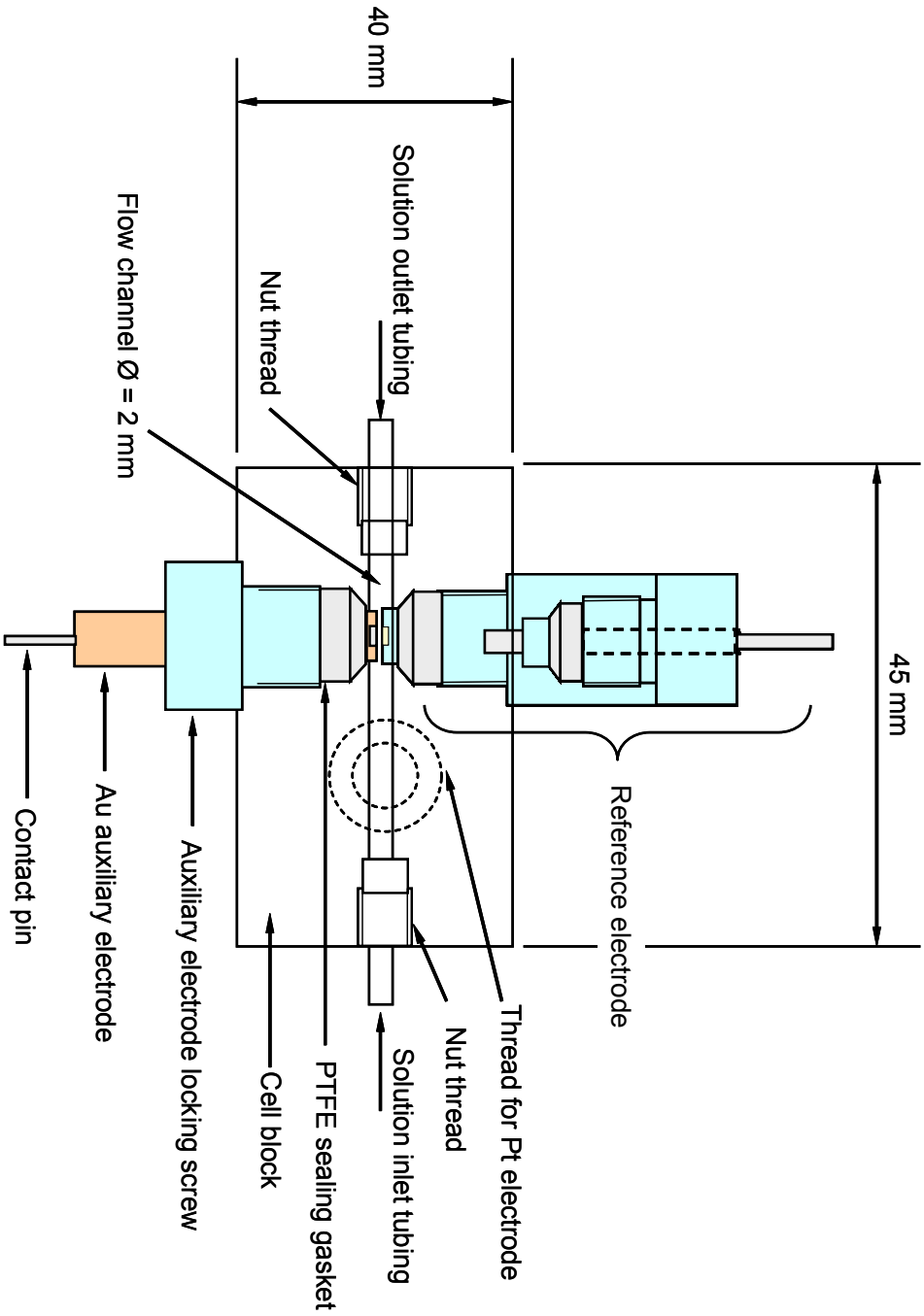

Figure 2.9: Illustration of flow by cell and components – side view.

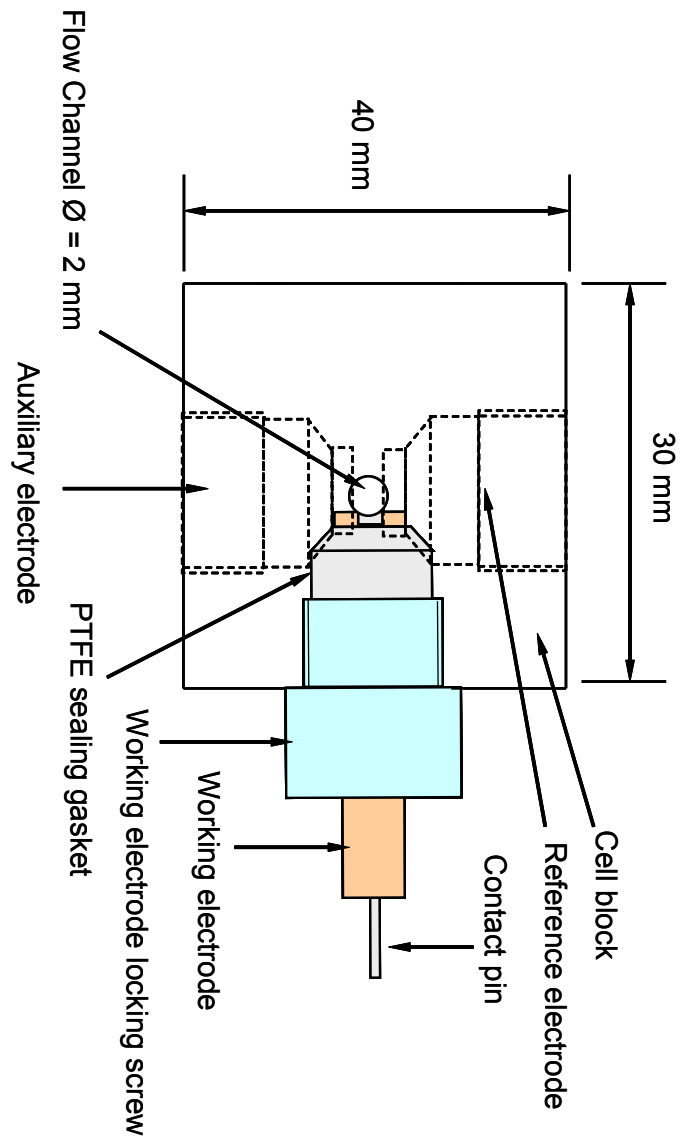

Figure 2.10: Illustration of flow by cell and components – front view.

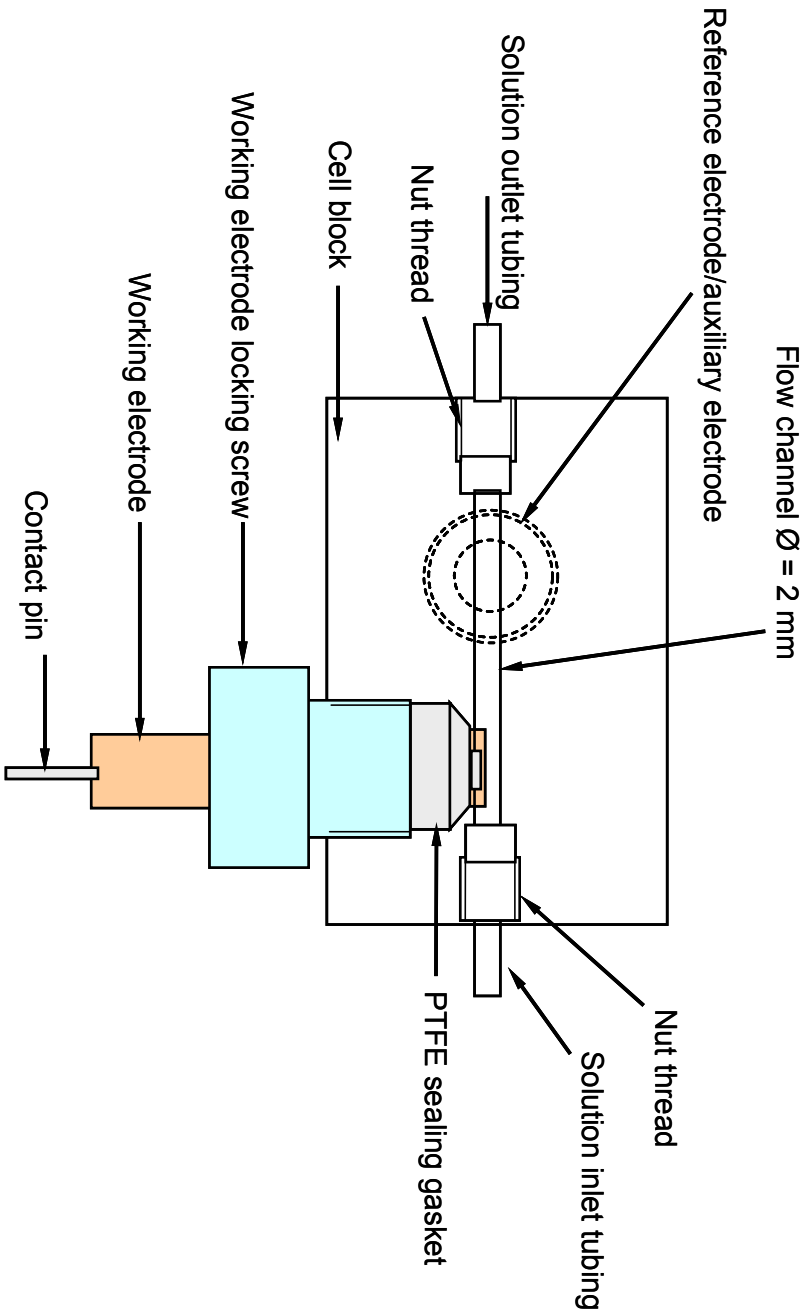

Figure 2.11: Illustration of flow by cell and components – top view.

2.1.2 Pumps

The background electrolyte pump was utilised to continuously pump background electrolyte towards the detectors, whilst the sample pump was used to pump the electroactive species into the sample loop.

The background electrolyte pump was a piston pump; model 765 Dosimat, (Metrohm, Herisau, Switzerland) with a PTFE Teflon piston. The sample pump was a gear pump which consisted of the pump drive; model 78004-02 (Ismatec, Glattbrugg, Switzerland) and pump head; model 1840 (Micropump, Vancouver, USA). The pump head body was constructed of 316 stainless steel, the gears were made of PEEK and the seals were PTFE Teflon.

Both the background electrolyte and the sample pump were controlled via a personal computer using the RS-232 interface. Pump parameters that could be controlled were the flow rate and volume of solution dispensed.

2.1.3 Six port loop valve

A six port loop valve furnished with an external sample loop was utilised as the injection device. The volume of the sample loop was 20 μl. The valve assembly consisted of a valve head (or valve); model R36781 (Hamilton, Bonaduz, Switzerland) and an electric valve drive; model R77810 (Hamilton, Bonaduz, Switzerland). The valve consisted of a fixed stator and a movable rotor. The stator was connected to the valve body in a manner that allowed attachment of tubing, sample loops and other devices. The rotor contained small passages that connected the stator passages as required. The movable rotor was driven by the electric motor. The diagram below illustrates the fixed stator, stator passages, movable rotor and rotor passages.

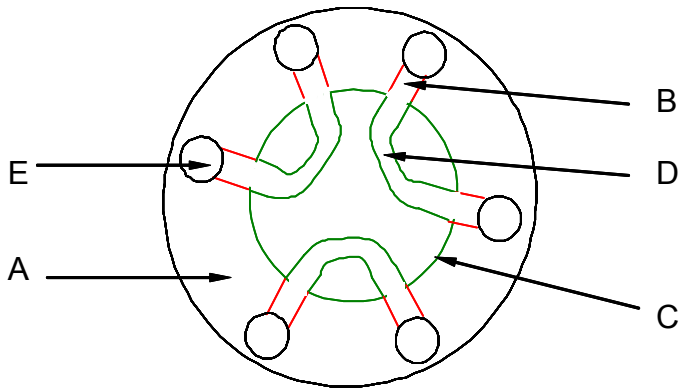

Figure 2.12: Illustration of six port loop valve. A – fixed stator, B – stator passages, C – movable rotor, D – rotor passages and E – nut threads.

The diagrams shown below illustrate the operation of the six port loop valve.

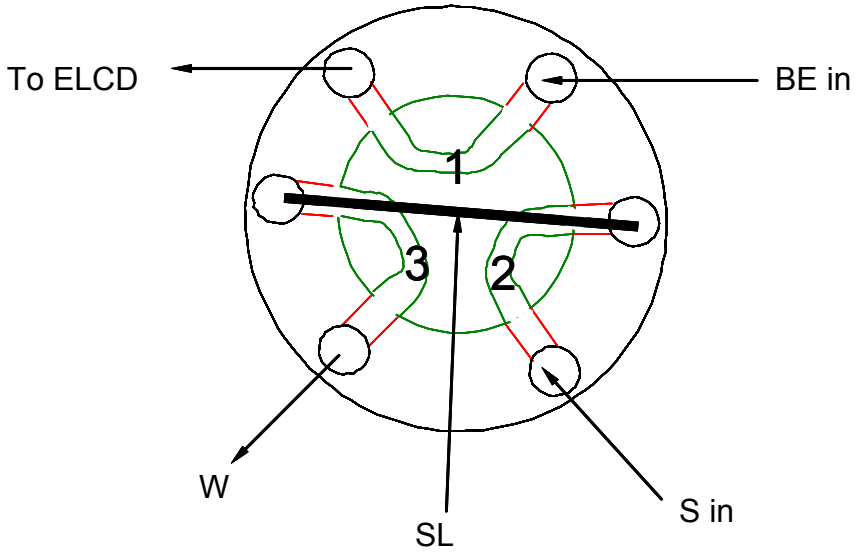

Figure 2.13: Operation of six port loop valve – load position. BE in – background electrolyte flows into the valve, To ELCD – background electrolyte flows towards the electrochemical cell detector, SL – sample loop, S in – Sample flows into the valve and through the sample loop, and W – excess sample flows to waste.

When the six port loop valve was in the load position as illustrated in Figure 2.13 above, a volume much greater than the volume of the sample loop was pumped through the sample loop. This ensured that the sample loop was flushed and filled with electroactive species. The excess solution was discarded as waste.

At the same time the background electrolyte was pumped towards the detector and bypassed the sample loop.

When the six port loop valve was in the inject position, as shown below in Figure 2.14, the rotor and stator passages were aligned in a manner such that the background electrolyte flowed through the sample loop, transporting with it the electroactive species to the input detector. The alignment of the rotor and stator passages can be noted by observing the relative positions of rotor passages 1 – 3 as illustrated in Figures 2.13 and 2.14. When the six port loop valve was in the inject position, the sample pump was inactive, therefore no sample was pumped to the valve. However, if for some reason the sample pump was pumping sample towards the valve when the valve was in the inject position; the sample did not flow through the sample loop, but flowed to the waste line.

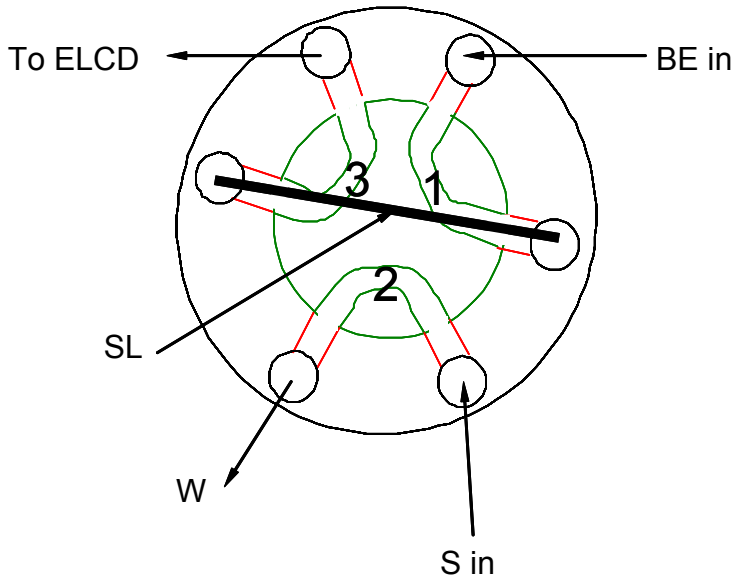

Figure 2.14: Operation of six port loop valve – inject position. BE in – Background electrolyte flows into the valve and through the sample loop, To ELCD – the background electrolyte and the sample flow towards the electrochemical cell detector, SL – sample loop, S – sample inlet port and W – to waste port.

Switching the six port loop valve from the load to inject position and vice versa was achieved by actuating the electric motor. The electric motor was controlled by a personal computer via the RS-232 interface.

2.1.4 Potentiostats

The potentiostats used were model 791 VA detector (Metrohm, Herisau, Switzerland). The input and output detectors were connected to separate potentiostats as illustrated in Figure 2.1. The applied potential or the polarization potential on both the working electrodes of the input and output detectors in all the experimental runs was 300 mV vs. the silver/ silver nitrate reference electrode. Connections to the potentiostats from the electrodes were via shielded electrode cables.

2.1.5 Narrow bore tubing

The narrow bore tubing was manufactured from FEP Teflon (Upchurch Scientific, Oak Harbor, USA). The outside diameter of the tubing was 1/16“, and the inner diameter was 0.02“(0.508 mm). The lengths of the tubing between the injection and detection points that were used were 0.25, 0.5, 0.8 and 1 m.

2.1.6 Data acquisition system and personal computer

The data acquisition system consisted of a PCI data acquisition card, model NI 6036E (National Instruments, Texas, USA) and a 68 pin shielded connector block, model SCB 68 (National Instruments, Texas, USA). The potentiostat signals were configured as differential inputs to the shielded connector block. The CPU of the personal computer was an Intel Pentium™ 3 microprocessor, with a clock speed of 667 MHz. The personal computer had 256 MB of RAM. The software used to control the equipment, and also to read from the data acquisition system was LabVIEW™ version 7.0 (National Instruments, Texas, USA).

2.2 Procedure

The experimental procedure consisted of two parts and for the sake of convenience; the experimental procedure will be discussed as two parts. The first phase or part, which was the pre-measurement phase, will be called the assembly and equilibration phase, and the second phase will be called the measurement phase. These phases are explained below.

2.2.1 Assembly and equilibration phase

As the name implies, this phase deals partly with the assembly of the system and components. If the system had been disassembled for whatever reason, then it was necessary to perform this phase, but if the system was not disassembled and all necessary connections were made then this phase was omitted.

The reference electrolyte vessels shown in Figure 2.5 were filled with reference electrolyte solution. The reference electrolyte was filled to the brim of the electrolyte storage vessels, and thereafter the silver rods were screwed into the electrolyte storage vessels. Filling the electrolyte storage vessels to the brim ensured that there were no air bubbles in the reference electrodes.

Thereafter the reference electrodes were screwed into the electrochemical cell detector bodies and connected to the potentiostats via shielded electrode cables. Similarly, the working electrodes were screwed into the electrochemical cell detector bodies and at this stage were not yet connected to the potentiostats. Lastly, the auxiliary electrode was screwed into the electrochemical cell detector body (for the flow by cell design) and then the auxiliary electrodes were connected to the potentiostats via shielded electrode cables.

Then all tubing and electrical connections were made, i.e. the system was assembled as depicted in Figures 2.1 and 2.2 or 2.3.

Thereafter the background electrolyte pump was started and background electrolyte was delivered to the cells at a certain flow rate. The data-recording program was switched on, the potentiostats were set to the standby mode and the potentiometers located on the VA 791 potentiostats were adjusted such that the display on the personal computer read zero (or close to zero) current. Once the display on the personal computer read zero (or close to zero) current, the polarization voltage (E_{appl}) was set on both the potentiostats to 300 mV, and the working electrodes were connected to the potentiostats via shielded electrode cables. The potentiostats were then set to the measure mode and the current recorded as a function of time was then monitored. This phase is called the equilibration phase. The working electrodes are said to be equilibrated when the current recorded did not vary substantially with time, i.e. a stable baseline current was obtained. If the steady baseline

current value was not zero (or close to zero) it was adjusted to zero (or close to zero) using the potentiometers located on the potentiostats.

It has been observed from experiments that the time required for the working electrodes to equilibrate was several hours, when the apparatus was assembled for the first time, or after the electrodes were removed from the cells and then reinserted into the cell bodies. However if the electrodes were not removed from the cell bodies, the time required for equilibration was approximately 10 to 20 minutes or even shorter when performing measurements the next day. Measurements were performed only after the working electrodes have reached a stable or steady baseline current.

2.2.2 Measurement phase

Background electrolyte was continuously pumped towards the electrochemical cell detectors. After a steady baseline current was observed, the six port loop valve was switched to the load position. A volume of approximately 1 to 2 ml of electroactive sample was pumped through the sample loop, using the sample pump, in order to flush the sample loop. After flushing of the sample loop, the six port loop valve was set to the inject position. The background electrolyte now flowed through the sample loop, carrying with it the injected sample. The current as a function of time was recorded on both detectors. After a steady baseline was reached on both detectors, the system was again pulsed with electroactive species.

2.3 Reagents

The background electrolyte or carrier stream was 0.05 M analytical grade tetrabutylammonium hexafluorophosphate (Sigma-Aldrich, Steinheim, Germany) dissolved in analytical grade acetonitrile (Sigma-Aldrich, Steinheim, Germany).

Silver nitrate dissolved in background electrolyte was used as the reference electrolyte. The silver nitrate concentration was 0.05 M. The

silver nitrate salt used was analytical grade (Saarchem, Merck, Darmstadt, Germany). The reference electrolyte was prepared by first dissolving tetrabutylammonium hexafluorophosphate salt in acetonitrile; thereafter the silver nitrate salt was added.

Ferrocene (Sigma-Aldrich, Steinheim, Germany) dissolved in background electrolyte was used as the tracer. A stock solution of 1000 mg/l ferrocene in background electrolyte was prepared by first dissolving tetrabutylammonium hexafluorophosphate salt in acetonitrile, then adding the required mass of ferrocene.

3 PRESENTATION AND DISCUSSION OF RESULTS

3.1 Calibration

One of the requirements for a successful pulse test is that the recorded signal should be linearly proportional to the tracer concentration. Standard solutions of 1 mg/l, 2 mg/l, 25 mg/l, 50 mg/l, 100 mg/l and 200 mg/l ferrocene in background electrolyte were prepared by dilution of the 1000 mg/l stock solution. These solutions were injected in increasing strength of the tracer solution. From these injections a plot of signal area vs. tracer concentration was obtained. From the calibration plot shown below it is clear that a linear relation is observed up to concentrations of about 75 mg/l for both input and output detectors. It is also clear from the calibration plot that as the concentration increased the difference in areas between the input and output signals increased. The output detector signal area was greater than the input detector signal area. An explanation for this will be discussed below. However at low concentrations (1 mg/l) the difference between areas of the input and output signals were negligible (approx 1% difference). It is for this reason, solutions with concentrations of 1 mg/l or 2 mg/l ferrocene were chosen in experimental runs where the residence time distribution of the system was determined.

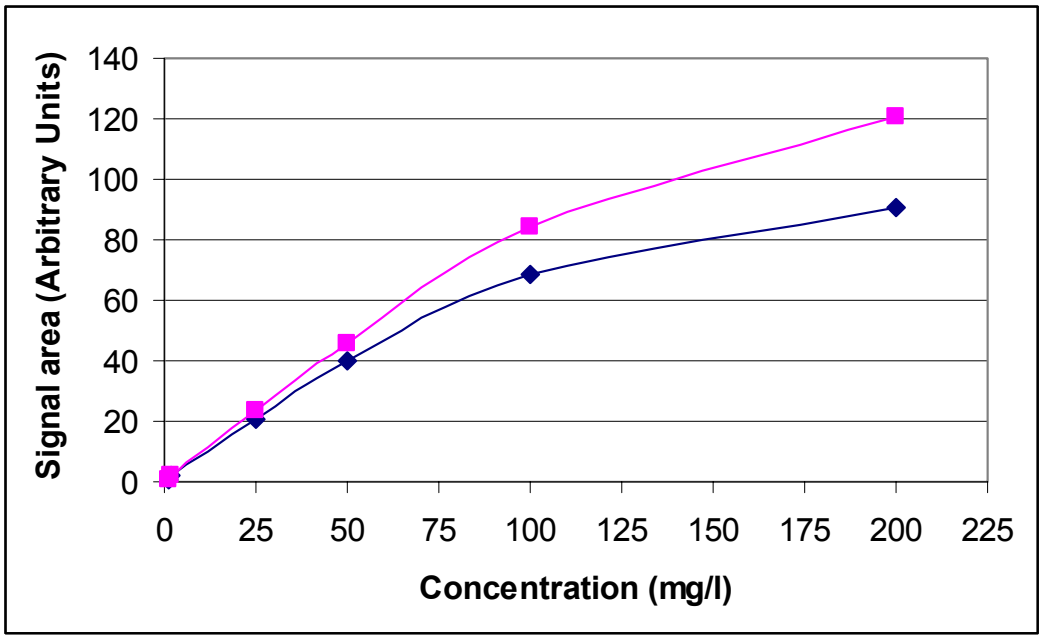

Figure 3.1: Calibration plot – Plot of signal area vs. tracer concentration. input electrochemical cell detector signal and output electrochemical cell detector signal. Both detectors were wall jet cell detectors.

The concentration signals that are measured are converted into electronic signals as shown in the scheme below [15].

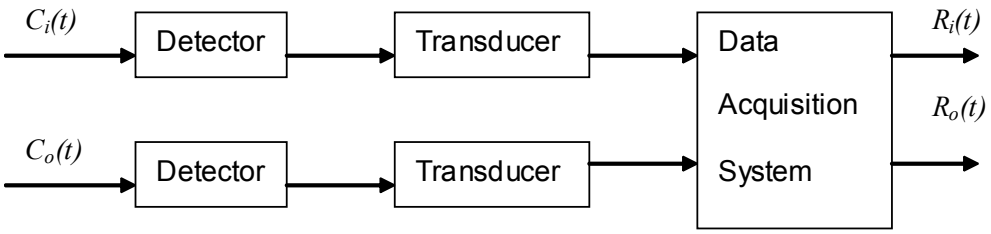

Figure 3.2: General scheme of signal recording

$R_i(t)$ and $R_o(t)$ are the recorded input and output signals respectively. It is required that the recorded signal is proportional to the concentration of tracer. Therefore the relationship between the recorded signal and concentration may be expressed by:

$$R_i(t) = K_i C_i(t) \quad \textbf{3-1}$$

$$R_o(t) = K_o C_o(t) \quad \textbf{3-2}$$

where C_i is defined as the tracer inlet – the reading from the input detector

C_o is defined as the tracer outlet – the reading from the output detector

K_i and K_o are the input and output signal proportionality factors respectively.

t is time

These proportionality factors are not always the same, since no two detectors are exactly the same. The area under the curve of the recorded signals is the integral of equations 3-1 and 3-2 i.e.

$$\int_0^\infty R_i(t)dt = \int_0^\infty K_i C_i(t)dt = K_i \int_0^\infty C_i(t)dt \quad \textbf{3-3}$$

$$\int_0^\infty R_o(t)dt = \int_0^\infty K_o C_o(t)dt = K_o \int_0^\infty C_o(t)dt \quad \textbf{3-4}$$

The proportionality factors can be placed outside the integrals since these are not a function of time. Now for the system under review the amount of tracer injected into the system must be equal to the amount of tracer leaving the system, hence $\int_0^\infty C_i(t) = \int_0^\infty C_o(t)$. Therefore it can be concluded that the difference between the input and output signal areas was due to the different proportionality factors.

3.2 Pulse testing experimental results

Experimental runs were performed using four different lengths of tubing between the input and output detectors. The lengths used were 0.25, 0.5, 0.8 and 1 m. Five different flow rates were tested for each length. These flow rates were 0.5, 0.75, 1.0, 1.5 and 2.0 ml/min. These twenty runs were performed using two wall jet cell detectors as the input and output detectors and these twenty runs were repeated, this time the input detector was a flow by cell detector and the output detector was a wall jet cell detector. It was believed, based on the design of the flow by detector, that the flow by detector caused less dispersion of tracer than the wall jet cell detector.

For the sake of clarity when presenting the results a system or convention will be adhered to. Runs A refer to tests performed where both detectors were the wall jet cell detectors and Runs B refer to tests when the other combination was used. The convention that will be adhered to is as follows. First the type of detectors used is stated then the length of the tubing between the detectors and lastly the flow rate of fluid is stated. For example A0.25-1.5 means a run where two wall jet cell detectors were used, the length of tubing between the detectors was 0.25 m and the flow rate was 1.5 ml/min.

The input and output detector readings for all experimental runs are tabulated in Appendix I (stiffy diskette).

A typical set of results is shown in Figures 3.3 and 3.4 below. These runs were randomly selected and the results are representative of the behaviour of the systems.

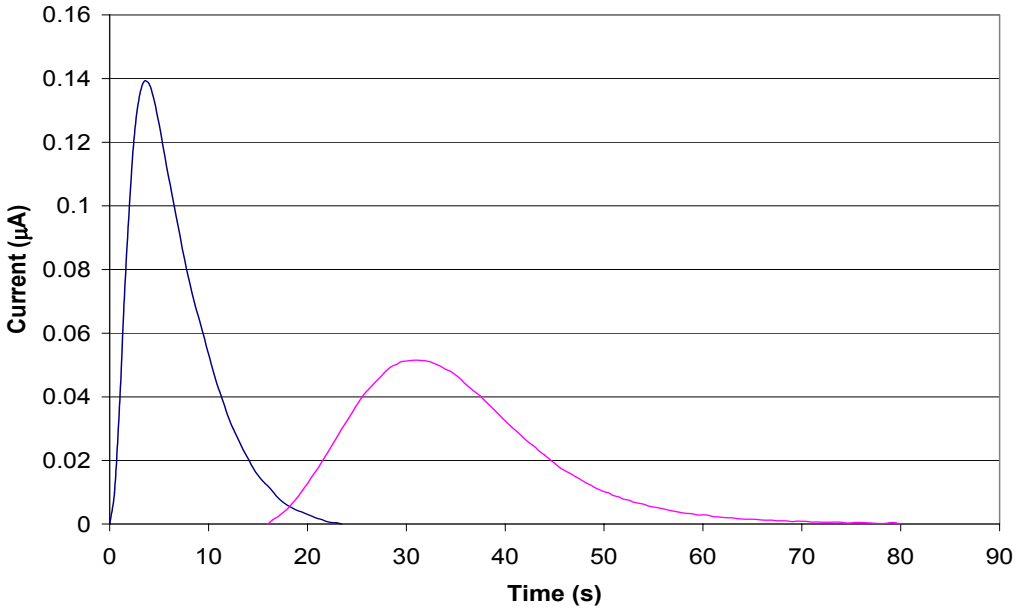

Figure 3.3: Plot of current vs. time for run A0.8-0.5. —Input signal and —output signal.

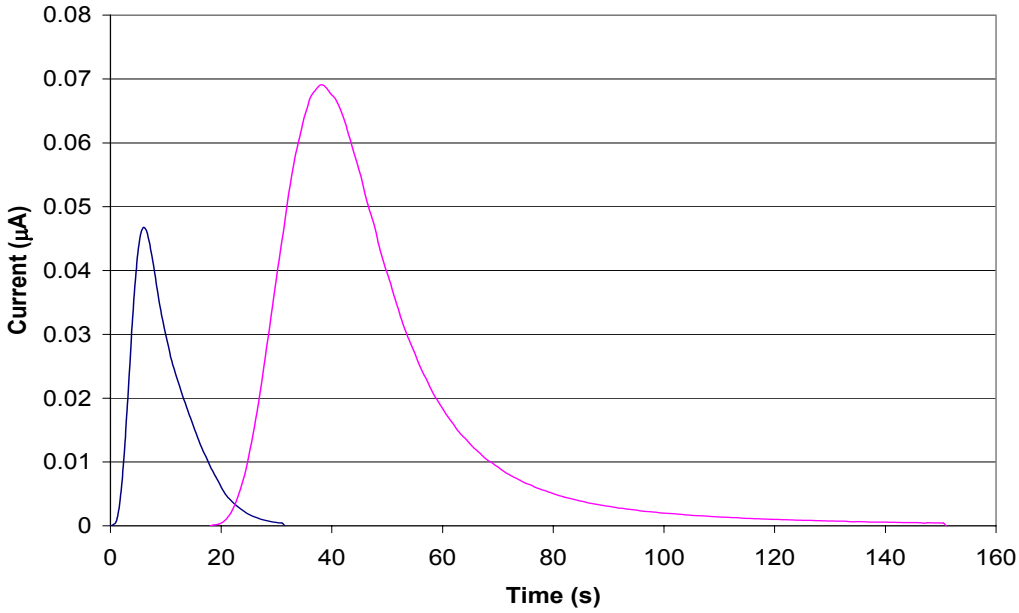

Figure 3.4: Plot of current vs. time for run B0.8-0.5. —Input signal and —output signal.

As expected, the output signals in Figures 3.3 and 3.4 show relatively broader peaks. Both the input and output curves are fairly smooth, indicating that dispersion of the tracer is relatively uniform within the system.

From Figure 3.4 above it is noted that the output signal has a greater peak height than the corresponding input signal. This fact illustrates a very important factor regarding the two different cell detectors. It indicates that the cell detector based on the wall jet design has a greater sensitivity than the cell detector based on the flow by design.

Shown in Figures 3.5 and 3.6 is the relationship between the input, output functions and the system response or system residence time distribution for the abovementioned runs.

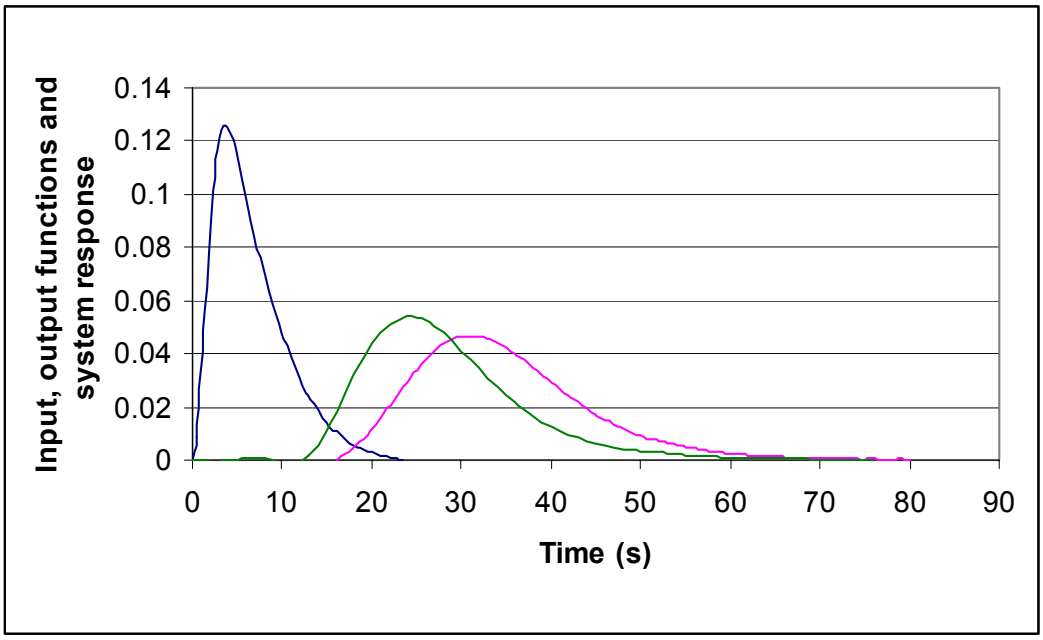

Figure 3.5: Graphical representation of input, output functions and system response for Run A0.8-0.5. — Input function, — output function and — system response or system residence time distribution.

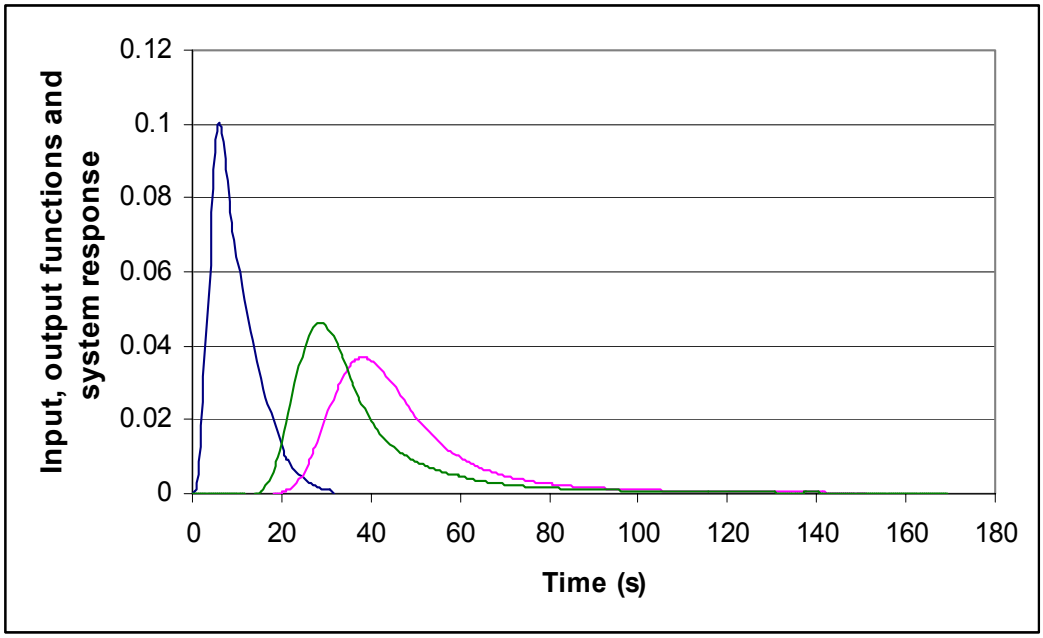

Figure 3.6: Graphical representation of input, output functions and system response for Run B0.8-0.5. — Input function, — output function and — system response or system residence time distribution.

The input and output functions shown in Figures 3.5 and 3.6 are normalized functions. The equations used for normalization of the input and output signals are shown below:

$$\theta_i(t) = \frac{C_i(t)}{\int_0^\infty C_i(t)dt} \qquad \textbf{3-5}$$

$$\theta_o(t) = \frac{C_o(t)}{\int_0^\infty C_o(t)dt} \qquad \textbf{3-6}$$

where $\theta_i(t)$ is defined as the input function

$\theta_o(t)$ is defined as the output function

The experimentally determined system responses or system residence time distributions shown in Figures 3.5 and 3.6 were obtained using the frequency analysis technique, which is explained in Section A.3.2.

The system response was calculated from a Fourier series of the form:

$$\mathbf{E}(t) = \sum_{n=0}^{\infty} \left(a_n \sin \omega t + b_n \cos \omega t \right) \quad \textbf{3-7}$$

where $\boldsymbol{E}(t)$ is the system residence time distribution

a_n and b_n are Fourier coefficients of the system response or the system residence time distribution

$\omega = \frac{n\pi}{T}$ is frequency

n is the coefficient number

T is a constant (T has units of time and has to be carefully selected, as discussed in Section A.3.2)

The Fourier coefficients a_n and b_n were obtained using the following equations:

$$a_n = \frac{q_n u_n - p_n v_v}{T\left(q_n^2 + p_n^2\right)} \quad \textbf{3-8}$$

$$b_n = \frac{q_n v_n - p_n u_v}{T\left(q_n^2 + p_n^2\right)} \quad \textbf{3-9}$$

where p_n and q_n are Fourier coefficients of the input function

u_n and v_n are Fourier coefficients of the output function

The coefficients p_n, q_n, u_n and v_n were obtained using the following equations:

$$p_n = \frac{1}{T} \int_0^{2T} \theta_i(t) \sin \omega t \, dt \quad \textbf{3-10}$$

$$q_n = \frac{1}{T} \int_0^{2T} \theta_i(t) \cos \omega t \, dt \quad \textbf{3-11}$$

$$q_0 = \frac{1}{2T}\int_0^{2T} \theta_i(t)\, dt \qquad \textbf{3-12}$$

$$u_n = \frac{1}{T}\int_0^{2T} \theta_o(t) \sin \omega t\, dt \qquad \textbf{3-13}$$

$$v_n = \frac{1}{T}\int_0^{2T} \theta_o(t) \cos \omega t\, dt \qquad \textbf{3-14}$$

$$v_0 = \frac{1}{2T}\int_0^{2T} \theta_o(t)\, dt \qquad \textbf{3-15}$$

The integrals in equations 3-10 to 3-15 were evaluated using a numerical technique. The numerical technique chosen was Simpson's rule.

The number of coefficients to be used in Equation 3-7 is set by the amplitude of the noise in the signal. A signal may be conceived as being made up of the true signal and noise. In the frequency spectrum of a signal, noise appears as irregular sharp pulses. As the frequency (or number of coefficients) increases, the amplitude ratio, A_n, of the signal drops below the amplitude of the noise.

The amplitude ratio, A_n, of the system response or system residence time distribution (called the system amplitude ratio) is defined by the following equation:

$$A_n = T\sqrt{a_n^2 + b_n^2} \qquad \textbf{3-16}$$

By examining plots of the system amplitude ratio vs. frequency, noise can be easily distinguished from the true signal. This is clearly evident from a plot of the logarithm of the system amplitude ratio against frequency as shown in Figure 3.7 below. In order to avoid the inclusion of noise in the calculation of the system residence time distribution, the Fourier series should be truncated at the point where the system amplitude falls below the level of the noise. According to Turner [13], by truncating at this point a

major portion of the noise is eliminated and truncation of the Fourier series at this point performs smoothing of the signal. Appendix C contains a program that was used to determine the system amplitude ratio and system response or system residence time distribution from the input and output detector readings.

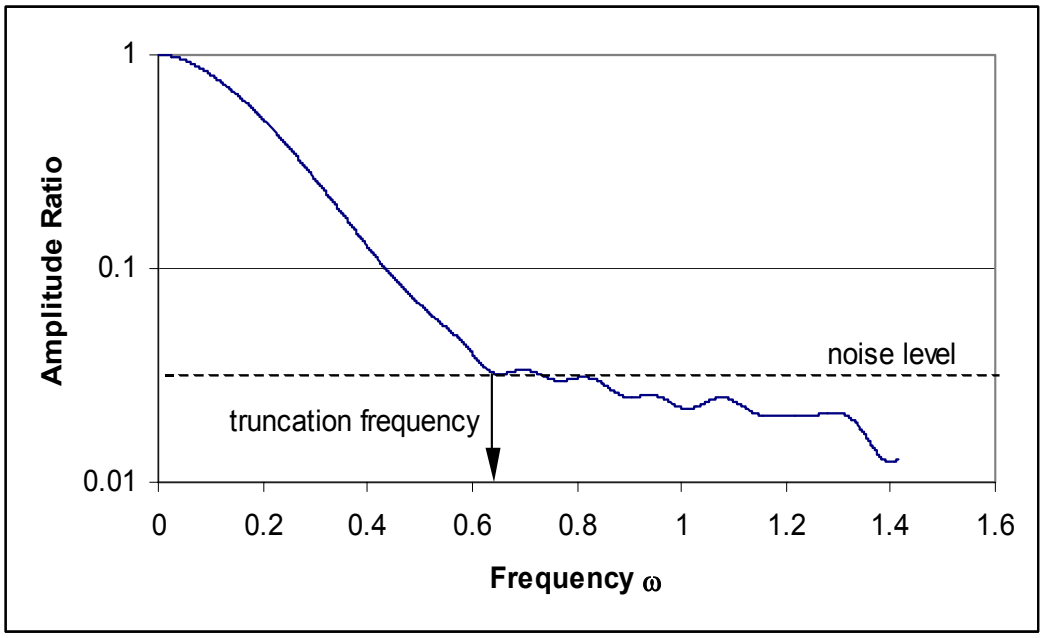

Figure 3.7: Plot of amplitude ratio vs. frequency.

Shown below in Figures 3.8 and 3.9 are plots of various system residence time distributions. In these cases the length of tubing between the injection and detection points was kept constant, but the flow rate of carrier solution was varied.

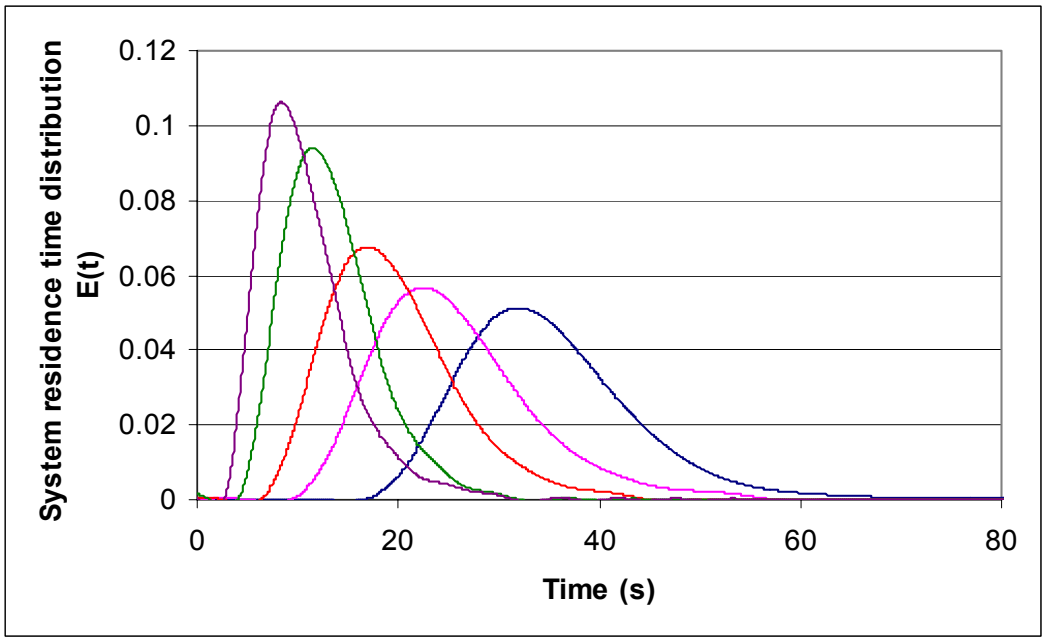

Figure 3.8: Plot of system residence time distributions for Runs A. The length of tubing between the injection and detection points was 1 m. — 0.5 ml/min, — 0.75 ml/min, — 1.0 ml/min, — 1.5 ml/min and — 2.0 ml/min.

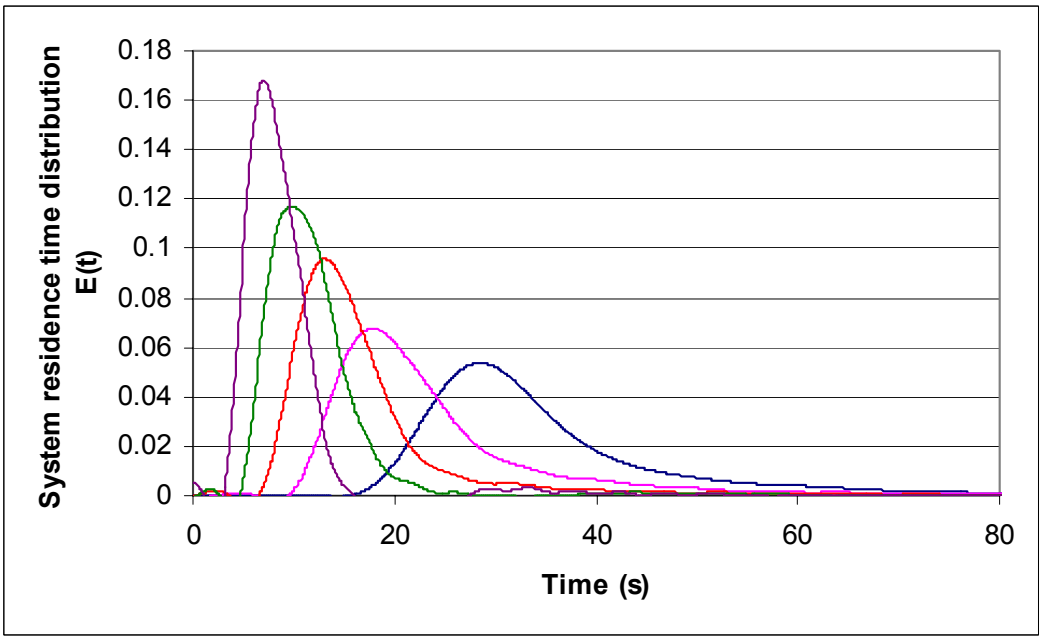

Figure 3.9: Plot of system residence time distributions for Runs B. The length of tubing between the injection and detection points was 1 m. — 0.5 ml/min, — 0.75 ml/min, — 1.0 ml/min, — 1.5 ml/min and — 2.0 ml/min.

From Figures 3.8 and 3.9 above, the effect of varying the flow rate of carrier solution on injected sample can be clearly seen. It is noted from these diagrams that as the flow rate increased, the system residence time distributions became sharper and narrower, indicating that the dispersion of the injected sample decreased as the flow rate of carrier solution increased. The effect of varying the flow rate on the dispersion of injected sample has been illustrated for Runs A and B, when the length of tubing between the injection and detection points was 1 m. However this finding is also applicable to the runs where the lengths of tubing were 0.25, 0.5 and 0.8 m.

Similarly the effect of varying the length of tubing between the injection and detection points, at a fixed flow rate, on the extent of injected sample dispersion was obtained by examining the shapes of the residence time distributions. For the sake of brevity this plots will not be shown.

It was noted that for a fixed flow rate, as the length of tubing between the injection and detection points increased, the system residence time distributions became broader and flatter, implying that as the tubing length increased so too did the dispersion of injected sample.

3.3 Moment analysis

Using the input and output detector readings, it was possible to determine the moments of the input and output functions. The moments of the input and output functions were obtained using the following equations:

$$\alpha_{ni} = \int_0^\infty t^n \theta_i(t)\, dt \qquad \textbf{3-17}$$

$$\alpha_{no} = \int_0^\infty t^n \theta_o(t)\, dt \qquad \textbf{3-18}$$

where α_{ni} is the nth moment, about the origin, of the input function

α_{no} is the nth moment, about the origin, of the output function

Using the moments of the input and output functions, it was possible to determine the analyser system mean residence time and distribution variance using the following equations:

$$\tau = \tau_o - \tau_i \qquad \textbf{3-19}$$

$$\sigma^2 = \sigma_o^2 - \sigma_i^2 \qquad \textbf{3-20}$$

where τ, τ_i and τ_o are the system, input function and output function mean residence times respectively,

σ^2, σ_i^2 and σ_o^2 are the system, input function and output function distribution variances respectively.

A comprehensive derivation of the above equations is presented in Section A.2.3. The integrals in equations 3-17 and 3-18 were evaluated using a suitable numerical integration technique. The technique used was Simpson's rule. Appendix E contains a program that was used for the calculation of the system mean residence time and variance of the distribution from the moments of the input and output functions.

The system distribution variance, σ^2, is a direct measure of peak width. As the system distribution variance, σ^2, increases, so too does the dispersion of injected sample [20]. Using the values of σ^2 calculated under various conditions, comparisons on the extent of sample dispersion could be made. Shown below in Figures 3.10 and 3.11 are plots of the system distribution variances, σ^2, vs. flow rate for both Runs A and B.

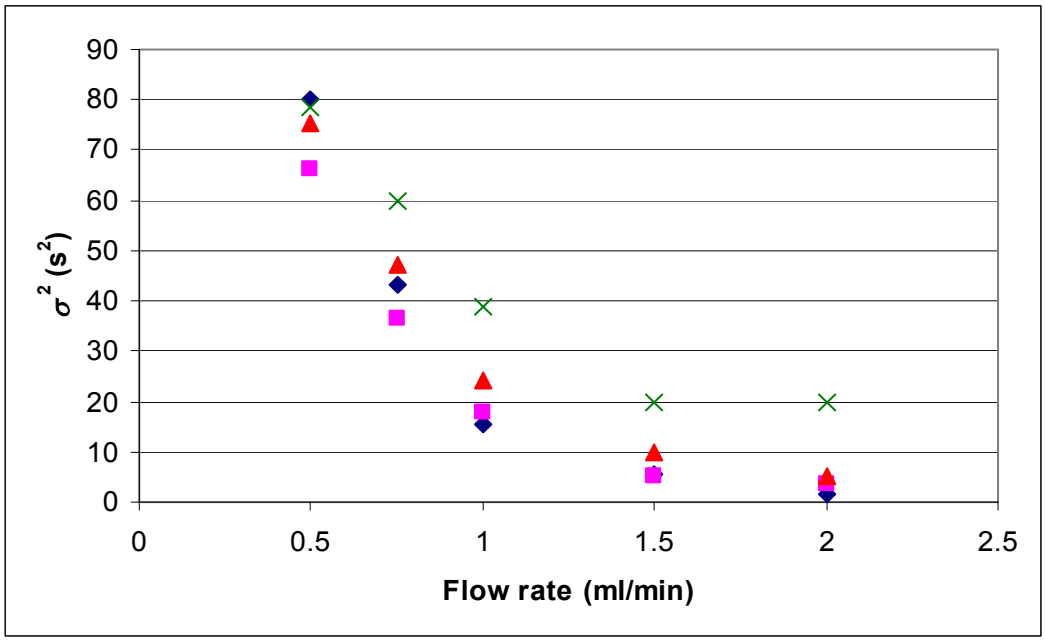

Figure 3.10: Plot of system distribution variance (σ^2) vs. flow rate for Runs A.

◆ – 0.25 m, ■ – 0.5 m, ▲ – 0.8 m and X – 1 m.

Both Figures 3.10 and 3.11 indicate that the system distribution variances, σ^2, are dependent on the flow rate of the carrier solution. For both Runs A and B, as the flow rate increased, the system distribution variances, σ^2, decreased. The findings from both Figures 3.10 and 3.11 imply that the dispersion of injected sample decreased as the flow rate of carrier solution increased. These findings are in agreement with the earlier findings of Section 3.2. From both Figures 3.10 and 3.11, it appears that the system distribution variance, σ^2, and hence the dispersion of injected sample is linearly dependent on the carrier solution flow rate.

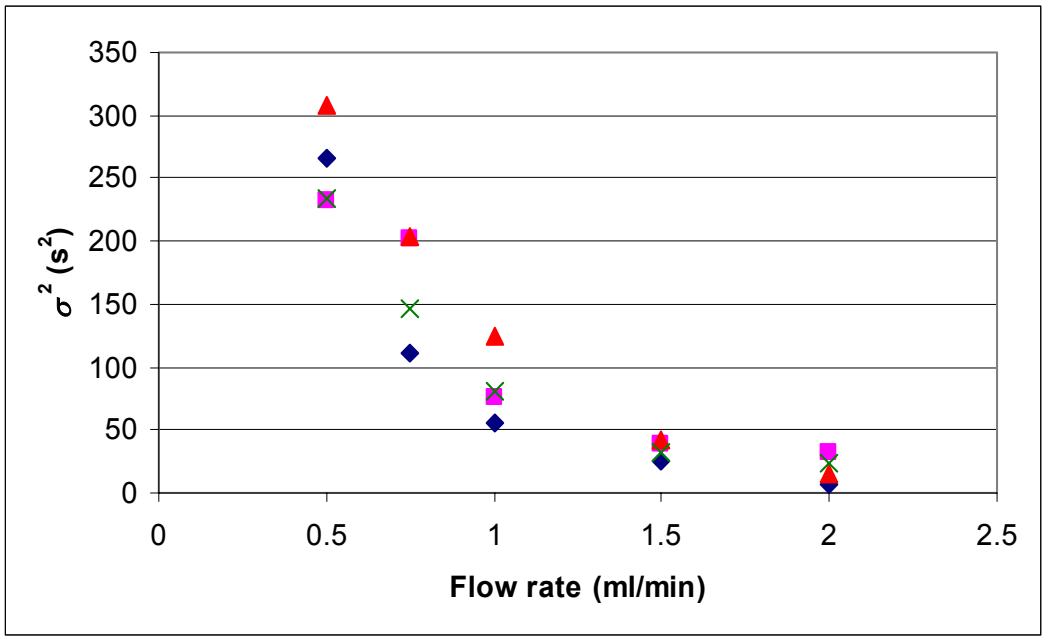

Figure 3.11: Plot of system distribution variance (σ^2) vs. flow rate for Runs B.
◆ – 0.25 m, ■ – 0.5 m, ▲ – 0.8 m and X – 1 m.

Shown below in Figures 3.12 and 3.13 are plots of system distribution variances, σ^2, vs. length of tubing between the injection and detection points for both Runs A and B.

From both Figures 3.12 and 3.13 it is clear that the system distribution variance, σ^2, shows no dependence on the length of tubing between the injection and detection points. The independence of the system distribution variance, σ^2, with respect to length of tubing situated between the injection and detection points, implies that the length of tubing between the injection and detection points does not affect the dispersion of injected sample. It has been shown above in Section 3.2, by examining the system response curves or the system residence time distributions that the dispersion of sample increased as the length of tubing between the injection and detection points increased. Růžička and Hansen in their work [2-4] have also found that the dispersion of sample increased as the length of tubing between the injection and detection points increased. There exists a discrepancy between the earlier findings of Section 3.2 and

the findings from Figures 3.12 and 3.13. It is a well known fact that there are large errors associated in calculating higher moments, especially due to tailing [23, 24], and the discrepancy between the findings could be attributed to the errors in calculating moments. This discrepancy between the experimental findings highlights the disadvantages of moment analysis, where the tail of the signals is disproportionately weighted to the rest of the signal, resulting in erroneous calculations. The results obtained from frequency analysis confirm the results obtained in Section 3.2. The results obtained from frequency analysis are more reliable than the results obtained from moment analysis, since frequency analysis is less sensitive to the tail portion of the signals [13]. The results obtained from frequency analysis are shown in Section 3.4.

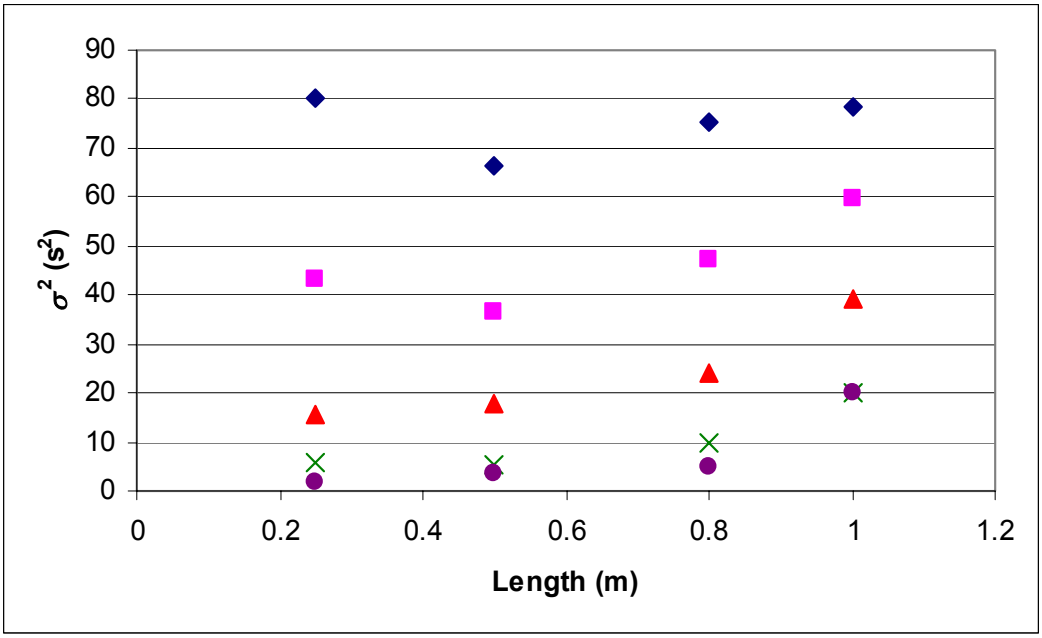

Figure 3.12: Plot of system distribution variance (σ^2) vs. tubing length for Runs A. ◆ – 0.5 ml/min, ■ – 0.75 ml/min, ▲ – 1.0 ml/min, X – 1.5 ml/min and ● – 2.0 ml/min.

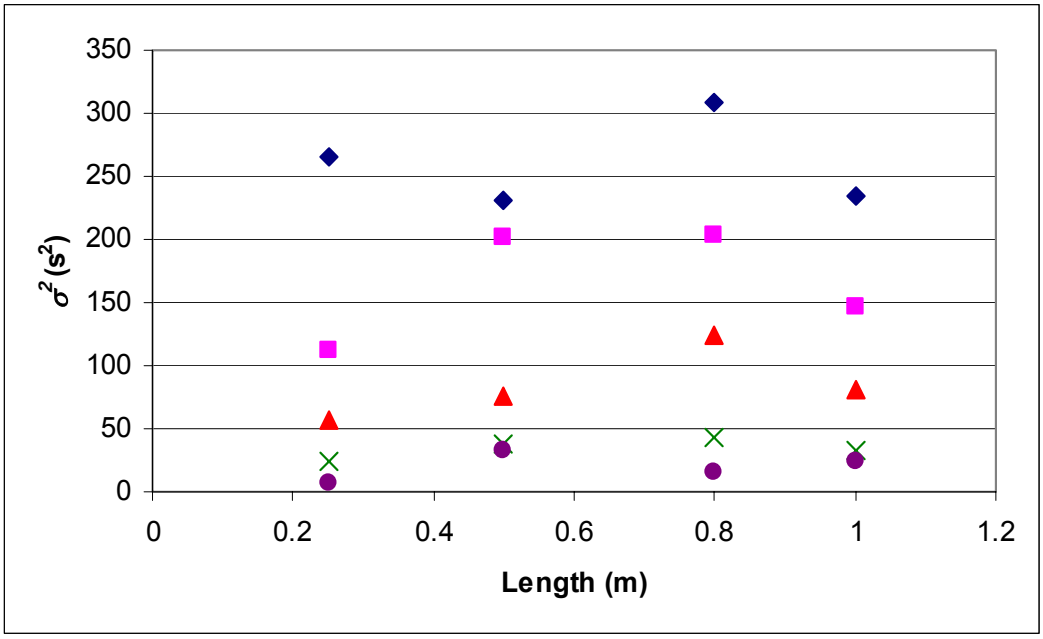

Figure 3.13: Plot of system distribution variance (σ^2) vs. tubing length for Runs B.
◆ – 0.5 ml/min, ■ – 0.75 ml/min, ▲ – 1.0 ml/min, X – 1.5 ml/min and ● – 2.0 ml/min.

3.4 Frequency analysis

The relationship between the amplitude ratio of the input signal, output signal and system response or system residence time distribution is shown below in Figure 3.14. The distances A and C are the same. The distance A is an indication of how far the input signal deviates from an ideal impulse, since the amplitude ratio of an ideal pulse is equal to one for all frequencies [23]. The distance indicated by B is an indication of how far the flow in the analyser system deviates from the amplitude ratio of an ideal pulse or plug flow. In general, as the distance B increases, the flow in the analyser system deviates further from plug flow.

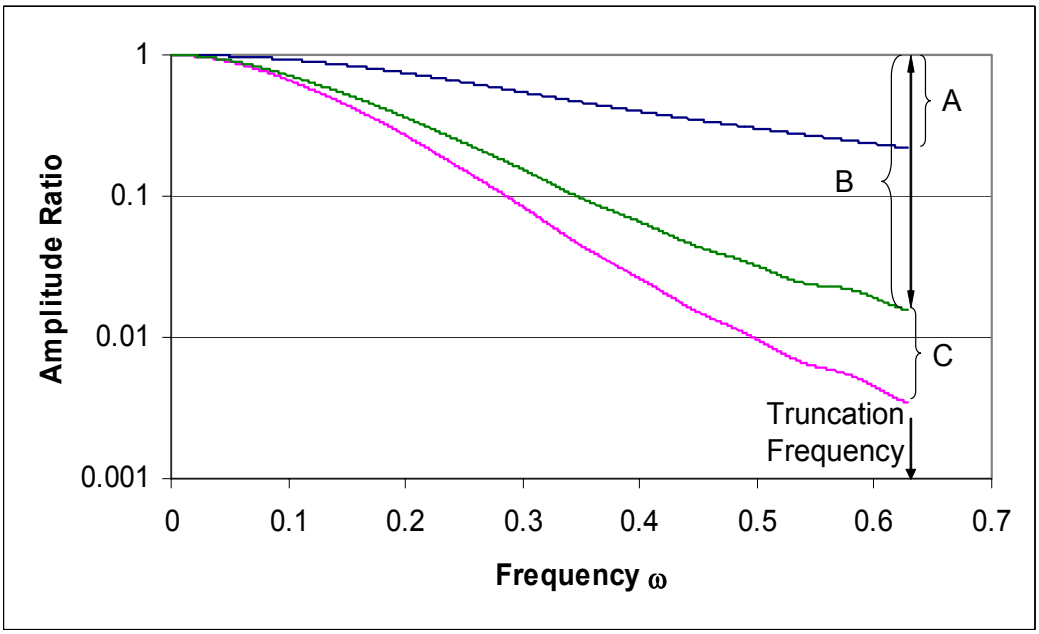

Figure 3.14: Plot of amplitude ratio vs. frequency. —Input signal, —output signal and —system response.

Therefore by examining how the amplitude ratio varies with frequency deductions can be made how the dispersion of sample changes as the length of tubing between the injection and detection points and the flow rate of carrier solution is varied. Shown in Figures 3.15 and 3.16 are plots of the system amplitude ratio vs. frequency, at a fixed flow rate, for various tubing lengths between the injection and detection points for both Runs A and B.

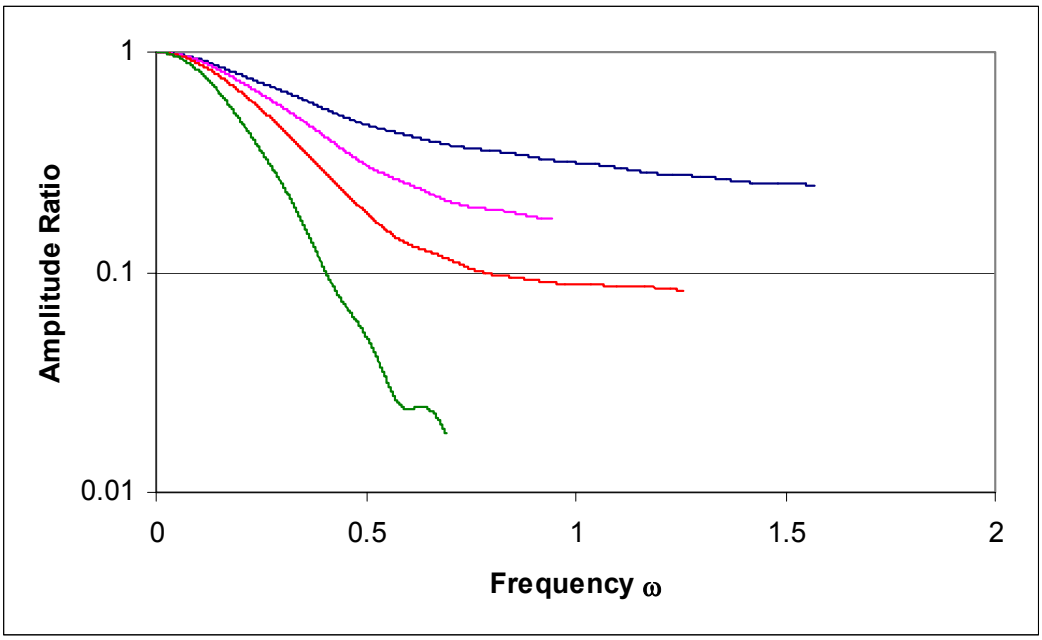

Figure 3.15: Plot of system amplitude ratio vs. frequency for Runs A. The flow rate was 1 ml/min. — 0.25 m, — 0.5 m, — 0.8 m and — 1m.

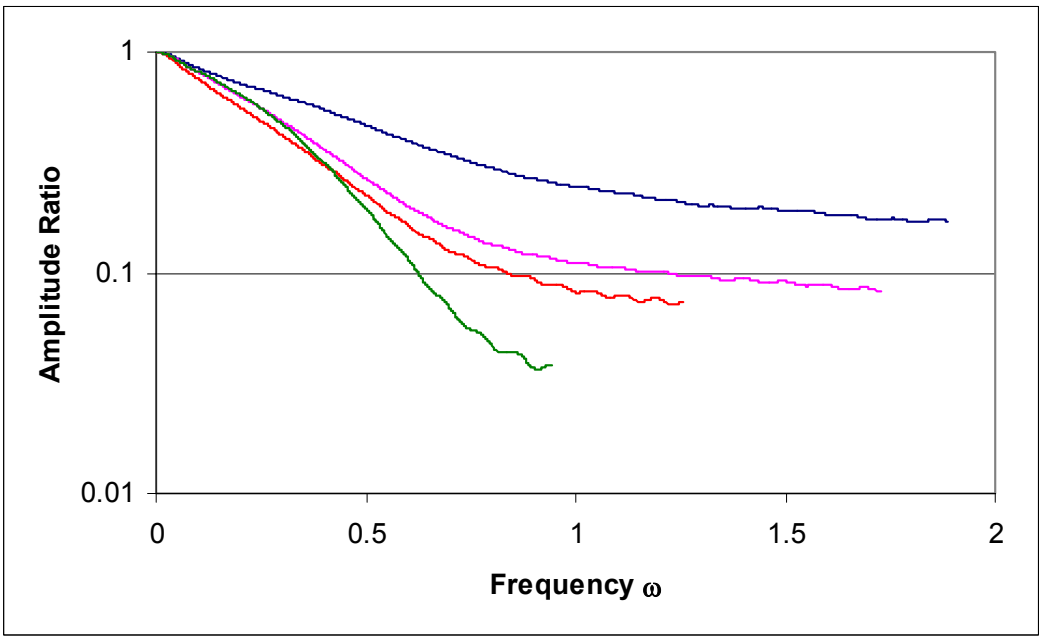

Figure 3.16: Plot of system amplitude ratio vs. frequency for Runs B. The flow rate was 1 ml/min. — 0.25 m, — 0.5 m, — 0.8 m and — 1m.

Clearly the above figures indicate that for a particular flow rate as the tubing length between the injection and detection points increased the system amplitude ratios, at the truncation frequency, deviated further from an ideal pulse amplitude ratio or plug flow. This indicates that the dispersion of sample increased as the length of tubing between the injection and detection points increased. Plots of the system amplitude ratio vs. frequency for various lengths of tubing between the injection and detection points have been shown only for the case where the flow rate was 1 ml/min. The results shown above are also generally applicable to the cases where other flow rates were tested. Plots of the system amplitude ratio vs. frequency for all the experimental runs are shown in Appendix D.

The above finding is in agreement with and confirms the finding from Section 3.2, where it was found that as the tubing length increased, the dispersion of injected sample increased. Both these findings prove that the deduction drawn from moment analysis results is incorrect. The results from moment analysis indicated that the dispersion of sample was independent of the length of tubing between the injection and detection points.

By examining how the amplitude ratio varies with frequency at a fixed tubing length and for various flow rates, the effect of flow rate on sample dispersion can be obtained. Shown below in Figures 3.17 and 3.18 are plots of the system amplitude ratio vs. frequency for a fixed length of tubing between the injection and detection points for various flow rates, for both Runs A and B.

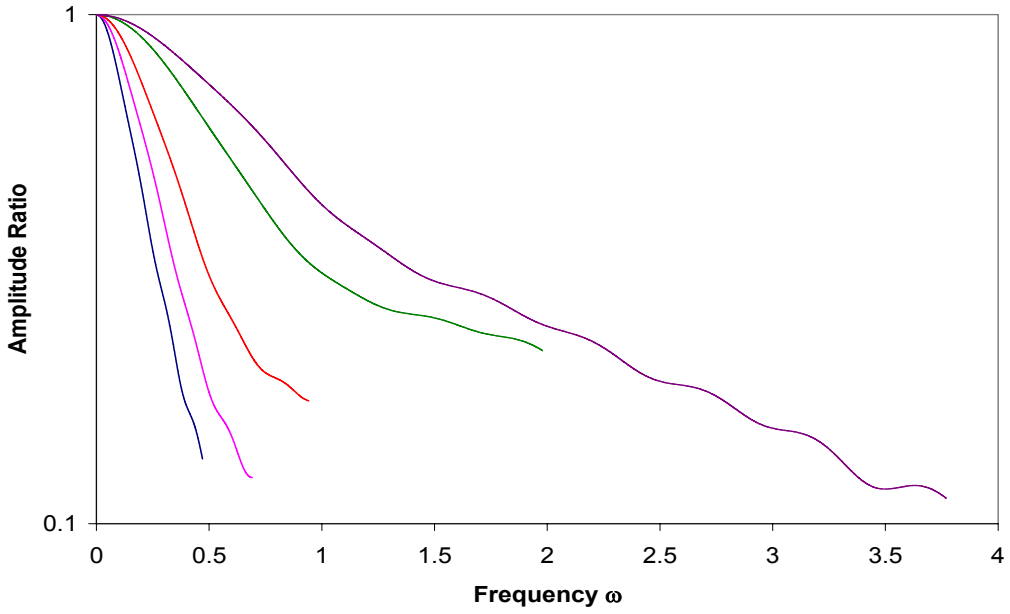

Figure 3.17: Plot of system amplitude ratio vs. frequency for Runs A. The length of tubing was 0.5 m. — 0.5 ml/min, — 0.75 ml/min, — 1.0 ml/min, — 1.5 ml/min and — 2.0 ml/min.

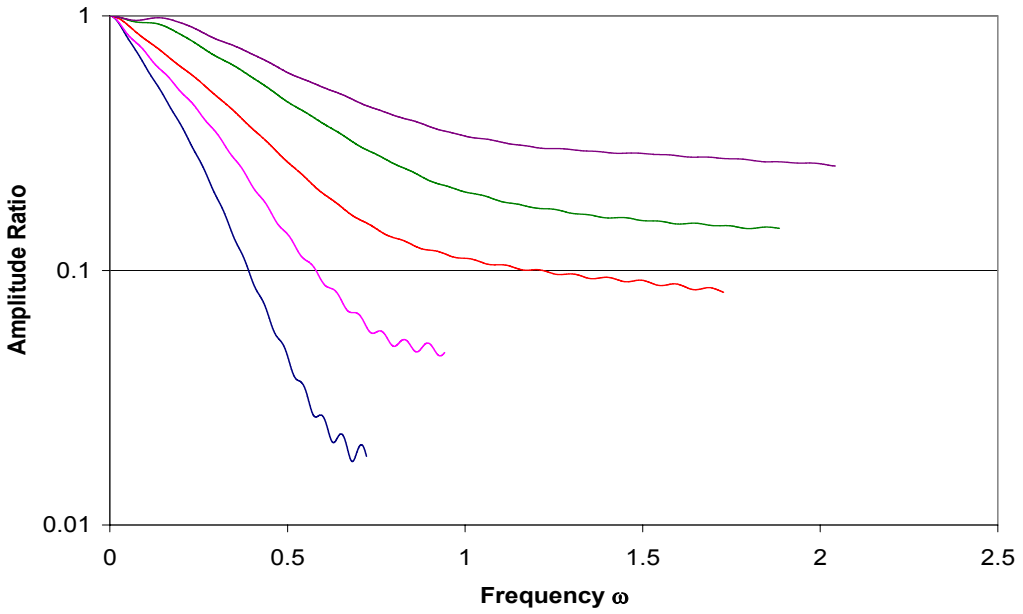

Figure 3.18: Plot of system amplitude ratio vs. frequency for Runs B. The length of tubing was 0.5 m. — 0.5 ml/min, — 0.75 ml/min, — 1.0 ml/min, — 1.5 ml/min and — 2.0 ml/min.

The results from frequency analysis illustrate that for a particular tubing length as the flow rate of background electrolyte increased, the system amplitude ratios, at the truncation frequency, approached the amplitude ratio of an ideal pulse or plug flow. This indicates that the dispersion of sample decreased as the flow rate of carrier solution increased. Using this method it was found, for each of the lengths of tubing tested for various carrier solution flow rates, that the sample dispersion decreased as the flow rate increased. For the sake of brevity, plots of the system amplitude ratio vs. frequency for various carrier solution flow rates were presented only for the case when the tubing length between the injection and detection points was 0.5 m. Plots of the system amplitude ratio vs. frequency for all the experimental runs are shown in Appendix D.

A comparison of the dispersion of injected sample caused by the different detectors designs can be made by examining plots of the amplitude ratio vs. frequency of the input signals only, for cases when the flow rates were the same. This comparison can be made, since the connection from the injection valve to the input detectors was the same. The connection from the injection valve to the input detectors was in any case very short, and its contribution to the dispersion of injected sample can be considered negligible. Shown below in Figure 3.19 is a plot of the input signal amplitude ratios vs. frequency for the wall jet cell and flow by cell detectors when the flow rate was 0.5 ml/min. For the sake of brevity this plot has been shown only for the case when the flow rate was 0.5 ml/min. The trend shown in Figure 3.19 was also observed for the cases when the flow rates were 0.75, 1.0, 1.5 and 2.0 ml/min.

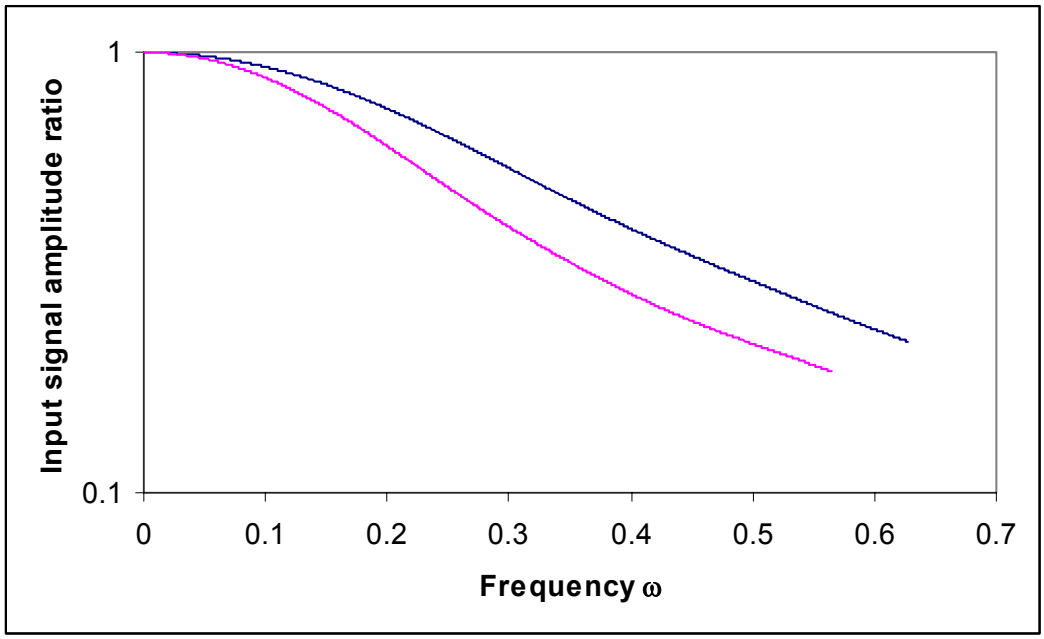

Figure 3.19: Plot of input signal amplitude ratios. — wall jet cell detector and — flow by cell detector. The flow rate was 0.5 ml/min.

From Figure 3.19 above it can be seen that, at the truncation frequencies, the input signal amplitude ratio of the wall jet cell detector is closer to the amplitude ratio of an ideal pulse or plug flow than the input signal amplitude ratio of the flow by cell detector. This implies that the wall jet cell detector caused less dispersion of the injected sample compared to the flow by cell detector, however the difference was small.

4 MATHEMATICAL MODELLING OF RESULTS

4.1 The dispersion model

The dispersion model or the axially dispersed plug flow model is a commonly used model for the description of the flow in flow injection analyser systems [2, 3, 18, 25-27].

For the experimental setup and conditions under consideration, the axially dispersed plug flow model is given by the following equation [28, 29, 30]:

$$\mathbf{E}(t) = \frac{L}{2\sqrt{\pi D t}} e^{-\frac{(L-ut)^2}{4Dt}} \qquad \textbf{4-1}$$

where D is the axial dispersion coefficient

L is the length of tubing between the injection and detection points

u is the mean velocity

The derivation of equation 4-1 is presented in Section A.4.

The transfer function in the Laplace domain of the axially dispersed plug flow model for the experimental conditions under consideration is given by [31, 32]:

$$\bar{\mathbf{E}}(s) = \exp\left(\frac{uL}{2D}\left(1-\sqrt{1+\frac{4sD}{u^2}}\right)\right) \qquad \textbf{4-2}$$

where s is the Laplace transform variable

4.1.1 Moment analysis of the dispersion model

In order to evaluate the moments or cumulants of the dispersion model, use is made of equation A-14. Using equation A-14 the following expressions are obtained for the system mean residence time τ and distribution variance σ^2:

$$\tau = \frac{L}{u} \qquad \textbf{4-3}$$

$$\sigma^2 = \frac{2DL}{u^3} \qquad \textbf{4-4}$$

The expressions derived above are consistent with the results obtained by Bischoff [33], Bischoff and Levenspiel [34] and Michelsen and Østergaard [31].

From equations 4-3 and 4-4 above it is noted that both τ and σ^2 are proportional to the length of tubing between the injection and detection points. Therefore if the flow or dispersion of sample in the analyser system can be represented by the axially dispersed plug flow model, plots of τ and σ^2 against L should be straight lines. Shown below in Figures 4.1 and 4.2 are plots of the system mean residence time τ against L for both Runs A and B.

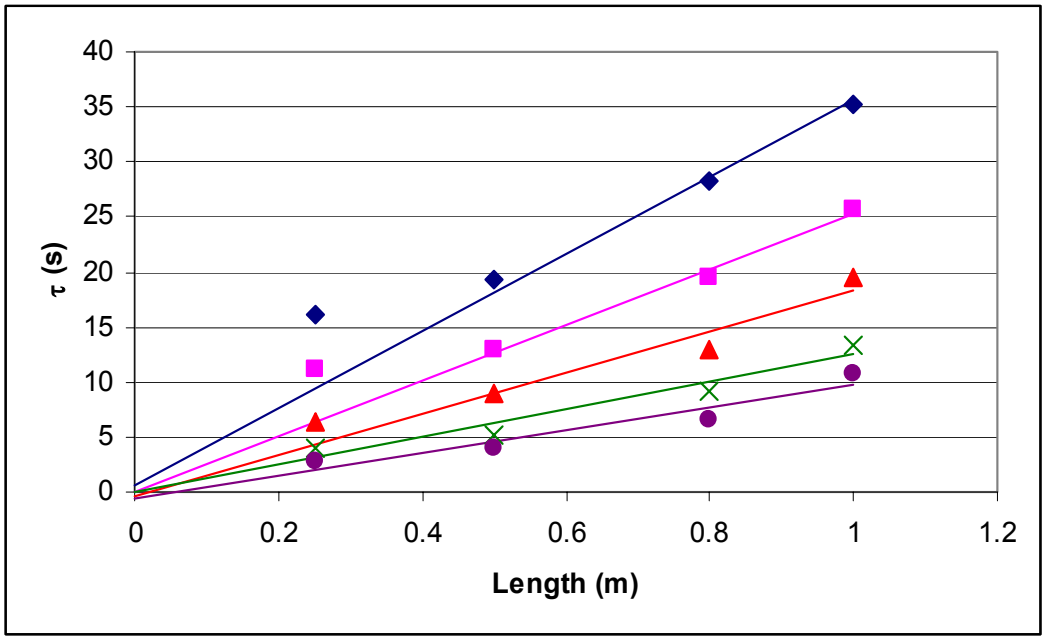

Figure 4.1: Plot of system mean residence time τ vs. tubing length for Runs A.
◆ – 0.5 ml/min, ■ – 0.75 ml/min, ▲ – 1.0 ml/min, X – 1.5 ml/min and ● – 2.0 ml/min.

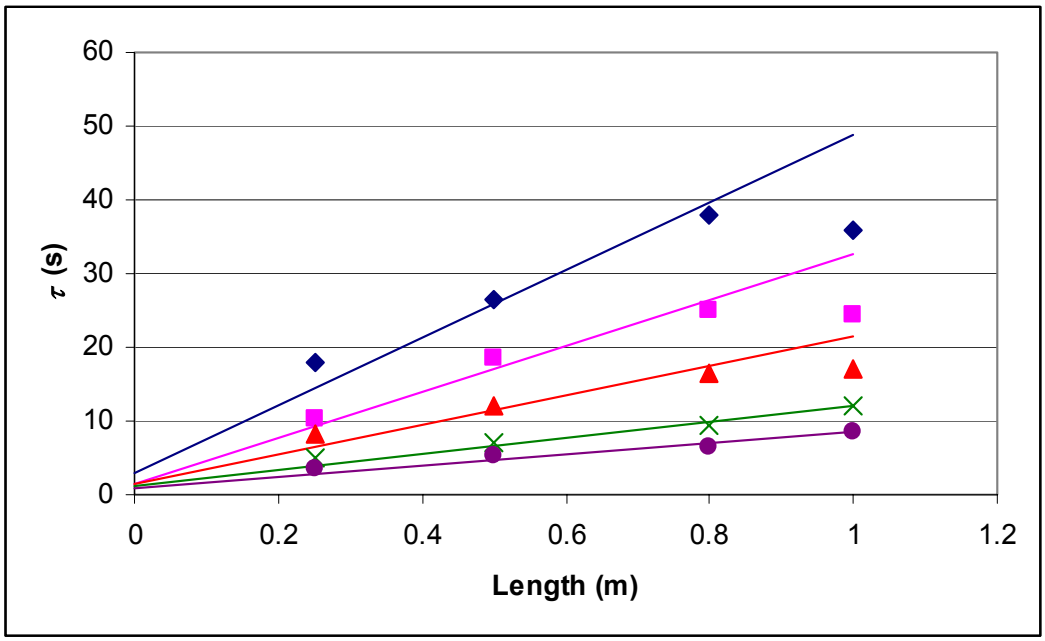

Figure 4.2: Plot of system mean residence time τ vs. tubing length for Runs B.
◆ – 0.5 ml/min, ■ – 0.75 ml/min, ▲ – 1.0 ml/min, X – 1.5 ml/min and ● – 2.0 ml/min.

From the above figures it is noted, for Runs A for the cases when the flow rate was 0.5 ml/min, 0.75 ml/min and 1 ml/min linearity was observed when the tubing length was greater than 0.5 m. For Runs B for the cases when the flow rate was 0.5 ml/min, 0.75 ml/min and 1 ml/min linearity was observed for lengths shorter than 1 m. For Runs A and B for the cases when the flow rate was 1.5 ml/min and 2 ml/min, linearity was observed for the whole range of lengths tested.

It has been shown above in Section 3.3 (see Figures 3.14 and 3.15) that the system distribution variances σ^2 are independent of the length of tubing between the injection and detection points. This was the case for all the flow rates that were tested.

4.1.2 Frequency analysis of the dispersion model

The transfer function given in equation 4-2 can be transformed into the frequency domain [13, 23], and is given by the following equation.

$$\bar{\mathbf{E}}(i\omega) = \exp\left(\frac{uL}{2D}\left(1-\sqrt{1+i\frac{4\omega D}{u^2}}\right)\right) \qquad \textbf{4-5}$$

where i is the imaginary variable

Now $\sqrt{1+i\frac{4\omega D}{u^2}}$ can be expressed in complex notation as:

$$\left(1+\frac{16D^2\omega^2}{u^4}\right)^{\frac{1}{4}}\left(\cos\frac{\theta}{2}+i\sin\frac{\theta}{2}\right) \qquad \textbf{4-6}$$

where $\theta = \arctan\left(\frac{4\omega D}{u^2}\right)$

The derivation of equation 4-6 is shown in Appendix F. Now substituting equation 4-6 into equation 4-5 and multiplying out, gives

$$\bar{\mathbf{E}}(i\omega) = \exp\left(\frac{uL}{2D} - \frac{uL}{2D}\left(1+\frac{16D^2\omega^2}{u^4}\right)^{\frac{1}{4}}\cos\frac{\theta}{2}\right)\cdot\exp-\left(i\frac{uL}{2D}\left(1+\frac{16D^2\omega^2}{u^4}\right)^{\frac{1}{4}}\sin\frac{\theta}{2}\right) \quad \textbf{4-7}$$

Equation 4-7 is now in the form of $A\exp(-i\Phi)$, where A is the amplitude ratio and Φ is the phase lag.

The experimentally determined system amplitude ratio A_n and system phase lag Φ_n are calculated from the following equations:

$$A_n = T\sqrt{a_n^2 + b_n^2} \quad \textbf{4-8}$$

$$\Phi_n = \arctan\left(\frac{a_n}{b_n}\right) \quad \textbf{4-9}$$

Plots of the experimentally determined system amplitude ratio and phase lag are shown in Appendix D.

Therefore from equation 4-7 the theoretical amplitude ratio and phase lag are given by:

$$A = \exp\left(\frac{uL}{2D} - \frac{uL}{2D}\left(1+\frac{16D^2\omega^2}{u^4}\right)^{\frac{1}{4}}\cos\frac{\theta}{2}\right) \quad \textbf{4-10}$$

$$\Phi = \frac{uL}{2D}\left(1+\frac{16D^2\omega^2}{u^4}\right)^{\frac{1}{4}}\sin\frac{\theta}{2} \quad \textbf{4-11}$$

By multiplying out both equations 4-10 and 4-11 and substituting for θ it is easy to show that

$$A = \exp\left(\frac{uL}{2D} - \left(\frac{u^4L^4}{16D^4} + \frac{\omega^2L^4}{D^2}\right)^{\frac{1}{4}}\cos\left(\frac{1}{2}\arctan\frac{4\omega D}{u^2}\right)\right) \quad \textbf{4-12}$$

and

$$\Phi = \left(\frac{u^4 L^4}{16 D^4} + \frac{\omega^2 L^4}{D^2} \right)^{\frac{1}{4}} \sin\left(\frac{1}{2} \arctan\left(\frac{4\omega D}{u^2} \right) \right) \qquad \textbf{4-13}$$

It is of value to obtain the flow model parameters D and u as functions of frequency, since this information is used to test the validity of the chosen model. By using a non-linear least squares fit algorithm it is possible to simultaneously fit equations 4-12 and 4-13 to the experimentally determined values of the amplitude ratio and phase lag to obtain the flow parameters D and u as functions of frequency. This procedure is used since the flow model parameters cannot be explicitly expressed in terms of frequency. It has been reported by Turner [13] that the log (natural log) of the amplitude ratio should be used, instead of the amplitude ratio, since the convergence is quicker. The non-linear least squares algorithm and the non-linear least squares fit program are presented in Appendix G.

The validity of the chosen model, the axially dispersed plug flow model, is tested by investigating how the parameters, the mean velocity (u) and the dispersion coefficient (D), vary with frequency. If the parameters show no variation with frequency, then the chosen model is an accurate representation of the flow characteristics in the analyser system. Shown below in Figures 4.3 and 4.4 are randomly selected plots of the mean velocity and dispersion coefficient vs. frequency for Runs A and B. For the sake of brevity, the results of only one experiment each from Runs A and B are shown below. Plots of the mean velocity and dispersion coefficient vs. frequency for all experimental runs are shown in Appendix H. The deductions obtained from these plots are presented below.

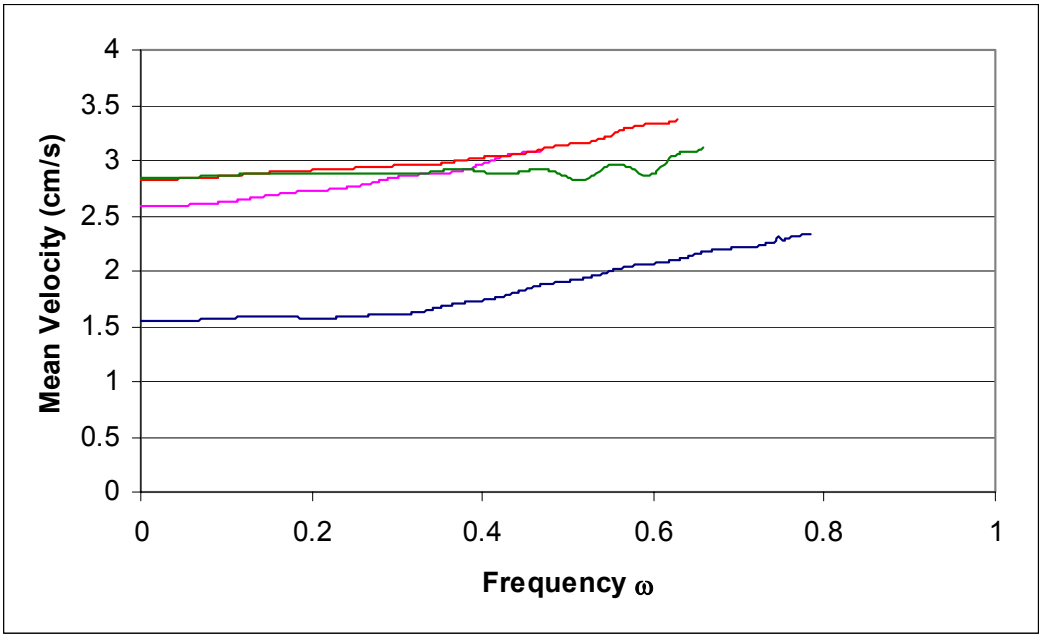

(a)

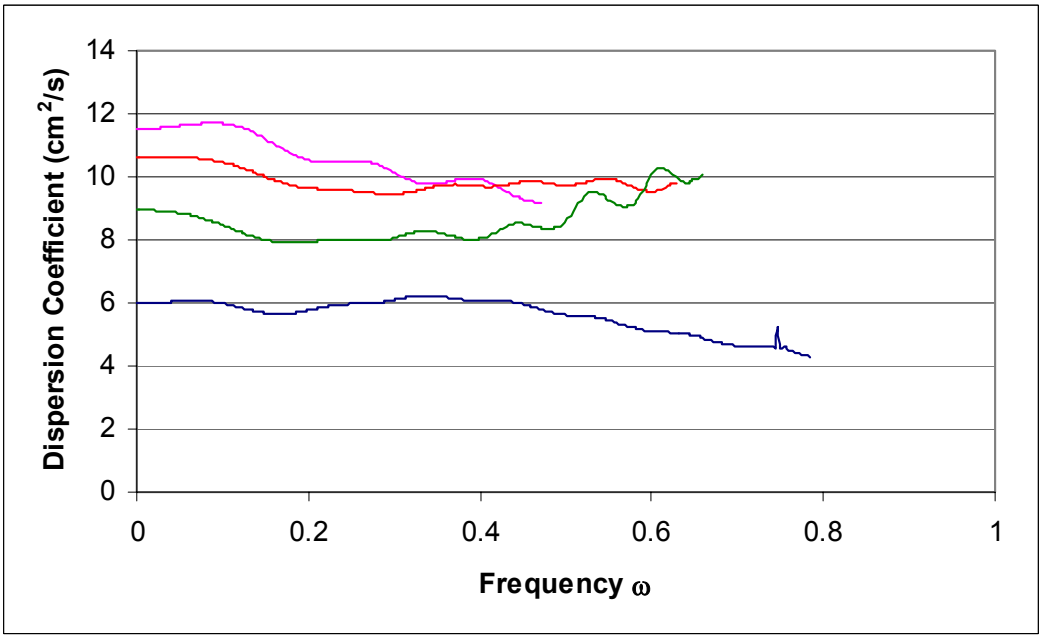

(b)

Figure 4.3: Plot of (a) mean velocity and (b) dispersion coefficient vs. frequency for Runs A. The flow rate was 0.5 ml/min. — 0.25 m, — 0.5 m, — 0.8 m and — 1m.

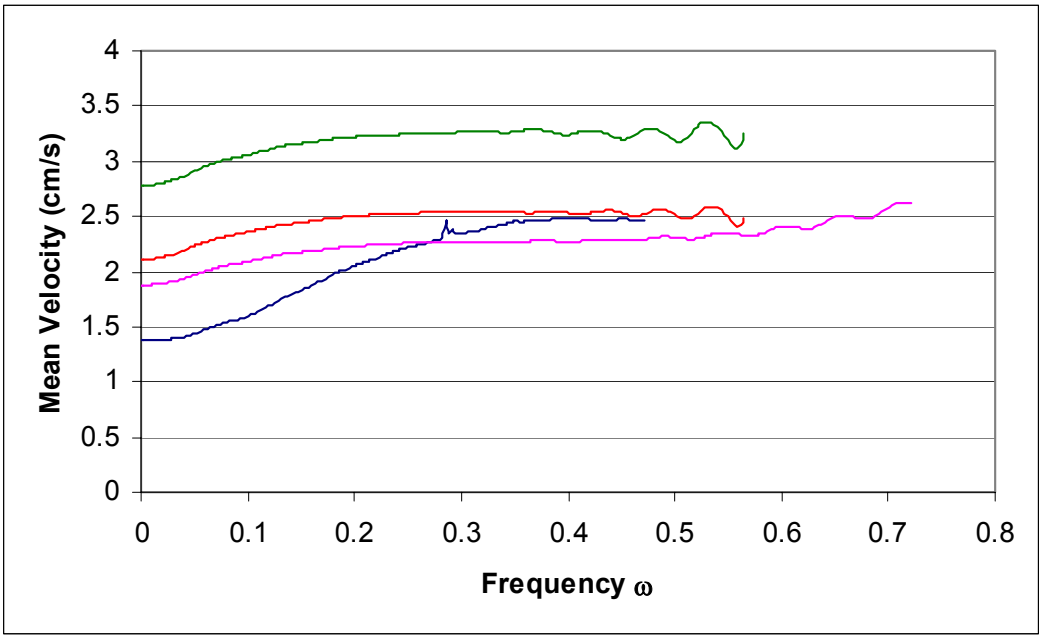

(a)

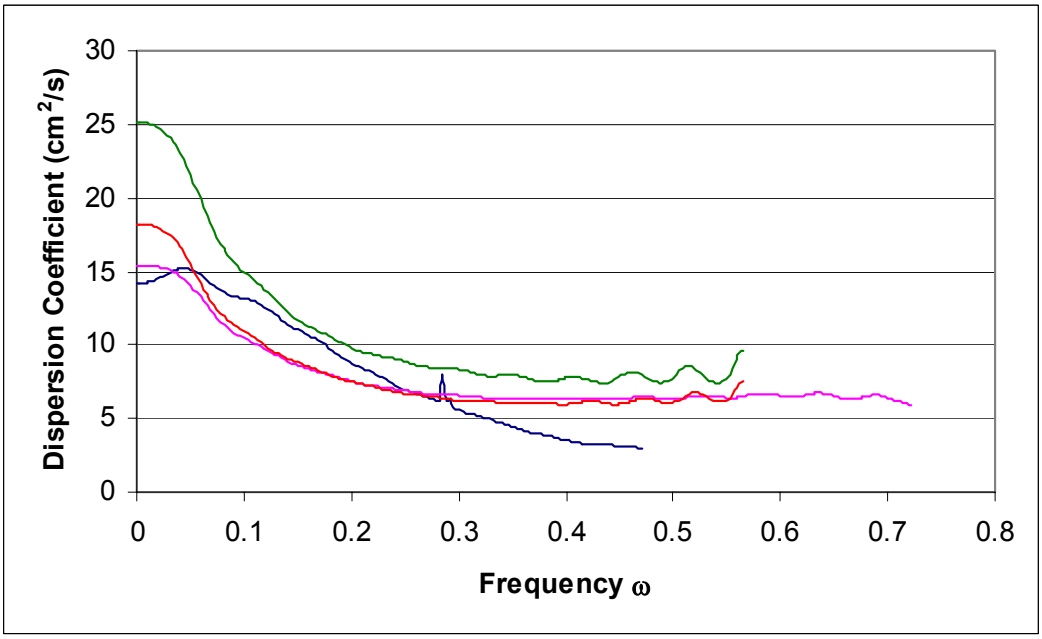

(b)

Figure 4.4: Plot of (a) mean velocity and (b) dispersion coefficient vs. frequency for Runs B. The flow rate was 0.5 ml/min. — 0.25 m, — 0.5 m, — 0.8 m and — 1m.

From Figures H.1 to H.10 (all shown in Appendix H), it is noted that for Run A0.25-2.0 and B0.25-2.0 both the parameters show the least variation with frequency. It may therefore be said that the axially dispersed plug flow model best fits the data For Runs A0.25-2.0 and B0.25-2.0. From the figures shown in Appendix H it appears that the axially dispersed plug flow model fits the data better when the flow rates are high and the length of tubing between the injection and detection points is short. The results from frequency analysis showed that for short tubing lengths and high flow rates, the flow pattern in the analyser system is closely approximated by plug flow. Therefore the axially dispersed plug flow model is a fair representation of the flow characteristics in the analyser system when the tracer dispersion is small.

5 CONCLUSIONS

From the experimental results shown in Section 3, it was concluded that the recorded signals were proportional to the tracer concentration up to about 75 mg/l.

By simply examining plots of the actual input and output detector readings vs. time on the same set of axes, it was observed that uniform dispersion of the injected sample occurred. Also by simply examining plots of the actual input and output detector readings, a very important factor regarding the different detector types became apparent. For Runs B, where the input detector was a flow by cell detector, and the output detector was a wall jet cell detector, the output signals had greater peak heights (and areas) than the corresponding input signals. This implied that the detector based on the wall jet cell design had a greater sensitivity than the detector based on the flow by design.

From the normalized input and output functions, the Fourier coefficients of the input and output signals were obtained. Using these coefficients it was possible to determine the coefficients of the experimental system response. Once the Fourier coefficients of the system response were determined, it was easy to obtain the system residence time distribution itself, the system amplitude ratio and system phase lag. The number of coefficients that were used in the Fourier series to calculate the system response was limited by the amplitude of noise in the system. The level of noise was easily determined by examining plots of the system amplitude ratio vs. frequency. In order to avoid the inclusion of noise in the system response, the Fourier series was truncated at the frequency where the signal dropped below the noise level. Truncation of the Fourier series at this point performed smoothing of the signal.

The effect of varying the length of tubing between the injection and detection points was obtained by comparing the system responses for cases where the flow rate was kept constant, but the length of tubing between the injection and detection points was varied. It was noted that

as the length of tubing between the injection and detection points increased, the system responses became broader and flatter. It was therefore concluded that the dispersion of injected sample increased as the length of tubing between the injection and detection points increased.

In a similar manner the effect of varying the flow rate on the injected sample was obtained. Plots of the system responses were compared for cases where the length of tubing was kept constant, but the flow rate was varied. From these plots it was evident that as the flow rate increased, the system responses became narrower and sharper, from which it was concluded that the dispersion of injected sample decreased as the flow rate increased.

The moments of the system residence time distribution were obtained from the experimental moments of the input and output signals. The system distribution variance σ^2 was found to vary linearly with the flow rate of carrier solution. It was also found that as the flow rate of carrier solution increased, the system distribution variance σ^2 decreased. This implied that the dispersion of sample decreased as the flow rate increased.

The results from moment analysis indicated that the system distribution variance σ^2 was independent of the length of tubing between the injection and detection points. This meant that the dispersion of sample was unaffected by the length of tubing between the injection and detection points. This finding from moment analysis was shown to be incorrect, using results obtained by examining the system responses and results obtained from frequency analysis.

The results obtained from frequency analysis were used to compare the extent of dispersion occurring under different conditions. This was achieved by comparing the system response amplitude ratios for various runs from which it was deduced that the dispersion of sample was dependent on both the flow rate of background electrolyte in the analyser system and the length of the tubing. To summarise, the results from frequency analysis indicated that the sample dispersion decreased as the

flow rate increased and tubing length between the injection and detection points decreased.

The results obtained from frequency analysis were also used to compare the extent of dispersion caused by the different detector cells themselves. This was achieved by comparing only the input signal amplitude ratios for Runs A and B for cases when the flow rates were the same. It was discovered from these comparisons that the detector cell based on the wall jet design caused less dispersion of sample than the flow by cell design, however the difference was small.

The model chosen to represent the flow pattern within the analyser system was the axially dispersed plug flow model. Very simple expressions for the theoretical mean residence time and system distribution variance were obtained from the system transfer function. The theoretical functions of the mean residence time and system distribution variance obtained from moment analysis of the dispersion model showed that the mean residence time and system distribution variance are linearly related to the length of tubing between the injection and detection points. However most of the plots of the experimentally determined system mean residence time τ vs. tubing length were not linear. Linearity was only observed for cases when the flow rates were greater than 1.5 ml/min for both Runs A and B. Plots of the experimentally determined system distribution variance σ^2 vs. tubing length for both Runs A and B did not show a linear relation with respect to tubing length. These plots showed that the system distribution variance σ^2 was independent of tubing length for all flow rates tested for both Runs A and B.

In evaluating the validity of the dispersion model, using frequency analysis and a non-linear least squares fit, it was revealed that the dispersion model best fitted data for Runs A0.25-2.0 and B0.25-2.0. Overall the parameters u and D showed variation with frequency, the variation reduced as the flow rate increased and tubing length decreased. In general the parameter D showed more variation with frequency than the

parameter u. It was concluded that the axially dispersed plug flow model fitted the data better at high flow rates and short tubing lengths. This means that the dispersion model is a fair representation of the flow characteristics in the analyser system when the tracer dispersion is small or when the flow is close to plug flow. It is not surprising that the dispersion model did not accurately represent the flow characteristics of the analyser systems. The deviation from the dispersed plug flow model could be attributed to the entrance and exit effects caused by the flow channels and electrodes of the detectors. Other models like the gamma distribution model; also known as the tanks in series model, could be evaluated for the purpose of describing the tracer dispersion in the analyser system.

Finally it may be recommended that high flow rates and short tubing lengths should be used in the Sasol analyser. High flow rates and short tubing lengths are recommended, since the findings from this study indicated that the tracer dispersion is small for these conditions. High flow rates and short tubing lengths also imply that the analysis time would be shorter. Also integration of sharp signals is more accurate than the integration of signals with long tails. However very high flow rates should be avoided, since very high flow rates could result in overpressure, causing electrodes to disengage from the cell block. Furthermore very high flow rates should be avoided since reagent consumption would increase.

6 REFERENCES AND BIBLIOGRAPHY

[1] C.B. Ranger in *Automated Stream Analysis For Process Control*, Vol. 1, edited by D.P. Manka, Academic Press, New York, 1982

[2] J. Růžička and E.H. Hansen, Flow injection analysis Part X. Theory, techniques and trends, *Analytica Chimica Acta*, vol. 99, 1978, pp. 37 – 76.

[3] J. Růžička and E.H. Hansen, Flow injection analysis Part IX. A new approach to continuous flow titrations, *Analytica Chimica Acta*, vol. 92, 1978, pp. 235 – 249.

[4] J. Růžička and E.H. Hansen, Flow injection analysis. Principles, applications and trends, *Analytica Chimica Acta*, vol. 114, 1980, pp. 19 – 44.

[5] K. Fukamachi and N.Ishibashi, Flow injection-atomic absorption spectrometry with organic solvents, *Analytica Chimica Acta*, vol. 119, 1980, pp. 383 – 387.

[6] C.B. Ranger, Flow injection analysis, *Analytical Chemistry*, vol. 53, 1981, pp. 20A – 32 A.

[7] J.F. Tyson and A.B. Idris, Flow injection sample introduction for atomic-absorption spectrometry: Applications of a simplified model for dispersion, *Analyst*, vol. 106, 1981, pp. 1125 – 1129.

[8] O. Åström, Flow injection analysis for the determination of bismuth by atomic absorption spectrometry with hydride generation, *Analytical Chemistry*, vol. 54, 1982, pp. 190 – 193.

[9] J. Růžička and E.H. Hansen, Recent developments in flow injection analysis: Gradient techniques and hydrodynamic injection, *Analytica Chimica Acta*, vol. 145, 1983, pp. 1 – 15.

[10] J.F. Tyson, Flow injection analysis techniques for atomic-absorption spectrometry, *Analyst*, vol. 110, 1985, pp. 419 – 429.

[11] T. Korenaga, Aspects of sample dispersion for optimising flow-injection analysis systems, *Analytica Chimica Acta*, vol. 261, 1992, pp. 539 – 548.

[12] L.G. Gibilaro, M.O. Stevens and S.P. Waldram, Evaluation of system moments from frequency response data, *Chemical Engineering Science*, vol. 33, 1978, pp. 1394 – 1396.

[13] G.M.S. Turner, *M.Sc. Thesis*, University of the Witwatersrand, Johannesburg, 1974

[14] P.A. Ramachandran and J.M. Smith, Transport rates by moment analysis of dynamic data, *Industrial And Engineering Chemistry Fundamentals*, vol. 17, no.3, 1978, pp. 148 – 160.

[15] C.Y. Wen and L.T. Fan, *Models For Flow Systems And Chemical Reactors*, Marcel Dekker Inc, New York, 1975

[16] M.A. Greenberg, *M.Sc. Thesis*, University of the Witwatersrand, Johannesburg, 1969

[17] S.K. Gangwal, R.R. Hudgins, A.W. Bryson and P.L. Silveston, Interpretation of chromatographic peaks by Fourier analysis, *The Canadian Journal Of Chemical Engineering*, vol. 49, 1971, pp. 113 – 119.

[18] S.D. Kolev and E. Pungor, Numerical solution of hydraulic models based on the axially-dispersed plug flow model by Laplace transforms, *Analytica Chimica Acta*, vol. 194, 1987, pp. 61 – 75.

[19] I.C. van Nugteren-Osinga, M. Bos and W.E. van der Linden, Impulse/response functions of individual components of flow-injection manifolds, *Analytica Chimica Acta*, vol. 214, 1988, pp. 77 – 86.

[20] S.H. Brooks and J.G. Dorsey, Moment analysis for evaluation of flow-injection manifolds, *Analytica Chimica Acta*, vol. 229, 1990, pp. 35 – 46.

[21] I.C. Van Nugteren-Osinga, E. Hoogendam, M. Bos and W.E. van der Linden, Impulse-response functions of several detectors used in flow-injection analysis, *Analytica Chimica Acta*, vol. 239, 1990, pp. 245 – 255.

[22] E.B. van Akker, M. Bos and W.E. van der Linden, Convection and diffusion in a micro-flow injection system, *Analytica Chimica Acta*, vol. 373, 1998, pp. 227 – 239.

[23] A.W. Bryson, Non-ideal flow models and pulse testing, Lecture notes, University of the Witwatersrand, Johannesburg

[24] A.W. Bryson, Test on the diffusion model for two-phase flow in a packed bed, *Reactor Journal Of Chemical Engineering*, vol. 2, 1963, pp. 9 – 11.

[25] J.H.M. Van Den Berg, R.S. Deelder and H.G.M. Egberink, Dispersion phenomena in reactors for flow analysis, *Analytica Chimica Acta*, vol. 114, 1980, pp. 91 – 104.

[26] S.D. Kolev, Solution of mathematical models of flow systems used in analytical chemistry and process analysis in the case of slug and time injection, *Analytica Chimica Acta*, vol. 229, 1990, pp. 183 – 189.

[27] S.D. Kolev, Mathematical modelling of flow-injection systems, *Analytica Chimica Acta*, vol. 308, 1995, pp. 36 – 66.

[28] E.B. Nauman, Continuous mixing, *Chemical Engineering Communications*, vol. 8, 1981, pp. 53 – 131.

[29] O. Levenspiel and W.K. Smith, Notes on the diffusion-type model for the longitudinal mixing of fluids in flow, *Chemical Engineering Science*, vol. 6, 1957, pp. 227 – 233.

[30] K.B. Bischoff and O. Levenspiel, Patterns of flow in chemical process vessels, *Advances In Chemical Engineering*, vol. 4, 1963, pp. 95 – 198.

[31] M.L. Michelsen and K. Østergaard, The use of residence time distribution data for estimation of parameters in the axial dispersion model, *Chemical Engineering Science*, vol. 25, 1970, pp. 583 – 592.

[32] M.L. Michelsen and K. Østergaard, On the use of the imperfect tracer pulse method for determination of hold-up and axial mixing, *The Canadian Journal Of Chemical Engineering*, vol. 47, 1969, pp. 107 – 112.

[33] K.B. Bischoff, Notes on the diffusion-type model for the longitudinal mixing of fluids in flow (Concerning papers by O. Levenspiel, W.K. Smith, E. van der Laan and R. Aris), *Chemical Engineering Science*, vol. 12, 1960, pp. 69 – 70.

[34] K.B. Bischoff and O. Levenspiel, Fluid dispersion-generalization and comparison of mathematical models – I Generalization of models, *Chemical Engineering Science*, vol. 17, 1962, pp. 245 – 255.

[35] O. Levenspiel, *Chemical Reaction Engineering*, 2nd edition, Wiley and Sons, New York, 1972

[36] K.H. Radeke, Discussing an idea negative order moments*, Chemical Engineering Science*, vol. 34, 1979, pp. 1347-1348.

[37] E.T. van der Laan, Notes on the diffusion-type model for the longitudinal mixing of fluids in flow (O. Levenspiel and W.K. Smith), *Chemical Engineering Science*, vol. 7, 1958, pp. 187 – 191.

[38] R. Aris, Notes on the diffusion-type model for the longitudinal mixing of fluids in flow (Levenspiel, Smith and van der Laan), *Chemical Engineering Science*, vol. 9, 1959, pp 266-267.

[39] K.B. Bischoff, The general use of imperfect pulse inputs to find characteristics of flow systems, *The Canadian Journal Of Chemical Engineering*, vol. 41, 1963, pp. 129.

[40] E. Kreyszig, *Advanced Engineering Mathematics*, 2nd edition, Wiley and Sons, New York, 1967

[41] O. Levenspiel, *Chemical Reaction Engineering*, 3rd edition, Wiley and Sons, New York, 1998

[42] A. Constantinides and N. Moustoufi, *Numerical Methods For Chemical Engineers with MATLAB Applications*, Prentice Hall, New Jersey, 1999

[43] P.V. Danckwerts, Continuous flow systems Distribution of residence times, *Chemical Engineering Science*, vol. 2, no.1, 1953, pp. 1 – 13.

[44] H. Kramers and G. Alberda, Frequency response analysis of continuous flow systems, *Chemical Engineering Science*, vol. 2, 1953, pp. 173 – 181.

[45] G.I. Taylor, Dispersion of soluble matter in solvent flowing slowly through a tube, *Proceedings Of Royal Society*, vol.A219, 1953, pp. 186 – 203.

[46] G.I. Taylor, The dispersion of matter in turbulent flow through a pipe, *Proceedings Of Royal Society*, vol. A223, 1954, pp. 446 – 468.

[47] J.F. Wehner and R.H. Wilhelm, Boundary conditions of flow reactor, *Chemical Engineering Science*, vol. 6, 1956, pp. 89 – 93.

[48] L.A. Barnstone and P. Harriot, Frequency response of gas mixing in a fluidized-bed reactor, *AIChE Journal*, vol. 13, no. 3, 1967, pp.465 – 475.

[49] L.G. Gibilaro, On the residence time distribution for systems with open boundaries, *Chemical Engineering Science*, vol. 33, 1978, pp. 487 – 492.

[50] A. Kreft and A. Zuber, On the physical meaning of the dispersion equation and its solutions for different initial and boundary conditions, *Chemical Engineering Science*, vol. 33, 1978, pp. 1471 – 1480.

[51] J.T. Hsu and J.S. Dranoff, On initial condition problems for reactor dispersion model, *Chemical Engineering Science*, vol. 41, no. 7, 1986, pp. 1930 – 1934.

A APPENDIX A - THEORY

A.1 Residence time distribution function $\mathbf{E}(t)$

Consider a continuous flow system, which is at steady state. Assume that a fluid, which does not undergo any reaction and with constant density flows through the system as illustrated below. Fluid elements enter the system, remain within the system for some period (referred to as ageing) and eventually leave the system. According to Bryson [23], a fluid element has a volume much smaller than the system but still large enough to contain sufficient molecules so that properties such as density and concentration can be defined.

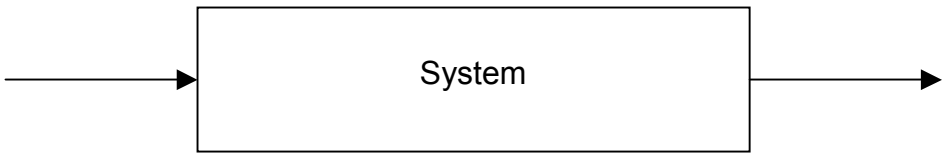

Figure A.1: Continuous flow system.

The residence time of a fluid element is defined as the time an element spends within the system. Fluid elements do not follow the same path or route through the system; therefore these fluid elements will spend different amounts of time within the system and will leave the system at different times. As a result a distribution of residence times occurs. The mathematical function describing this distribution is called the residence time distribution function denoted by $\mathbf{E}(t)$.

It is convenient to represent the residence time distribution in a manner such that the area under the curve is equal to one. This statement represented mathematically is:

$$\int_0^\infty \mathbf{E}(t)\,dt = 1 \qquad \text{A-1}$$

The fraction of fluid that spent time less than t_1 in the system is:

$$\int_0^{t_1} \mathbf{E}(t)\, dt \qquad \textbf{A-2}$$

and the fraction of fluid that spent time between t and $t + dt$ is:

$$\mathbf{E}(t)\, dt \qquad \textbf{A-3}$$

It is obvious that the fraction of fluid that spent time longer than t_1 in the system is:

$$\int_{t_1}^{\infty} \mathbf{E}(t)\, dt \qquad \textbf{A-4}$$

Knowledge of the residence time distribution of the fluid flowing through a system can be used to describe the type of flow occurring within that system.

Experimentally the residence time distribution is determined by techniques termed stimulus – response techniques. In these techniques the stimulus is a tracer input and the response is a time record of the tracer leaving the system. According to Bryson [23] and Levenspiel [35] a tracer is any material that has very similar properties to the fluid material flowing through the system, must be non reactive, must not be adsorbed by the surfaces within the system, must be detectable at low concentrations and must not disrupt the flow pattern. There should be a linear relationship between the tracer concentration and the recorded signal. The tracer input signal can be a pulse input, step input, periodic input or even a random input signal. The input signal chosen for this work was the pulse input. The output signal and the corresponding system response signal are also pulse shaped. The pulse input was chosen, since no complicated apparatus is required to achieve this input signal, the time required for pulse input testing is shorter than that of sinusoidal input testing and furthermore the same amount of information that can be

obtained from a whole range of sinusoidal input testing, is obtained from one pulse input test [13, 15]. By injecting a pulse, the system is excited with all frequencies at the same time [13, 15].

A.2 Characterization of E(t) by moment analysis

A.2.1 Definition of moments

The n^{th} moment (α_n) about the origin of the $\mathbf{E}(t)$ curve is defined by the following equation:

$$\alpha_n = \int_0^\infty t^n \mathbf{E}(t)\, dt \qquad \textbf{A-5}$$

where n = 0, 1, 2 … . Radeke [36] has defined non-integer and negative moments using equation A-5; however these non-integer and negative moments are infrequently used. The zeroth moment about the origin is equal to one and the first moment about the origin is called the mean or mean residence time, denoted by τ. The n^{th} moment about the mean, which is also called a cumulant [12, 28], is defined by the following equation:

$$\alpha_n' = \int_0^\infty (t-\tau)^n \mathbf{E}(t)\, dt \qquad \textbf{A-6}$$

Cumulants that are frequently used are the second and third cumulants. The second cumulant is called the variance of the distribution, denoted by σ^2, whilst the third cumulant is called the skewness. The second cumulant can also be expressed by the following equation:

$$\alpha_2' = \alpha_2 - \alpha_1^{\,2} = \alpha_2 - \tau^2 = \sigma^2 \qquad \textbf{A-7}$$

A.2.2 Moments and cumulants from the transfer function

The Laplace transform of a function *f(t)* is defined as:

$$\bar{\mathbf{f}}(s) = \int_0^\infty e^{-st} f(t)\, dt \qquad \textbf{A-8}$$

where s is the transform variable.

Using equation A-8, the Laplace transform of $\mathbf{E}(t)$ is:

$$\bar{\mathbf{E}}(s) = \int_0^\infty e^{-st} \mathbf{E}(t)\, dt \qquad \textbf{A-9}$$

$\bar{\mathbf{E}}(s)$ is also called the system transfer function.

The exponential term in equation A-9 can be expressed using the following expansion:

$$e^{-st} = 1 - st + \frac{s^2 t^2}{2!} - \frac{s^3 t^3}{3!} + \ldots \qquad \textbf{A-10}$$

Substituting equation A-10 into equation A-9 results in the following:

$$\bar{\mathbf{E}}(s) = \alpha_0 - \alpha_1 s + \alpha_2 \frac{s^2}{2} - \alpha_3 \frac{s^3}{6} + \ldots \qquad \textbf{A-11}$$

The moments can be obtained from equation A-11 above or by differentiating and evaluating the differential as the limit of s tends to zero, as shown below in equation A-12.

$$\alpha_n = (-1)^n \lim_{s \to 0} \frac{d^n \bar{\mathbf{E}}(s)}{ds^n} \qquad \textbf{A-12}$$

The cumulants can be obtained by taking the natural logarithm of equation A-11. The cumulants are the coefficients of s, shown in the equation below.

$$\ln \bar{\mathbf{E}}(s) = \ln \alpha_0 - \alpha_1' s + \alpha_2' \frac{s^2}{2} - \alpha_3' \frac{s^3}{6} + \ldots \qquad \textbf{A-13}$$

Analogously, differentiating $\ln \bar{\mathbf{E}}(s)$ and evaluating the differential, as the limit of s tends to zero gives the cumulants of the function.

$$\alpha_n' = (-1)^n \lim_{s \to 0} \frac{d^n \ln \bar{\mathbf{E}}(s)}{ds^n} \qquad \textbf{A-14}$$

A.2.3 Input - Output relation

It has been stated above (see Section A.1) that the residence time distribution of a flow system can be determined by means of stimulus – response techniques. In early reported work on stimulus – response techniques [29, 37]; it was assumed that the stimulus was a perfect pulse or a dirac delta function. The dirac delta function is a mathematical idealization, and injection of tracer as a perfect pulse can never be achieved experimentally. The theory by Aris [38], which was later extended by Bischoff [33] and Bischoff and Levenspiel [34], showed that by measuring the tracer concentration at two points, it was not necessary to inject the tracer as a perfect pulse. The tracer should be injected upstream of the test section or flow system and the first measuring point should also be located upstream of the test section. The second measuring point may be located either downstream of the test section or within the test section [34, 30]. This method is referred to as the imperfect pulse method. The points mentioned above are illustrated below.

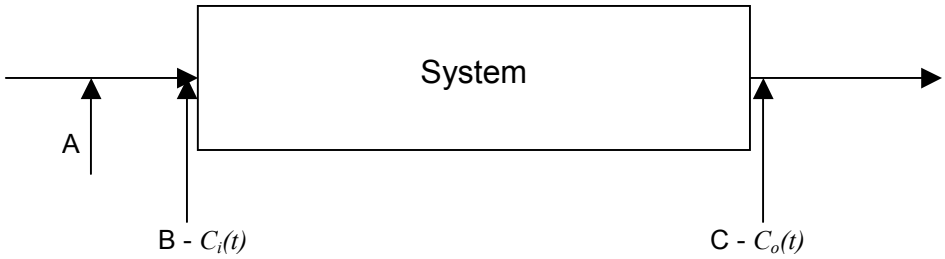

Figure A.2: A continuous flow system. A – tracer input location, B – input signal measuring point and C – output signal measuring point.

In the figure above $C_i(t)$ is defined as the tracer inlet or input concentration, and $C_o(t)$ is defined as the tracer outlet or output concentration. Also $\theta_i(t)$ is defined as the input function, $\mathbf{E}(t)$ is the system residence time distribution and $\theta_o(t)$ is defined as the output function. The functions $\theta_i(t)$ and $\theta_o(t)$ are normalized concentration functions. These normalized functions are obtained using the following equations.

$$\theta_i(t) = \frac{C_i(t)}{\int_0^\infty C_i(t)dt} \qquad \textbf{A-15}$$

$$\theta_o(t) = \frac{C_o(t)}{\int_0^\infty C_o(t)dt} \qquad \textbf{A-16}$$

Using equation A-8, $\bar{\theta}_i(s)$ is the Laplace transform of $\theta_i(t)$ and $\bar{\theta}_o(s)$ is the Laplace transform of $\theta_o(t)$. Analogous relations to equation A-12 can be defined for the input and output functions. These relations are shown below.

$$\alpha_{ni} = (-1)^n \lim_{s\to 0} \frac{d^n \bar{\theta}_i(s)}{ds^n} \qquad \textbf{A-17}$$

$$\alpha_{no} = (-1)^n \lim_{s\to 0} \frac{d^n \bar{\theta}_o(s)}{ds^n} \qquad \textbf{A-18}$$

where α_{ni} and α_{no} are the n^{th} moments for the input and output functions respectively.

Bischoff [39] showed that the system transfer function $\bar{\mathbf{E}}(s)$ is related to $\bar{\theta}_i(s)$ and $\bar{\theta}_o(s)$ by the following equation:

$$\frac{\bar{\theta}_o(s)}{\bar{\theta}_i(s)} = \bar{\mathbf{E}}(s) \qquad \textbf{A-19}$$

Equation A-19 can be rearranged to give:

$$\bar{\theta}_o(s) = \bar{\theta}_i(s)\,\bar{\mathbf{E}}(s) \qquad \textbf{A-20}$$

Taking the derivative of equation A-20, and also evaluating the limit as s tends to zero, results in the following:

$$\lim_{s\to 0}\frac{d\,\bar{\theta}_o(s)}{ds} = \lim_{s\to 0}\left[\bar{\theta}_i(s)\frac{d\,\bar{\mathbf{E}}(s)}{ds} + \bar{\mathbf{E}}(s)\frac{d\,\bar{\theta}_i(s)}{ds}\right] \qquad \textbf{A-21}$$

Using equations A-12, A-17 and A-18 gives the desired result, shown below.

$$-\alpha_{1o} = -\alpha_1 - \alpha_{1i} \qquad \textbf{A-22}$$

or by rearranging

$$\tau = \tau_o - \tau_i \qquad \textbf{A-23}$$

where τ, τ_i and τ_o are the system, input function and output function mean residence times respectively.

Similarly taking the second derivative of equation A-20, evaluating the limit as s tends to zero and using equations A-12, A-15 and A-16 gives:

$$\sigma^2 = \sigma_o^2 - \sigma_i^2 \qquad \textbf{A-24}$$

where σ^2, σ_i^2 and σ_o^2 are the system, input function and output function distribution variances respectively.

Therefore the system mean residence time and distribution variance are obtained from the input and output function moments and cumulants using equations A-23 and A-24. The moments and cumulants of the input and output functions are obtained from equations, which are similar to equations A-5 and A-6. These equations are shown below.

$$\alpha_{ni} = \int_0^\infty t^n \theta_i(t)\, dt \qquad \textbf{A-25}$$

$$\alpha'_{ni} = \int_0^\infty (t - \tau_i)^n \theta_i(t)\, dt \qquad \textbf{A-26}$$

$$\alpha_{no} = \int_0^\infty t^n \theta_o(t)\, dt \qquad \textbf{A-27}$$

$$\alpha'_{no} = \int_0^\infty (t - \tau_i)^n \theta_o(t)\, dt \qquad \textbf{A-28}$$

A.3 Characterization of E(t) by frequency analysis

A.3.1 Fourier series representation

Suppose any arbitrary function, $f(x)$, is a periodic function of period 2π. This arbitrary function can be represented by a trigonometric series of the form:

$$f(x) = \sum_{n=0}^{\infty} (a_n \sin nx + b_n \cos nx) \qquad \textbf{A-29}$$

This trigonometric series is also referred to as a Fourier series. The coefficients a_n and b_n in equation A-29 are called Fourier coefficients, and these coefficients are obtained from Euler's formulae shown below.

$$a_n = \frac{1}{\pi}\int_0^{2\pi} f(x)\sin nx\,dx \qquad \textbf{A-30}$$

$$b_n = \frac{1}{\pi}\int_0^{2\pi} f(x)\cos nx\,dx \qquad \textbf{A-31}$$

$$b_0 = \frac{1}{2\pi}\int_0^{2\pi} f(x)\,dx \qquad \textbf{A-32}$$

However there are many functions that have arbitrary period, periods other than 2π. For a function *f(t)*, with period $2T$, it can be shown (see Appendix B and Kreyszig [40]) that this function can be represented by a Fourier series of the form:

$$f(t) = \sum_{n=0}^{\infty}\left(a_n \sin\omega t + b_n \cos\omega t\right) \qquad \textbf{A-33}$$

where $\omega = \frac{n\pi}{T}$ is the frequency.

The coefficients a_n and b_n in equation A-33 above are obtained from Euler formulae, which have the following form:

$$a_n = \frac{1}{T}\int_0^{2T} f(t)\sin\omega t\,dt \qquad \textbf{A-34}$$

$$b_n = \frac{1}{T}\int_0^{2T} f(t)\cos\omega t\,dt \qquad \textbf{A-35}$$

$$b_0 = \frac{1}{2T}\int_0^{2T} f(t)\,dt \qquad \textbf{A-36}$$

The amplitude ratio, A_n, and the phase lag, Φ_n, are defined by the following equations:

$$A_n = T\sqrt{a_n^2 + b_n^2} \qquad \textbf{A-37}$$

$$\Phi_n = \arctan(\frac{a_n}{b_n}) \qquad \textbf{A-38}$$

In order for an arbitrary function to be represented as a Fourier series, certain conditions must be fulfilled [13, 16]. These conditions are:

- *f(t)* is defined at every point in the chosen interval
- *f(t)* is a single valued function, finite and sectionally continuous
- *f(t)* must not have an infinite number of minima and maxima in the chosen interval.

These conditions are referred to as the Dirichlet conditions [13, 16].

A.3.2 Input - Output relation

It was stated above (see Section A.2.3) that $C_i(t)$ is the tracer input concentration, and $\theta_i(t)$ is the input function. $C_o(t)$ is the output tracer concentration and $\theta_o(t)$ the output function. The input function, $\theta_i(t)$, can be represented by a Fourier series of the form:

$$\theta_i(t) = \sum_{n=0}^{\infty} \left(p_n \sin \omega t + q_n \cos \omega t\right) \qquad \textbf{A-39}$$

Similarly the output function and the system residence time distribution function can also be represented by Fourier series of the forms:

$$\theta_o(t) = \sum_{n=0}^{\infty} \left(u_n \sin \omega t + v_n \cos \omega t\right) \qquad \textbf{A-40}$$

and

$$\mathbf{E}(t) = \sum_{n=0}^{\infty} \left(a_n \sin \omega t + b_n \cos \omega t\right) \qquad \textbf{A-41}$$

The coefficients in equations A-39 and A-40 are obtained using the equations shown below.

$$p_n = \frac{1}{T}\int_0^{2T} \theta_i(t)\sin\omega t\ dt \qquad \textbf{A-42}$$

$$q_n = \frac{1}{T}\int_0^{2T} \theta_i(t)\cos\omega t\ dt \qquad \textbf{A-43}$$

$$q_0 = \frac{1}{2T}\int_0^{2T} \theta_i(t)\ dt \qquad \textbf{A-44}$$

$$u_n = \frac{1}{T}\int_0^{2T} \theta_o(t)\sin\omega t\ dt \qquad \textbf{A-45}$$

$$v_n = \frac{1}{T}\int_0^{2T} \theta_o(t)\cos\omega t\ dt \qquad \textbf{A-46}$$

$$v_0 = \frac{1}{2T}\int_0^{2T} \theta_o(t)\ dt \qquad \textbf{A-47}$$

These integrals are evaluated by using a suitable numerical integration technique. Once again, the technique employed was Simpson's rule.

The functions $\theta_i(t)$, $\theta_o(t)$ and $\mathbf{E}(t)$ are transformed into the frequency domain using the transform shown in [13, 23]. The transformed functions are shown below.

$$\theta_i(i\omega) = Tq_n - iTp_n \qquad \textbf{A-48}$$

$$\theta_o(i\omega) = Tv_n - iTu_n \qquad \textbf{A-49}$$

and

$$\mathbf{E}(i\omega) = Tb_n - iTa_n \qquad \textbf{A-50}$$

The relation between the system transfer function and the Laplace transform of the input and output functions shown in equation A-19, can also be expressed as:

$$\frac{\theta_o(i\omega)}{\theta_i(i\omega)} = \mathbf{E}(i\omega) \qquad \textbf{A-51}$$

Substitution of equations A-48, A-49 and A-50 into equation A-51 leads to:

$$Tb_n - iTa_n = \frac{Tv_n - iTu_n}{Tq_n - iTp_n} \qquad \textbf{A-52}$$

By equating real and imaginary parts, the coefficients a_n and b_n are obtained from the following relations:

$$a_n = \frac{q_n u_n - p_n v_v}{T\left(q_n^2 + p_n^2\right)} \qquad \textbf{A-53}$$

$$b_n = \frac{q_n v_n - p_n u_v}{T\left(q_n^2 + p_n^2\right)} \qquad \textbf{A-54}$$

The real time system response or the experimentally determined system response is obtained by substituting the values of a_n and b_n obtained from equations A-53 and A-54 into equation A-41 and evaluating this equation over the duration of the experiment. The experimental system amplitude ratio and phase lag are obtained by substituting the values of a_n and b_n obtained from equations A-53 and A-54 into equations A-37 and A-38. Appendix C contains a program that was used to determine the system amplitude ratio, phase lag and response from the input and output functions.

Questions which may arise at this point are, what the value of T is, how should the value of T be chosen and how many coefficients should be evaluated. According to Turner [13], T is an arbitrary constant, and thus the choice of T is not critical. However T should be chosen large enough to

define an adequate frequency range. Bryson [23] suggests that a value of T that is suitable can be calculated from the following expression:

$$T = 2\left(\tau + \frac{\sigma^2}{\tau}\right) \qquad \textbf{A-55}$$

Greenberg [16] states that the flow model parameters are independent of T so long as the value of T is chosen such that the tail region of the (output) peak is included. Gangwal *et al.* [17] state that the value of T should be at least two to five times the apparent time the peak tail vanishes. In general, the value of T should be large so that a suitable frequency range is defined. The value of T chosen in this work was 10 000 (seconds). The number of coefficients to evaluate depends on the amplitude of the noise in the frequency spectrum. As the frequency (or number of coefficients) increases, the amplitude of the signal (input, output or system) drops below the amplitude of the noise. This is clearly evident from a plot of the logarithm of the signal amplitude ratio against frequency as shown in Figure A.3 below. The Fourier series should be truncated at this point, as this performs smoothing of the data [13]. The number of data points, up to a specific frequency, for both the amplitude ratio and phase lag curves is influenced by the value of T. A large value of T gives a large number of data points for these curves. This is required in order to obtain reliable estimates of D and u as functions of frequency as explained in Appendix G. A value of T = 10 000 (seconds) was found to be adequate for the present study.

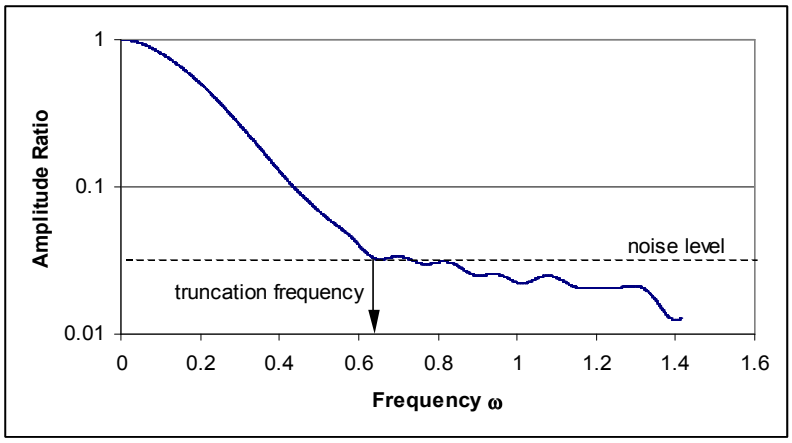

Figure A.3: Plot of amplitude ratio vs. frequency.

A.4 The dispersion model

The general mathematical form of the dispersion model is given by [15, 28, 30].

$$\frac{\partial C(t)}{\partial t} = \nabla \cdot (D \nabla C(t)) - u \cdot \nabla C(t) + \zeta(C(t)) \qquad \textbf{A-56}$$

where u is the mean velocity

$C(t)$ is the concentration

t is time

$\zeta(C(t))$ is the reaction rate or source term

For an isothermal system, with a constant fluid density, no reaction, no flow rate changes and fluid flowing in a cylindrical system, equation A-56 reduces to:

$$\frac{\partial C(t)}{\partial t} = D_z \frac{\partial^2 C(t)}{\partial z^2} + D_r \left(\frac{\partial^2 C(t)}{\partial r^2} + \frac{1}{r} \frac{\partial C(t)}{\partial r} \right) - u \frac{\partial C(t)}{\partial z} \qquad \textbf{A-57}$$

where z and r are the axial and radial directions respectively

D_z and D_r are the axial dispersion coefficient and radial dispersion coefficient respectively.

For the system investigated the tubing situated between the injection and detection point had an inner diameter much smaller than the length of the tubing. As a result the radial dispersion can be neglected in comparison to the axial dispersion [15, 30]. Using this fact equation A-57 simplifies to:

$$\frac{\partial C(t)}{\partial t} = D_z \frac{\partial^2 C(t)}{\partial z^2} - u \frac{\partial C(t)}{\partial z} \qquad \textbf{A-58}$$

Levenspiel and Smith [29] solved the axially dispersed plug flow model shown above in equation A-58, using the “infinite pipe” conditions for a pulse injection. Using these conditions it is assumed that the changes in

flow at the entrance and exit of the system are negligible. This means that the dispersion at the entrance, exit and within the system are the same. The solution to equation A-58, using the "infinite pipe" conditions for a pulse input is given below [28, 29, 30]. The axial dispersion coefficient D_z will now be denoted by D.

$$\mathrm{C}'(t) = \frac{L}{2\sqrt{\pi D t}} e^{-\frac{(L-ut)^2}{4Dt}} \qquad \textbf{A-59}$$

where L is the length of the tubing situated between the injection and detection points.

Equation A-59 is presented in terms of a dimensionless concentration, $\mathrm{C}'(t)$, which is $C(t)/C'_{ave}(t)$. According to Levenspiel and Bischoff [30] $C'_{ave}(t)$ is defined as "the concentration of injected tracer if evenly distributed throughout the vessel." $\mathrm{C}'(t)$ in equation A-59 is actually the residence time distribution function $\mathbf{E}(t)$ [28, 41]. Therefore the left hand side of equation A-59 can be replaced by $\mathbf{E}(t)$.

As mentioned in Section A.2.3 above, a perfect pulse can never be achieved experimentally. Aris [38] developed a theory, which was later extended by Bischoff [33] and Bischoff and Levenspiel [34] that allowed for the injection of a non-ideal pulse. This method was referred to as the imperfect pulse method. The transfer function of the axial dispersion model using the imperfect pulse method is given by the following equation [31, 32]:

$$\bar{\mathbf{E}}(s) = \exp\left(\frac{uL}{2D}\left(1 - \sqrt{1 + \frac{4sD}{u^2}}\right)\right) \qquad \textbf{A-60}$$

B APPENDIX B – MODIFIED FOURIER SERIES

Suppose $f(t)$ is a function with period $2T$. A variable called x is introduced such that $f(t)$, as a function of x, has period 2π. Now let

$$t = \frac{2T}{2\pi} x = \frac{T}{\pi} x \qquad \textbf{B-1}$$

Therefore

$$x = \frac{\pi}{T} t \qquad \textbf{B-2}$$

Using equations B-1 and B-2, when $x = 0$, $t = 0$ and when $x = 2\pi$, $t = 2T$.

Now $f(t)$, as a function of x, has a Fourier series of the form:

$$f(t) = f\left(\frac{T}{\pi} x\right) = \sum_{n=0}^{\infty} \left(a_n \sin nx + b_n \cos nx\right) \qquad \textbf{B-3}$$

with coefficients a_n and b_n given by:

$$a_n = \frac{1}{\pi} \int_0^{2\pi} f(x) \sin nx \, dx \qquad \textbf{B-4}$$

$$b_n = \frac{1}{\pi} \int_0^{2\pi} f(x) \cos nx \, dx \qquad \textbf{B-5}$$

$$b_0 = \frac{1}{2\pi} \int_0^{2\pi} f(x) \, dx \qquad \textbf{B-6}$$

Substituting equation B-2, for x, into equation B-3 gives the desired form of the Fourier series for $f(t)$.

$$f(t) = \sum_{n=0}^{\infty} \left(a_n \sin \omega t + b_n \cos \omega t \right) \qquad \textbf{B-7}$$

where $\omega = \frac{n\pi}{T}$.

Since $x = \frac{\pi}{T} t$,

$$dx = \frac{\pi}{T} dt \qquad \textbf{B-8}$$

The limits of integration in equations B-4, B-5 and B-6 are transformed using equation B-1.

Equations B-2 and B-8 are substituted into equations B-4, B-5 and B-6 to give:

$$a_n = \frac{1}{T} \int_0^{2T} f(t) \sin \omega t \; dt \qquad \textbf{B-9}$$

$$b_n = \frac{1}{T} \int_0^{2T} f(t) \cos \omega t \; dt \qquad \textbf{B-10}$$

$$b_0 = \frac{1}{2T} \int_0^{2T} f(t) \; dt \qquad \textbf{B-11}$$

The coefficients of equation B-7 are obtained from equations B-9, B-10 and B-11, which are shown above.

C APPENDIX C – PROGRAM FOR CALCULATION OF SYSTEM AMPLITUDE RATIO, PHASE LAG AND RESPONSE

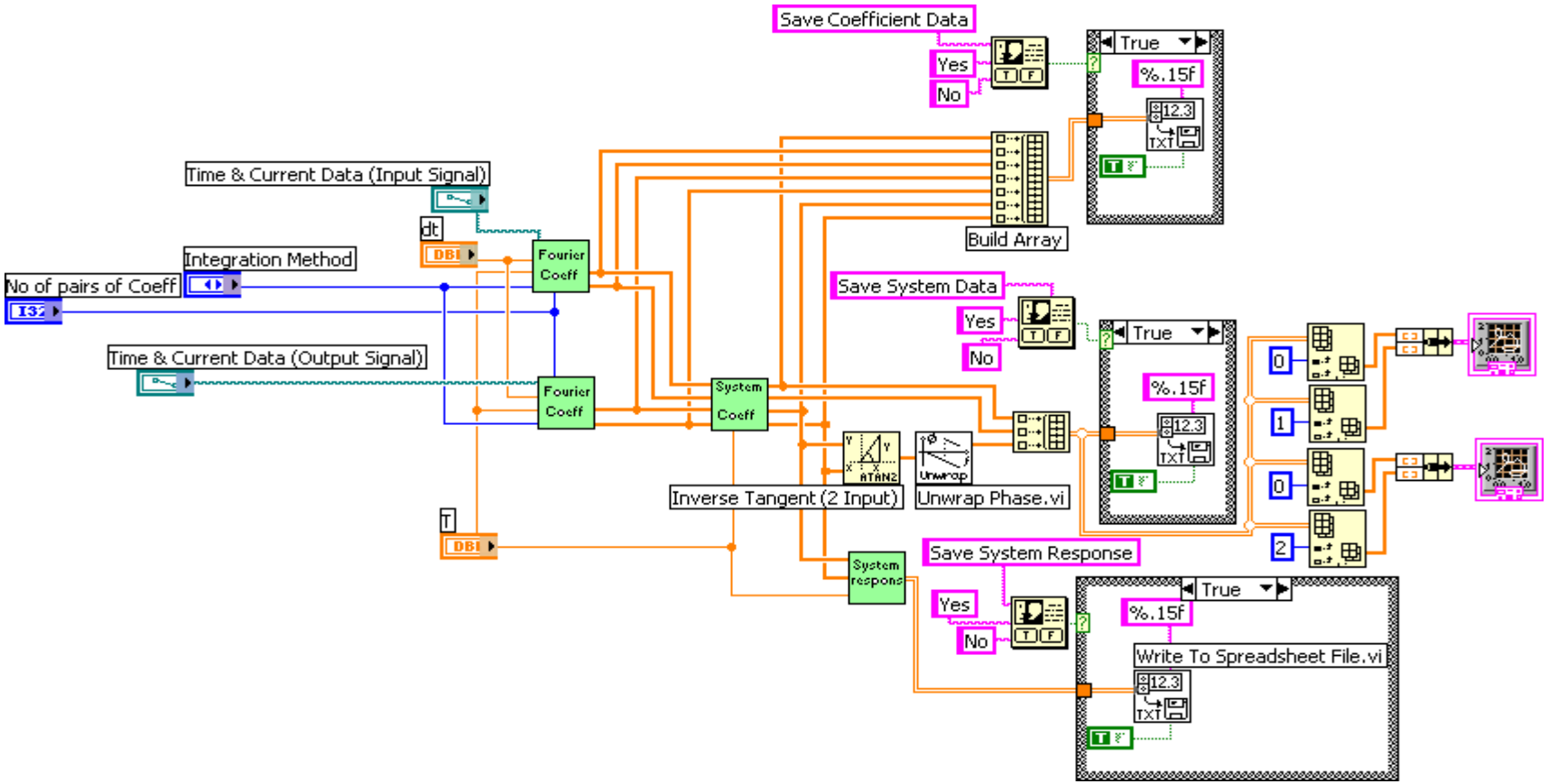

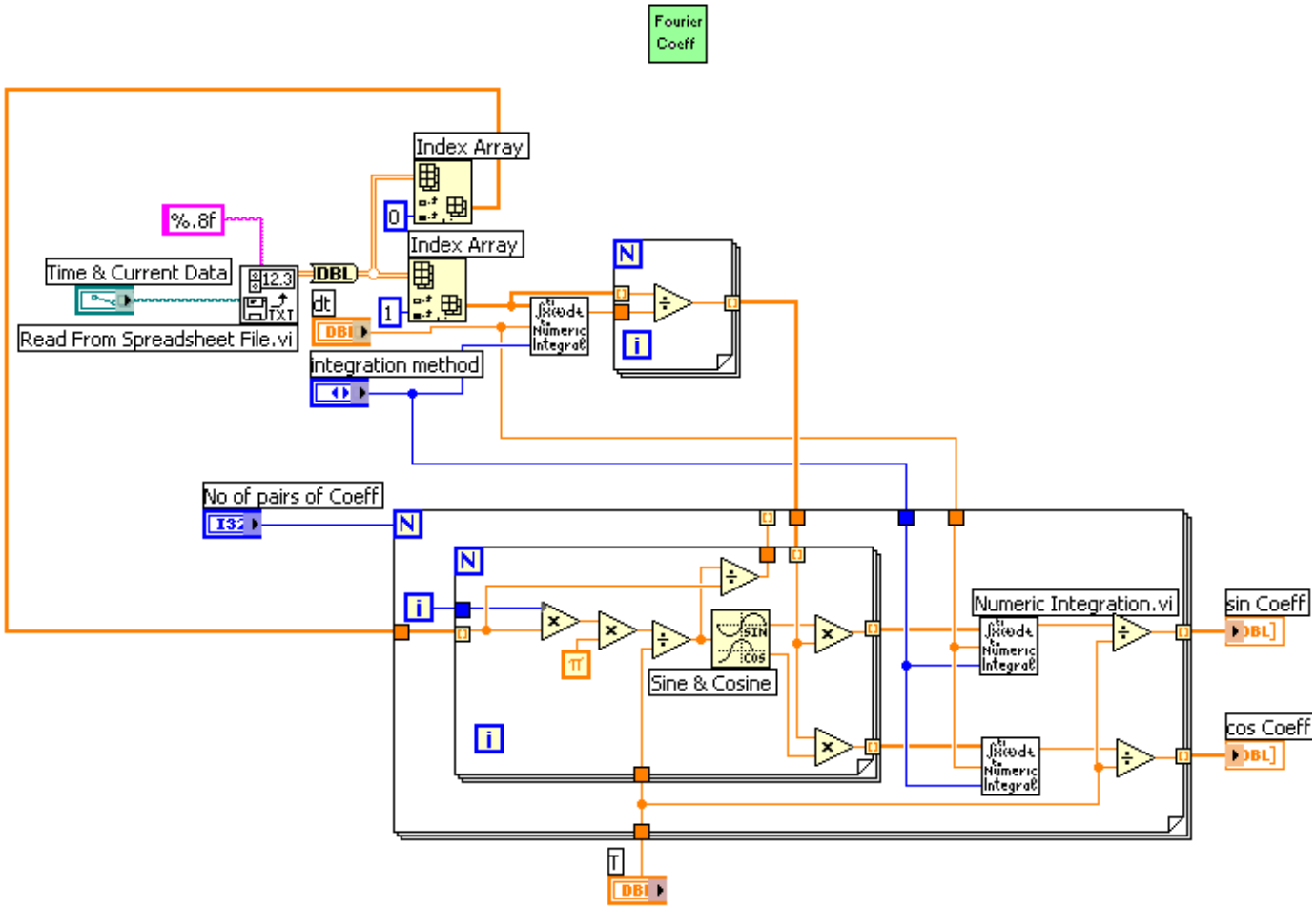
Fourier Coeff
Index Array
%.8f
0
Index Array
Time & Current Data
12.3
TXT
DBL
dt
1
DBL
Read From Spreadsheet File.vi
integration method
N
i
No of pairs of Coeff
I32
N
N
i
i
Sine & Cosine
Numeric Integration.vi
sin Coeff
DBL
cos Coeff
DBL
T
DBL

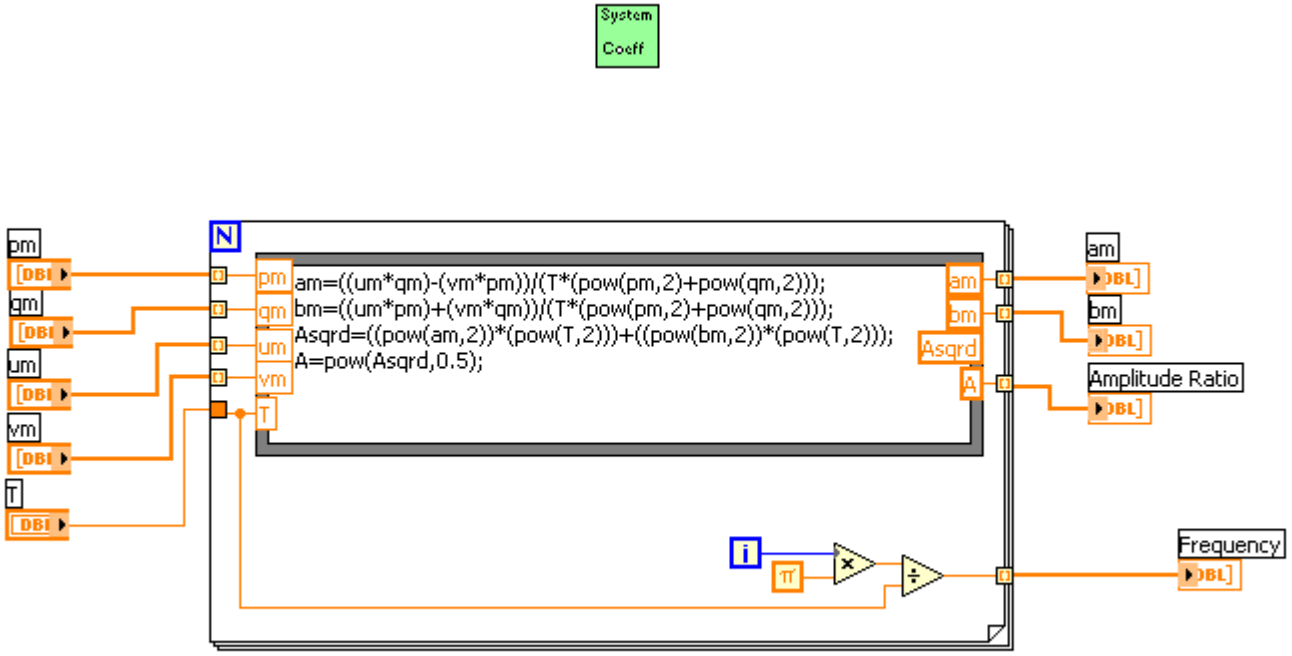
System
Coeff
pm
qm
um
vm
T
N
am=((um*qm)-(vm*pm))/(T*(pow(pm,2)+pow(qm,2)));
bm=((um*pm)+(vm*qm))/(T*(pow(pm,2)+pow(qm,2)));
Asqrd=((pow(am,2))*(pow(T,2)))+((pow(bm,2))*(pow(T,2)));
A=pow(Asqrd,0.5);
am
bm
Asqrd
A
Amplitude Ratio
Frequency
i
π

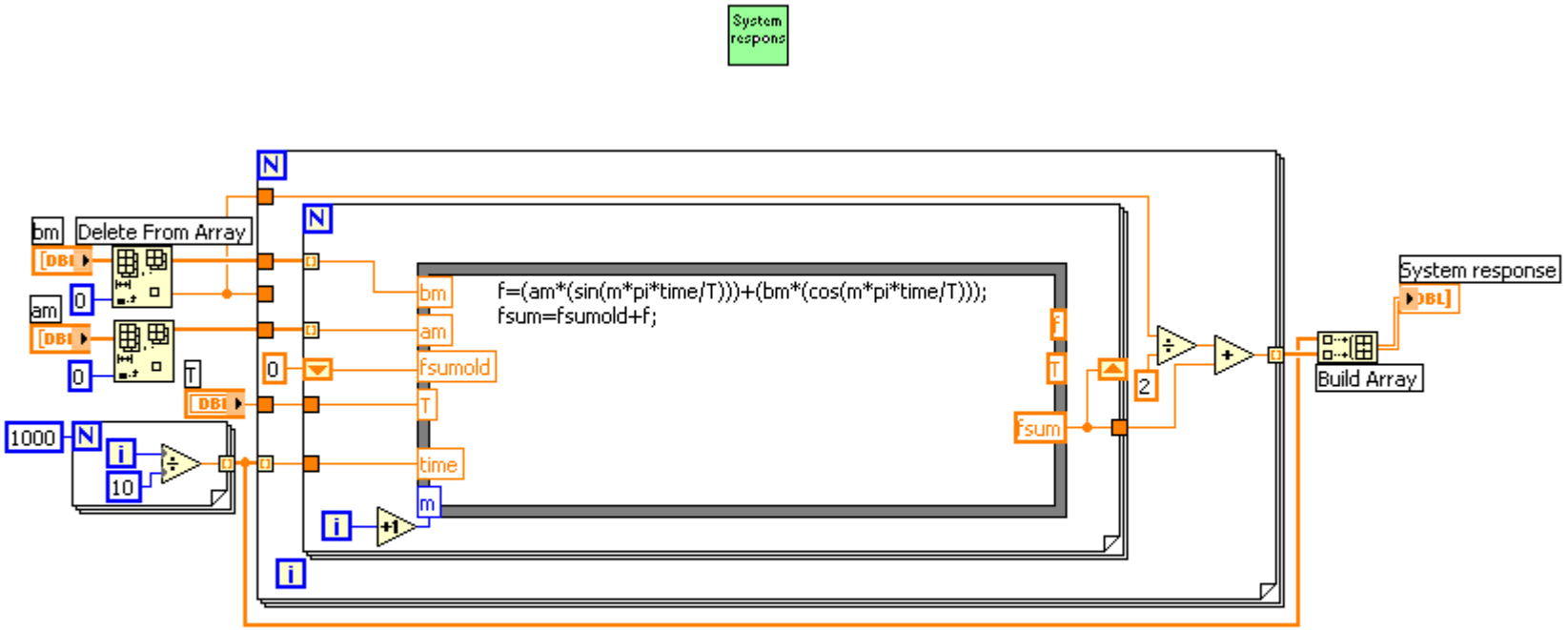
System respons
bm
Delete From Array
am
0
0
T
1000
10
bm
am
fsumold
T
time
m
0
f=(am*(sin(m*pi*time/T)))+(bm*(cos(m*pi*time/T)));
fsum=fsumold+f;
fsum
2
Build Array
System response
DBL

D APPENDIX D – PLOTS OF SYSTEM AMPLITUDE RATIOS AND PHASE LAGS VS. FREQUENCY

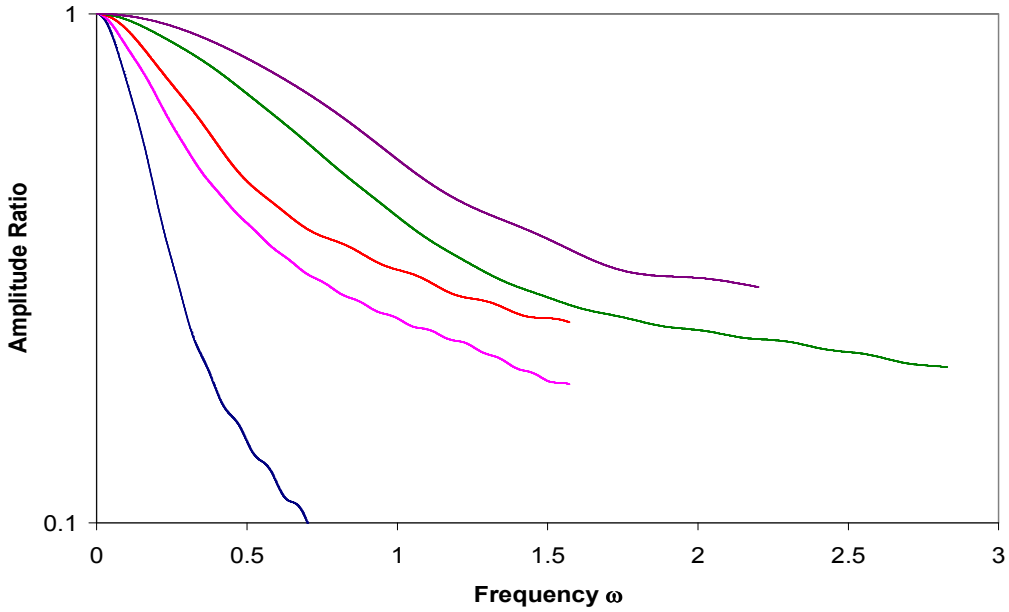

Figure D.1: Plot of system response amplitude ratio vs. frequency for Runs A. The length of tubing was 0.25 m. — 0.5 ml/min, — 0.75 ml/min, — 1.0 ml/min, — 1.5 ml/min and — 2.0 ml/min.

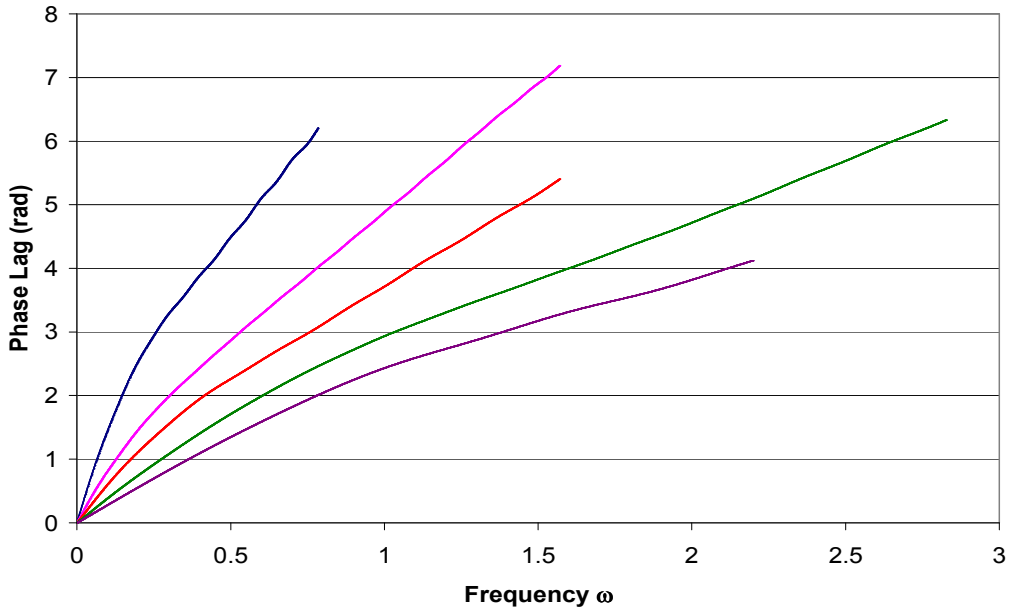

Figure D.2: Plot of system response phase lag vs. frequency for Runs A. The length of tubing was 0.25 m. — 0.5 ml/min, — 0.75 ml/min, — 1.0 ml/min, — 1.5 ml/min and — 2.0 ml/min.

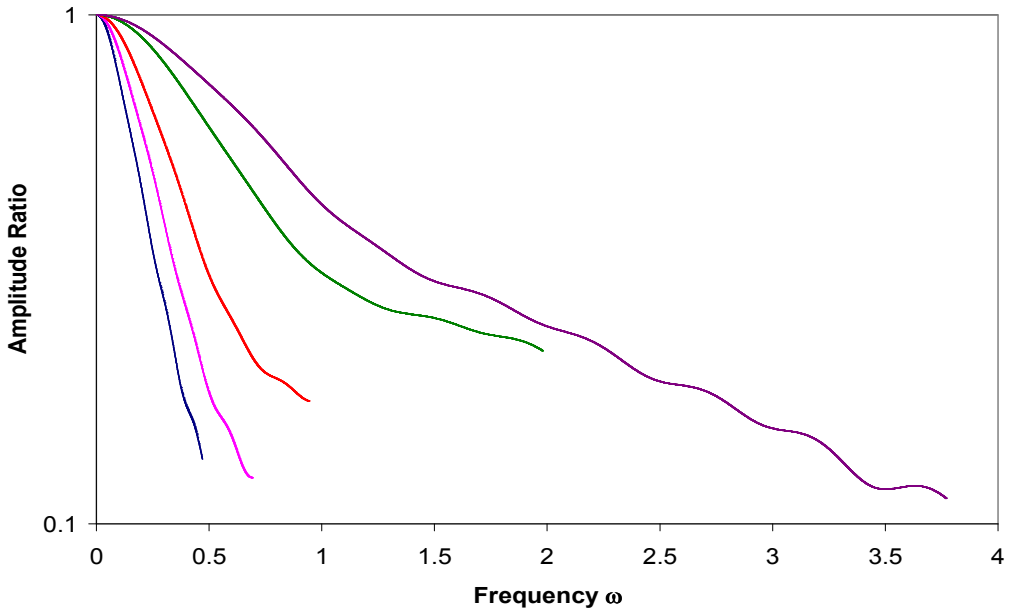

Figure D.3: Plot of system response amplitude ratio vs. frequency for Runs A. The length of tubing was 0.5 m. — 0.5 ml/min, — 0.75 ml/min, — 1.0 ml/min, — 1.5 ml/min and — 2.0 ml/min.

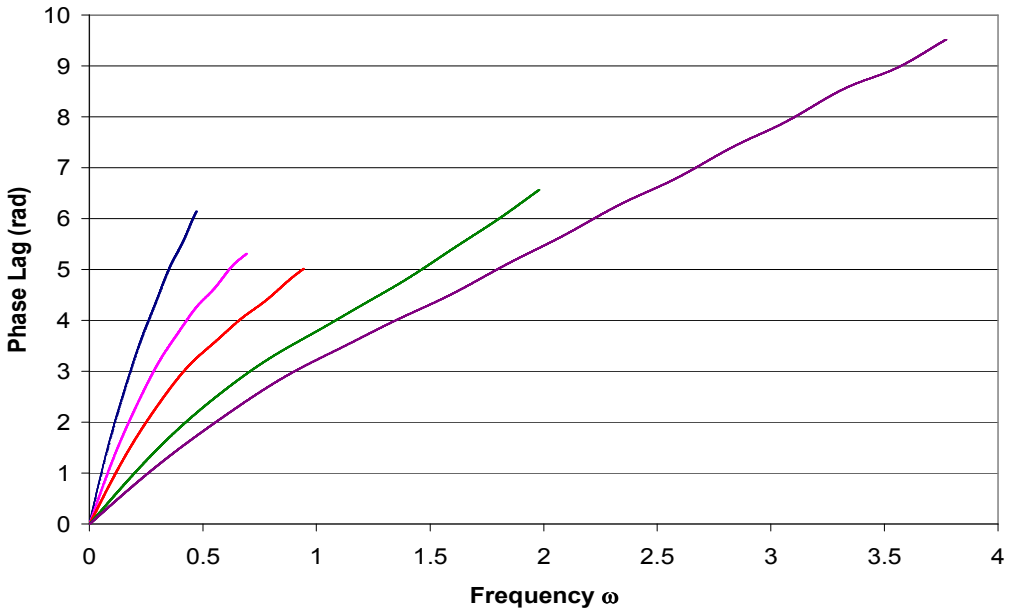

Figure D.4: Plot of system response phase lag vs. frequency for Runs A. The length of tubing was 0.5 m. — 0.5 ml/min, — 0.75 ml/min, — 1.0 ml/min, — 1.5 ml/min and — 2.0 ml/min.

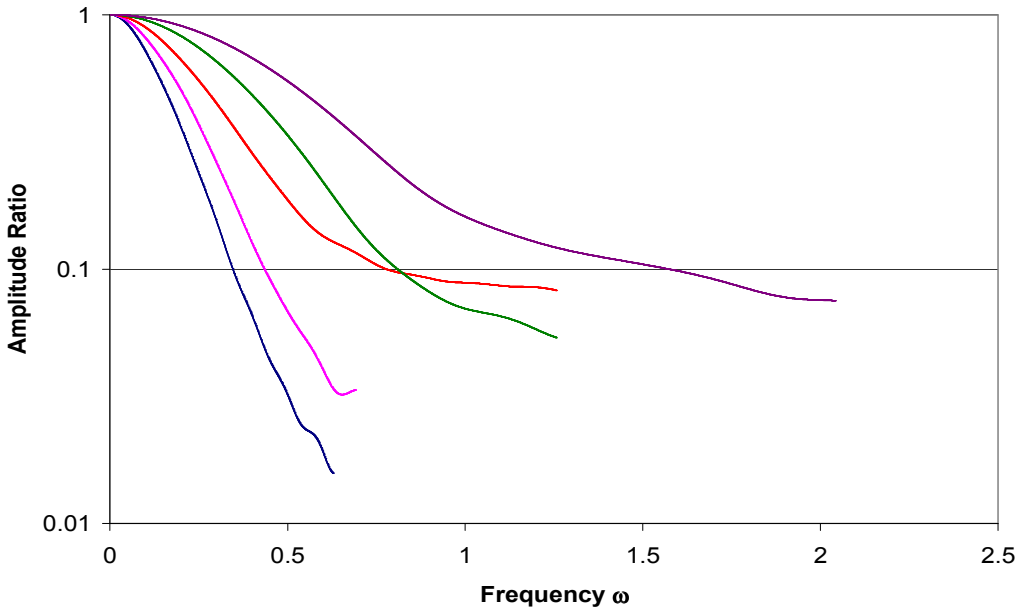

Figure D.5: Plot of system response amplitude ratio vs. frequency for Runs A. The length of tubing was 0.8 m. – 0.5 ml/min, – 0.75 ml/min, – 1.0 ml/min, – 1.5 ml/min and – 2.0 ml/min.

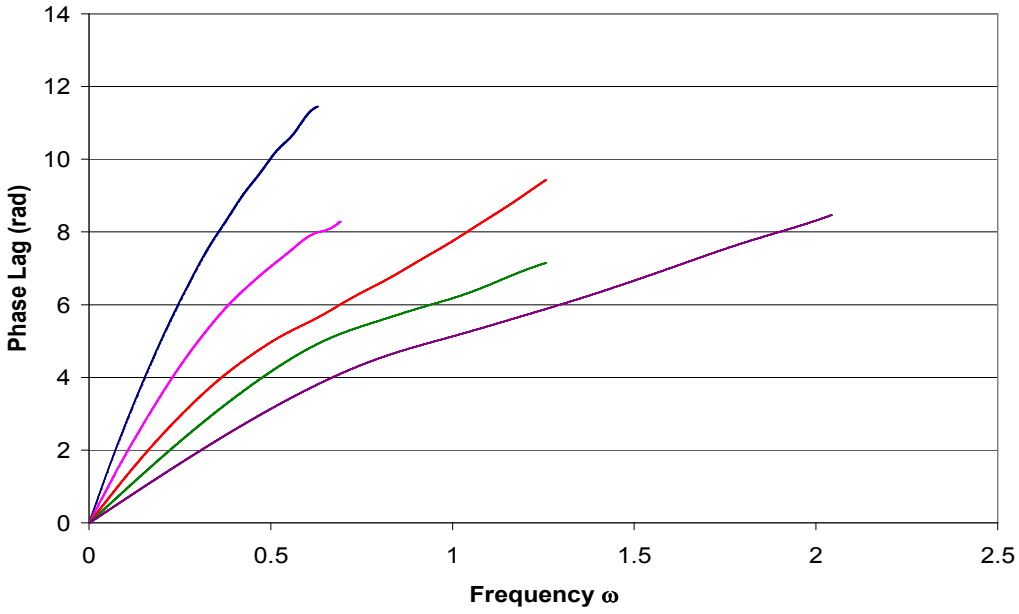

Figure D.6: Plot of system response phase lag vs. frequency for Runs A. The length of tubing was 0.8 m. – 0.5 ml/min, – 0.75 ml/min, – 1.0 ml/min, – 1.5 ml/min and – 2.0 ml/min.

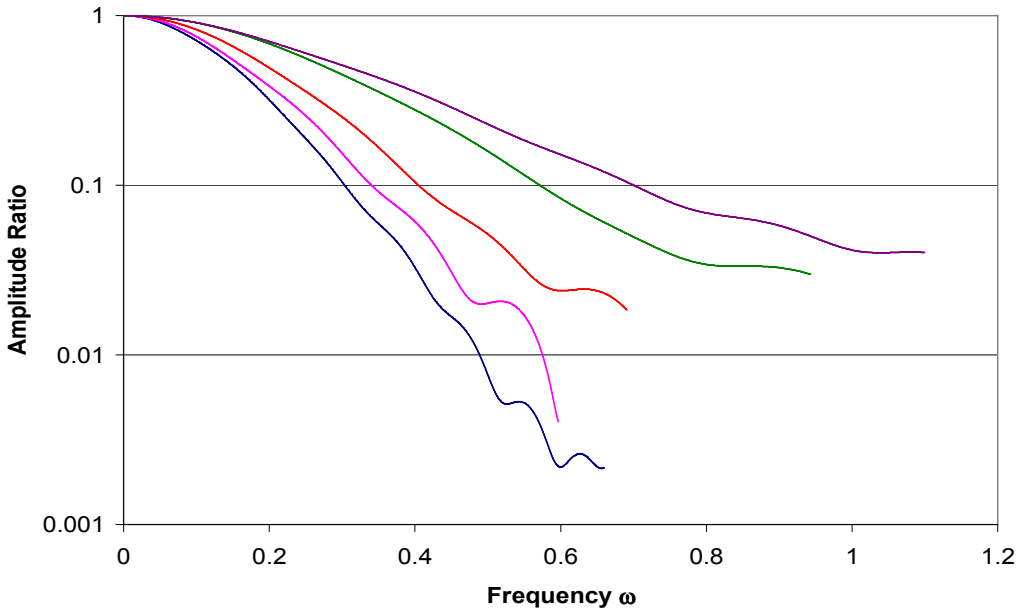

Figure D.7: Plot of system response amplitude ratio vs. frequency for Runs A. The length of tubing was 1 m. — 0.5 ml/min, — 0.75 ml/min, — 1.0 ml/min, — 1.5 ml/min and — 2.0 ml/min.

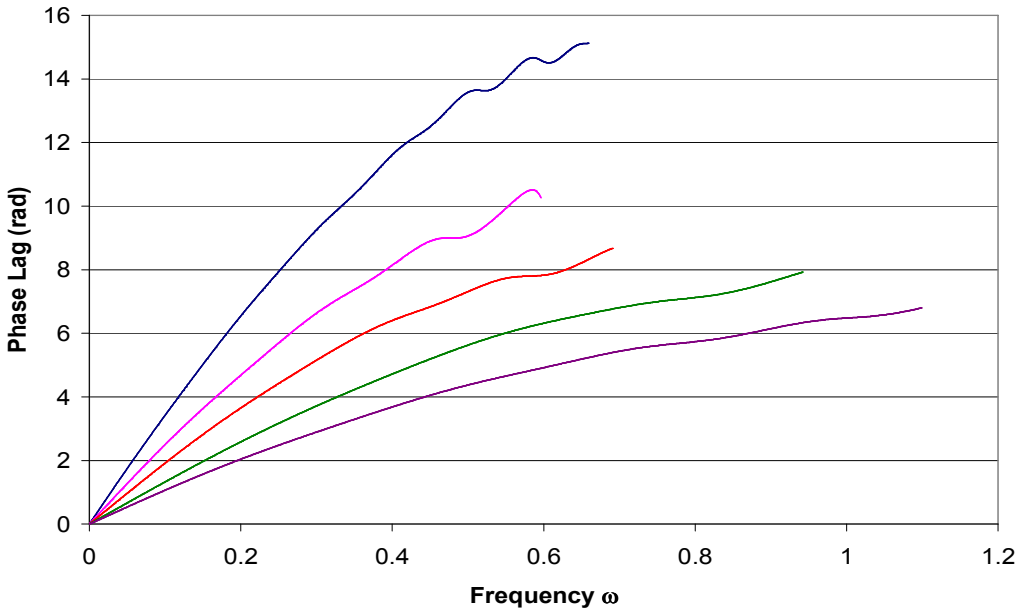

Figure D.8: Plot of system response phase lag vs. frequency for Runs A. The length of tubing was 1 m. — 0.5 ml/min, — 0.75 ml/min, — 1.0 ml/min, — 1.5 ml/min and — 2.0 ml/min.

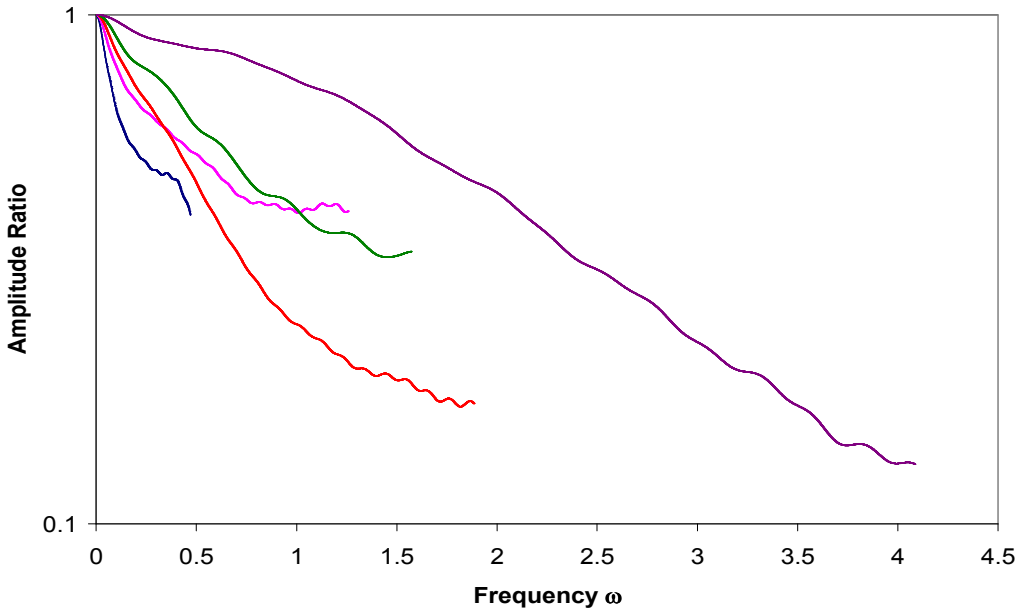

Figure D.9: Plot of system response amplitude ratio vs. frequency for Runs B. The length of tubing was 0.25 m. — 0.5 ml/min, — 0.75 ml/min, — 1.0 ml/min, — 1.5 ml/min and — 2.0 ml/min.

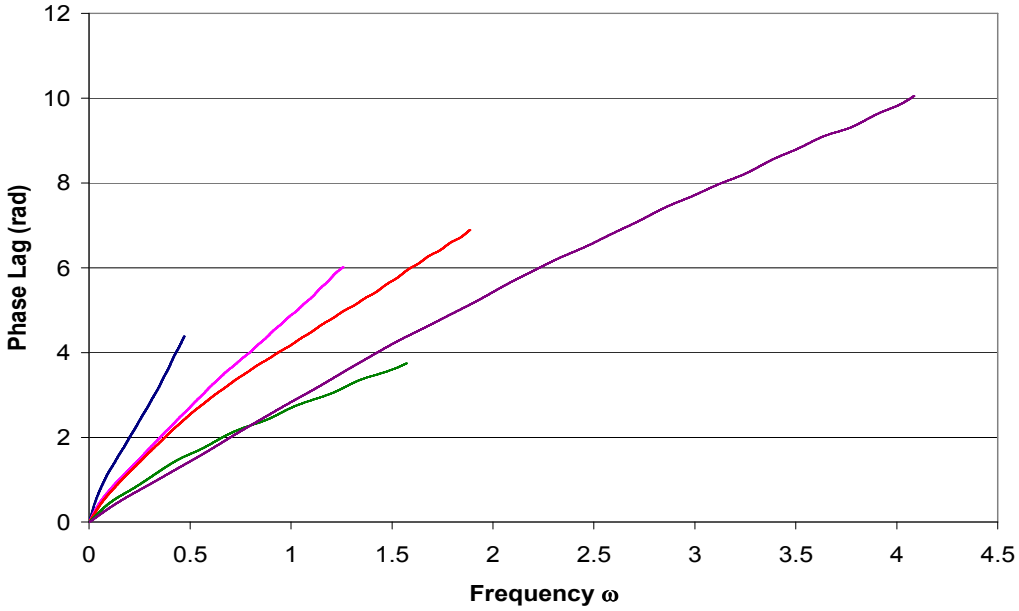

Figure D.10: Plot of system response phase lag vs. frequency for Runs B. The length of tubing was 0.25 m. — 0.5 ml/min, — 0.75 ml/min, — 1.0 ml/min, — 1.5 ml/min and — 2.0 ml/min.

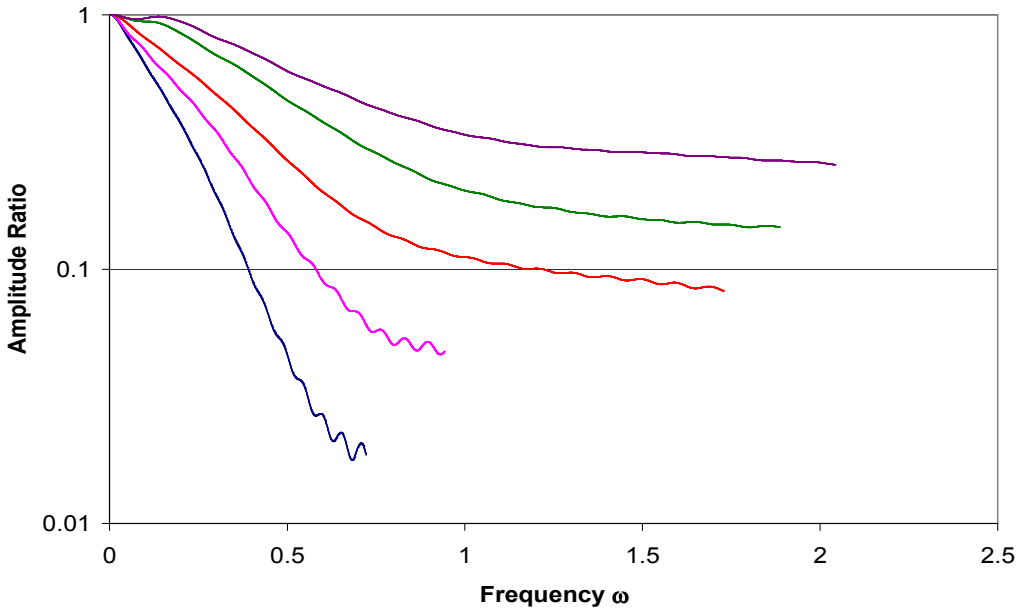

Figure D.11: Plot of system response amplitude ratio vs. frequency for Runs B. The length of tubing was 0.5 m. — 0.5 ml/min, — 0.75 ml/min, — 1.0 ml/min, — 1.5 ml/min and — 2.0 ml/min.

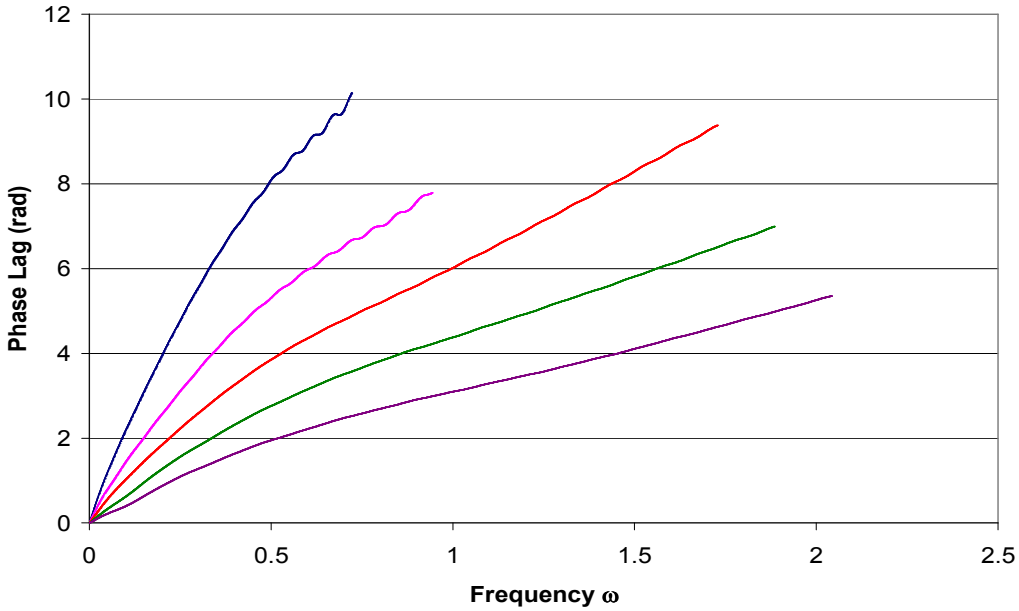

Figure D.12: Plot of system response phase lag vs. frequency for Runs B. The length of tubing was 0.5 m. — 0.5 ml/min, — 0.75 ml/min, — 1.0 ml/min, — 1.5 ml/min and — 2.0 ml/min.

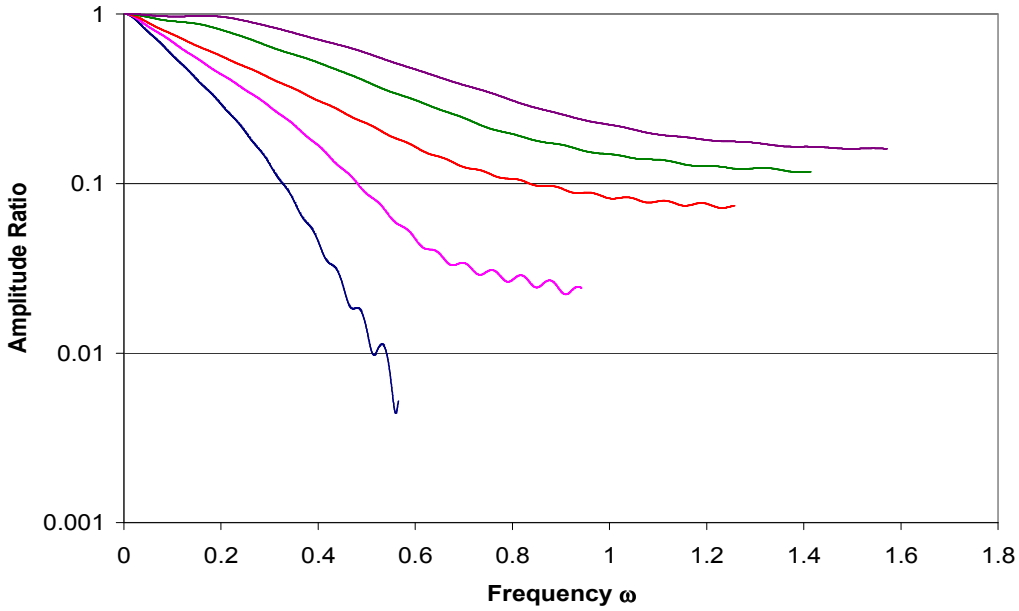

Figure D.13: Plot of system response amplitude ratio vs. frequency for Runs B. The length of tubing was 0.8 m. — 0.5 ml/min, — 0.75 ml/min, — 1.0 ml/min, — 1.5 ml/min and — 2.0 ml/min.

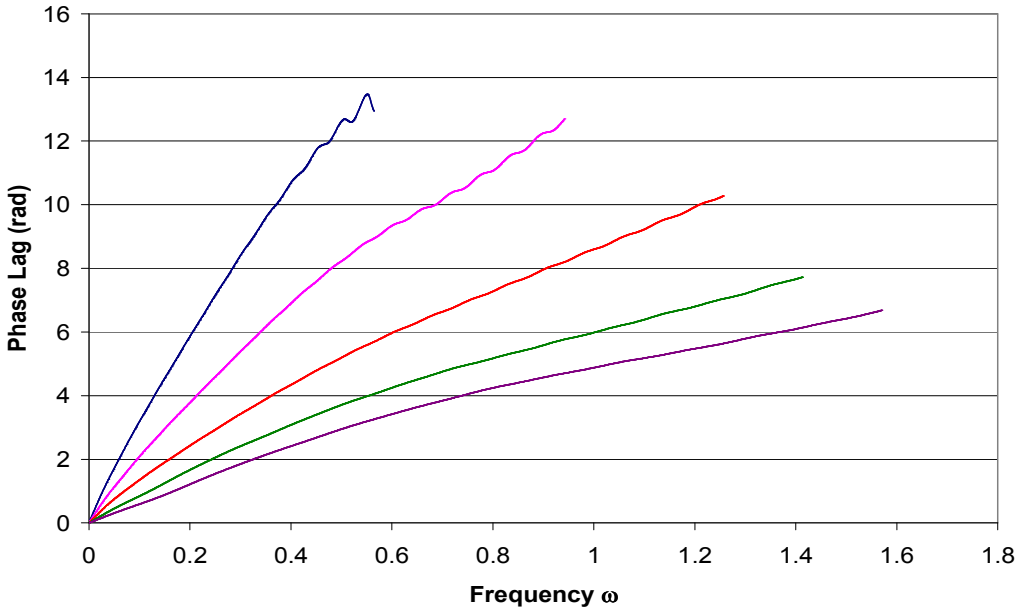

Figure D.14: Plot of system response phase lag vs. frequency for Runs B. The length of tubing was 0.8 m. — 0.5 ml/min, — 0.75 ml/min, — 1.0 ml/min, — 1.5 ml/min and — 2.0 ml/min.

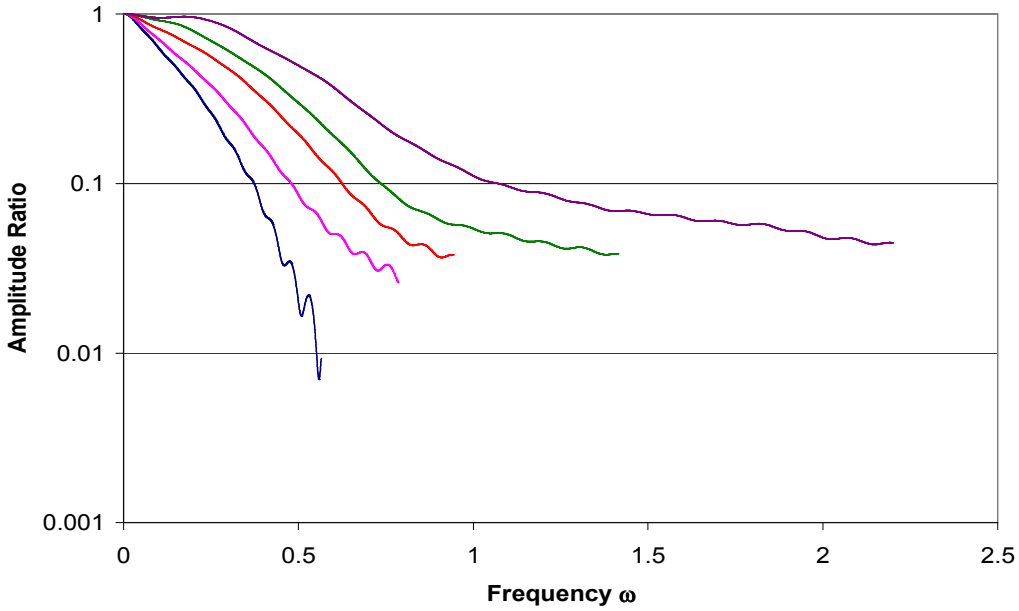

Figure D.15: Plot of system response amplitude ratio vs. frequency for Runs B. The length of tubing was 1 m. — 0.5 ml/min, — 0.75 ml/min, — 1.0 ml/min, — 1.5 ml/min and — 2.0 ml/min.

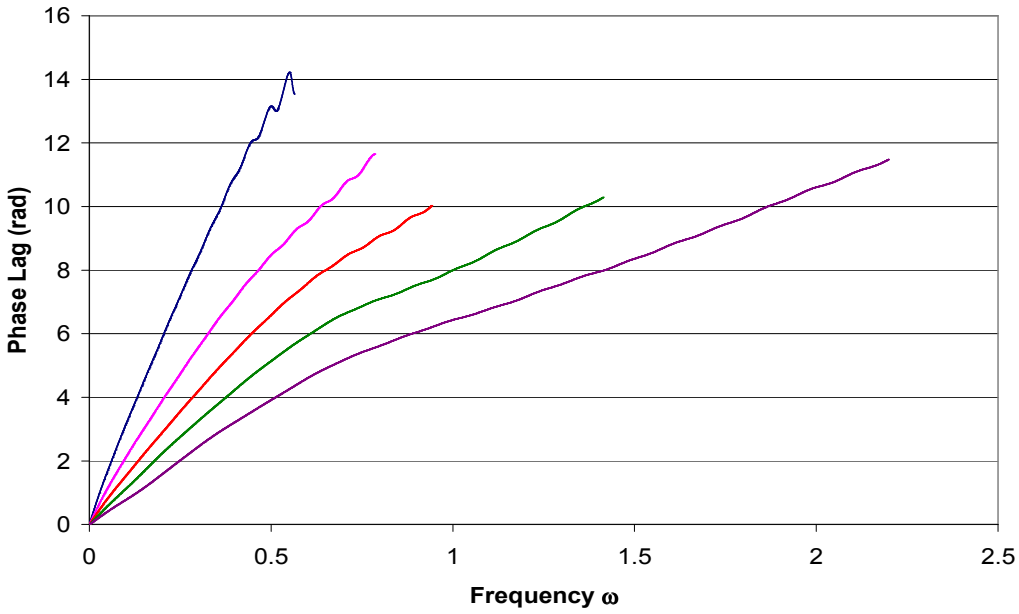

Figure D.16: Plot of system response phase lag vs. frequency for Runs B. The length of tubing was 1 m. — 0.5 ml/min, — 0.75 ml/min, — 1.0 ml/min, — 1.5 ml/min and — 2.0 ml/min.

E APPENDIX E – PROGRAM FOR CALCULATION OF SYSTEM MOMENTS

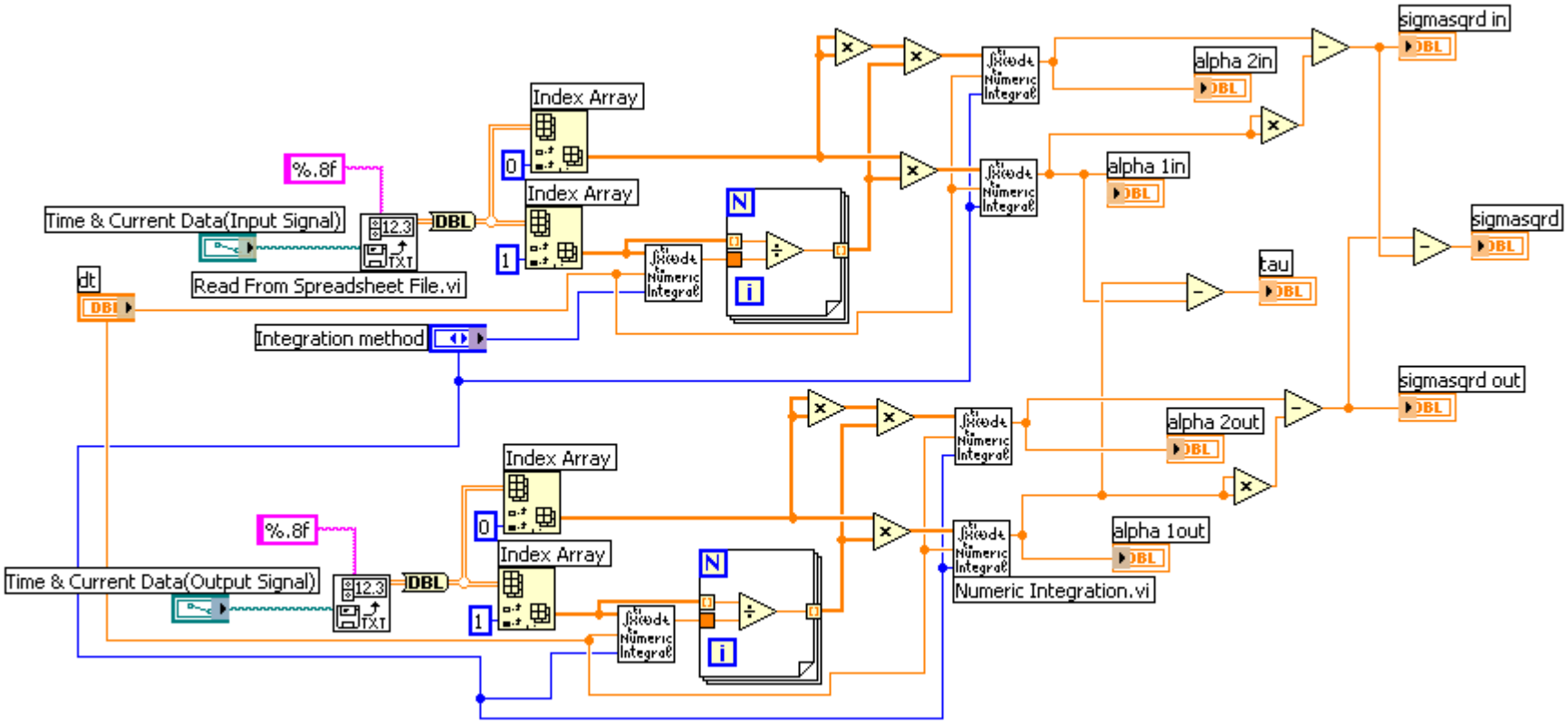

F APPENDIX F – DERIVATION OF EQUATION 4-6

Consider a complex number g. If g is complex, then

$$g = x + iy = r(\cos\theta + i\sin\theta) \quad \text{F-1}$$

where

$$r = \sqrt{x^2 + y^2} \quad \text{F-2}$$

Substituting equation F-2 into equation F-1 results in equation F-3

$$g = \sqrt{x^2 + y^2}\,(\cos\theta + i\sin\theta) \quad \text{F-3}$$

Now expressing $1 + i\frac{4\omega D}{u^2}$ in complex notation. Let $1 + i\frac{4\omega D}{u^2}$ = g. By comparing with equation F-1 it is easy to see that x = 1 and y = $\frac{4\omega D}{u^2}$. Substituting these expressions for x and y into equation F-3 results in:

$$\left(1 + i\frac{4\omega D}{u^2}\right) = g = \sqrt{1^2 + \left(\frac{4\omega D}{u^2}\right)^2}\,(\cos\theta + i\sin\theta) \quad \text{F-4}$$

Therefore $\sqrt{1 + i\frac{4\omega D}{u^2}}$ = $\sqrt{\sqrt{1^2 + \left(\frac{4\omega D}{u^2}\right)^2}\,(\cos\theta + i\sin\theta)}$ F-5

Using the relation $\cos\theta + i\sin\theta = e^{i\theta}$ equation F-5 can be simplified to

$$\sqrt{1 + i\frac{4\omega D}{u^2}} = \left(1 + \frac{16\omega^2 D^2}{u^4}\right)^{\frac{1}{4}} e^{i\frac{\theta}{2}} \quad \text{F-6}$$

Expanding equation F-6 gives the desired result shown below

$$\sqrt{1 + i\frac{4\omega D}{u^2}} = \left(1 + \frac{16D^2\omega^2}{u^4}\right)^{\frac{1}{4}}\left(\cos\frac{\theta}{2} + i\sin\frac{\theta}{2}\right) \quad \text{F-7}$$

G APPENDIX G – NON-LINEAR LEAST SQUARES ALGORITHM

Consider any non-linear function or dependant variable $\boldsymbol{Y}$. $\boldsymbol{Y}$ can be represented by an equation of the form:

$$\boldsymbol{Y} = f(x, \mathbf{b}) \qquad \text{G-1}$$

where $\mathbf{b}$ is a vector of parameters.

x is the independent variable

The sum of squared residuals, φ, is given by:

$$\varphi = (\boldsymbol{Y}^* - \boldsymbol{Y})' (\boldsymbol{Y}^* - \boldsymbol{Y}) \qquad \text{G-2}$$

where $\boldsymbol{Y}^*$ is a vector of experimental observations of the dependant variable

$\boldsymbol{Y}$ is a vector of calculated values of the dependant variable

$(\boldsymbol{Y}^* - \boldsymbol{Y})'$ is the transpose of $(\boldsymbol{Y}^* - \boldsymbol{Y})$

The least squares method requires that the sum of squared residuals, φ, is a minimum, which means that a value of the vector $\mathbf{b}$ must be found such that the sum of squared residuals, φ, is a minimum. This is achieved by solving:

$$\frac{\partial \varphi}{\partial \mathbf{b}} = 0 \qquad \text{G-3}$$

It will be difficult to obtain a solution for equation G-3 since the dependent variable is non-linear with respect to the parameters. In the Gauss-Newton method $\boldsymbol{Y}$ is linearized by a Taylor series expansion around estimates of the parameters. Therefore expanding $\boldsymbol{Y}$ as a Taylor series expansion of two terms:

$$\boldsymbol{Y}(x,\mathbf{b}) = \boldsymbol{Y}(x,\mathbf{b}^{(m)}) + \left.\frac{\partial \boldsymbol{Y}}{\partial \mathbf{b}}\right|_{\mathbf{b}^{(m)}} \Delta\mathbf{b} \quad = \boldsymbol{Y} + \boldsymbol{J}\Delta\mathbf{b} \qquad \textbf{G-4}$$

$$\Delta\mathbf{b} = \mathbf{b}^{(m+1)} - \mathbf{b}^{(m)} \qquad \textbf{G-5}$$

where m is the iteration counter

J is the Jacobian matrix of partial derivatives of $\boldsymbol{Y}$ with respect to b, evaluated at all points where experimental observations were made.

The Jacobian matrix is given by the following equation:

$$\mathbf{J} = \begin{bmatrix} \left.\frac{\partial \boldsymbol{Y}}{\partial \mathbf{b}_1}\right|_1 & \cdots & \left.\frac{\partial \boldsymbol{Y}}{\partial \mathbf{b}_k}\right|_1 \\ \vdots & & \vdots \\ \left.\frac{\partial \boldsymbol{Y}}{\partial \mathbf{b}_1}\right|_n & \cdots & \left.\frac{\partial \boldsymbol{Y}}{\partial \mathbf{b}_k}\right|_n \end{bmatrix} \qquad \textbf{G-6}$$

where $\left|_n\right.$ means a function evaluated at the independent variable value for

the n^{th} experimental observation

n is the number of experimental observations

k is the number of parameters

Substituting equation G-4 into equation G-2 gives:

$$\varphi = (\boldsymbol{Y}^* - \boldsymbol{Y} - \mathbf{J}\Delta\mathbf{b})^{/}(\boldsymbol{Y}^* - \boldsymbol{Y} - \mathbf{J}\Delta\mathbf{b}) \qquad \textbf{G-7}$$

Equation G-7 is linear with respect to $\Delta\mathbf{b}$. So in order to find $\mathbf{b}$, $\Delta\mathbf{b}$ must first be determined such that the sum of squared residuals, φ, is a minimum. Taking the partial derivative of φ with respect to $\Delta\mathbf{b}$, setting it equal to zero and solving for $\Delta\mathbf{b}$ gives:

$$\Delta\mathbf{b} = (\mathbf{J}^{/}\mathbf{J})^{-1}\mathbf{J}^{/}(\boldsymbol{Y}^* - \boldsymbol{Y}) \qquad \textbf{G-8}$$

Once has $\Delta\mathbf{b}$ has been found, $\mathbf{b}$ can be found using equation G-5. The Gauss-Newton method explained above has been explained for the case

where there is only one dependent variable. For the present study there were two dependent variables. For the case where there is more than one dependent variable the following equations are valid [42].

$$\varphi = \sum_{j=1}^{v} w_j (\boldsymbol{Y}_j^* - \boldsymbol{Y}_j - \mathbf{J}_j \Delta\mathbf{b})^{/} (\boldsymbol{Y}_j^* - \boldsymbol{Y}_j - \mathbf{J}_j \Delta\mathbf{b}) \qquad \textbf{G-9}$$

where w_j is the weighting factor of the j^{th} dependent variable

v is the number of dependent variables

The weighting factor is calculated by the following equation [42]:

$$w_j = \frac{1/\sigma_j^2}{\frac{1}{\sum_{b=1}^{v} n_b}\left[\sum_{b=1}^{v}\sum_{l=1}^{n_b}\frac{1}{\sigma_b^2}\right]} \qquad \textbf{G-10}$$

where σ_j^2 or σ_b^2 is the variance for each curve

n_b is the number of experimental points for each curve

For cases where there are v dependent variables, a total number of v Jacobian matrices have to be evaluated.

By taking the partial derivative of φ, given in equation G-9, with respect to $\Delta\mathbf{b}$, setting it equal to zero and solving for $\Delta\mathbf{b}$ gives [42]:

$$\Delta\mathbf{b} = \left[\sum_{j=1}^{v} w_j (\mathbf{J}_j{}^{/} \mathbf{J}_j)\right]^{-1}\left[\sum_{j=1}^{v} w_j \mathbf{J}_j{}^{/} (\boldsymbol{Y}_j^* - \boldsymbol{Y}_j)\right] \qquad \textbf{G-11}$$

As was for the case of a single dependent variable, once $\Delta\mathbf{b}$ has been found, $\mathbf{b}$ can be found using equation G-5.

Therefore to summarise, the Gauss-Newton method or algorithm for multiple non-linear regression consists of the following steps:

1) Assume or guess values for the parameters
2) Calculate the Jacobian matrices

3) Calculate $\Delta\mathbf{b}$ using equation G-11 and other relevant equations
4) Calculate the new values of the parameters using equation G-5
5) Repeat steps 1 to 3 until one or both of the following conditions are met
    a. $\Delta\mathbf{b}$ becomes very small
    b. φ does not change substantially

The Gauss-Newton method will now be explained in terms of the equations for the present study.

Let $\boldsymbol{Y_1} = \ln A$ and $\boldsymbol{Y_2} = \Phi$. For completeness sake these equations are repeated here.

$$\boldsymbol{Y}_1 = \ln A = \frac{uL}{2D} - \left(\frac{u^4L^4}{16D^4} + \frac{\omega^2L^4}{D^2}\right)^{\frac{1}{4}} \cos\left(\frac{1}{2}\arctan\frac{4\omega D}{u^2}\right) \qquad \textbf{G-12}$$

$$\boldsymbol{Y}_2 = \Phi = \left(\frac{u^4L^4}{16D^4} + \frac{\omega^2L^4}{D^2}\right)^{\frac{1}{4}} \sin\left(\frac{1}{2}\arctan\left(\frac{4\omega D}{u^2}\right)\right) \qquad \textbf{G-13}$$

$\boldsymbol{Y}_1^*$ and $\boldsymbol{Y}_2^*$ are the experimental values of $\ln A$ and Φ respectively. The vector $\mathbf{b}$ consists of two parameters, which are D and u. So let $D = \mathbf{b}_1$ and $u = \mathbf{b}_2$. The first and second Jacobian matrices are given by:

$$\mathbf{J}_1 = \begin{bmatrix} \left.\frac{\partial \ln A}{\partial D}\right|_1 & \left.\frac{\partial \ln A}{\partial u}\right|_1 \\ \vdots & \vdots \\ \left.\frac{\partial \ln A}{\partial D}\right|_n & \left.\frac{\partial \ln A}{\partial u}\right|_n \end{bmatrix} \qquad \textbf{G-14}$$

$$\mathbf{J}_2 = \begin{bmatrix} \left.\frac{\partial \Phi}{\partial D}\right|_1 & \left.\frac{\partial \Phi}{\partial u}\right|_1 \\ \vdots & \vdots \\ \left.\frac{\partial \Phi}{\partial D}\right|_n & \left.\frac{\partial \Phi}{\partial u}\right|_n \end{bmatrix} \qquad \text{G-15}$$

The partial derivatives of $\ln A$ and Φ with respect to D and u are given by the following equations:

$$\frac{\partial \ln A}{\partial D} = -\frac{uL}{2D^2} - \left(\frac{1}{4}\left(\frac{u^4L^4}{16D^4} + \frac{\omega^2 L^4}{D^2} \right)^{-\frac{3}{4}} \left(-\frac{u^4L^4}{4D^5} - \frac{2\omega^2 L^4}{D^3} \right) \cos\left(\frac{1}{2}\arctan\left(\frac{4\omega D}{u^2} \right) \right) \right)$$
$$+ 2\left(\frac{u^4L^4}{16D^4} + \frac{\omega^2 L^4}{D^2} \right)^{\frac{1}{4}} \sin\left(\frac{1}{2}\arctan\left(\frac{4\omega D}{u^2} \right) \right) \frac{\omega}{u^2\left(1 + \frac{16\omega^2 D^2}{u^4} \right)} \qquad \text{G-16}$$

$$\frac{\partial \ln A}{\partial u} = \frac{L}{2D} - \frac{1}{16}\left(\frac{u^4L^4}{16D^4} + \frac{\omega^2 L^4}{D^2} \right)^{-\frac{3}{4}} \cos\left(\frac{1}{2}\arctan\left(\frac{4\omega D}{u^2} \right) \right) \frac{u^3L^4}{D^4}$$
$$- 4\left(\frac{u^4L^4}{16D^4} + \frac{\omega^2 L^4}{D^2} \right)^{\frac{1}{4}} \sin\left(\frac{1}{2}\arctan\left(\frac{4\omega D}{u^2} \right) \right) \frac{\omega D}{u^3\left(1 + \frac{16\omega^2 D^2}{u^4} \right)} \qquad \text{G-17}$$

$$\frac{\partial \Phi}{\partial D} = \frac{1}{4}\left(\frac{u^4L^4}{16D^4} + \frac{\omega^2 L^4}{D^2} \right)^{-\frac{3}{4}} \sin\left(\frac{1}{2}\arctan\left(\frac{4\omega D}{u^2} \right) \right) \left(-\frac{u^4L^4}{4D^5} - \frac{2\omega^2 L^4}{D^3} \right)$$
$$+ 2\left(\frac{u^4L^4}{16D^4} + \frac{\omega^2 L^4}{D^2} \right)^{\frac{1}{4}} \cos\left(\frac{1}{2}\arctan\left(\frac{4\omega D}{u^2} \right) \right) \frac{\omega}{u^2\left(1 + \frac{16\omega^2 D^2}{u^4} \right)} \qquad \text{G-18}$$

$$\frac{\partial \Phi}{\partial u} = \frac{1}{16}\left(\frac{u^4L^4}{16D^4} + \frac{\omega^2 L^4}{D^2} \right)^{-\frac{3}{4}} \sin\left(\frac{1}{2}\arctan\left(\frac{4\omega D}{u^2} \right) \right) \frac{u^3L^4}{D^4}$$
$$- 4\left(\frac{u^4L^4}{16D^4} + \frac{\omega^2 L^4}{D^2} \right)^{\frac{1}{4}} \cos\left(\frac{1}{2}\arctan\left(\frac{4\omega D}{u^2} \right) \right) \frac{\omega D}{u^3\left(1 + \frac{16\omega^2 D^2}{u^4} \right)} \qquad \text{G-19}$$

Equations G-16 to G-19 are substituted into G-14 and G-15. The Jacobian matrices are then evaluated at all points where experimental observations were made using estimates or guesses of the parameters D and u. Thereafter $\boldsymbol{Y}_1$ and $\boldsymbol{Y}_2$ are calculated using equations G-12 and G-13 also where experimental observations were made using estimates or guesses of the parameters D and u. Using the experimental data i.e. $\boldsymbol{Y}_1^*$ and $\boldsymbol{Y}_2^*$, the weighting factors are calculated by means of equation G-10. Then $\Delta\mathbf{b}$ is calculated using equation G-11. The sum of squared residuals, φ, is calculated using equation G-9.The above mentioned steps are repeated until both or one of the following conditions are met:

a) $\Delta\mathbf{b}$ becomes very small

b) φ does not change substantially

When one or both of the conditions mentioned above are satisfied, then the vector $\mathbf{b}$ is calculated using equation G-5. The values now obtained for the vector $\mathbf{b}$ are the desired values. Shown below is the non-linear least squares fit program coded in LabVIEW ™ version 7.0.

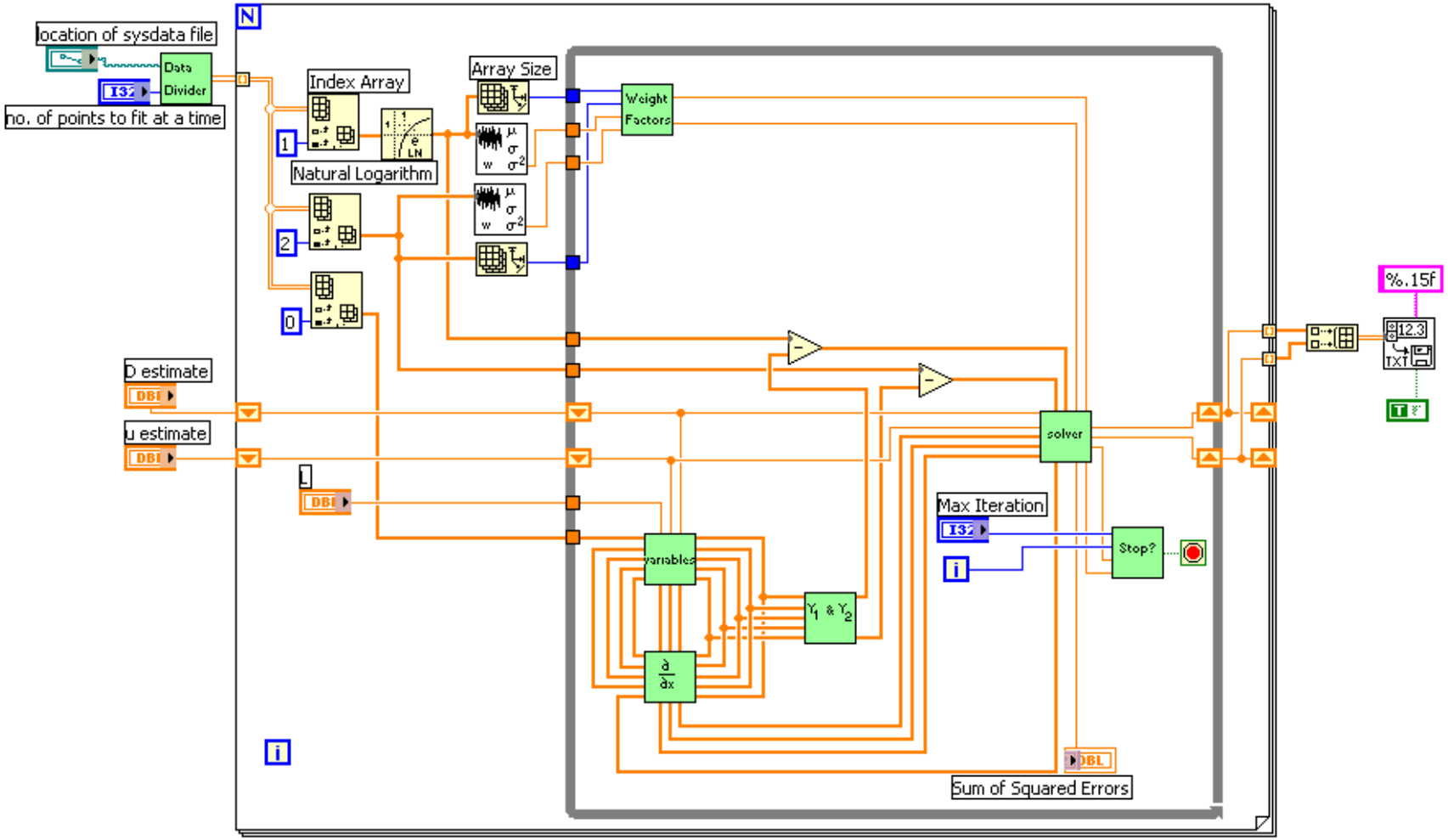
location of sysdata file
Data Divider
no. of points to fit at a time
Index Array
Array Size
Natural Logarithm
Weight Factors
D estimate
u estimate
L
variables
solver
Max Iteration
Stop?
Sum of Squared Errors
%.15f

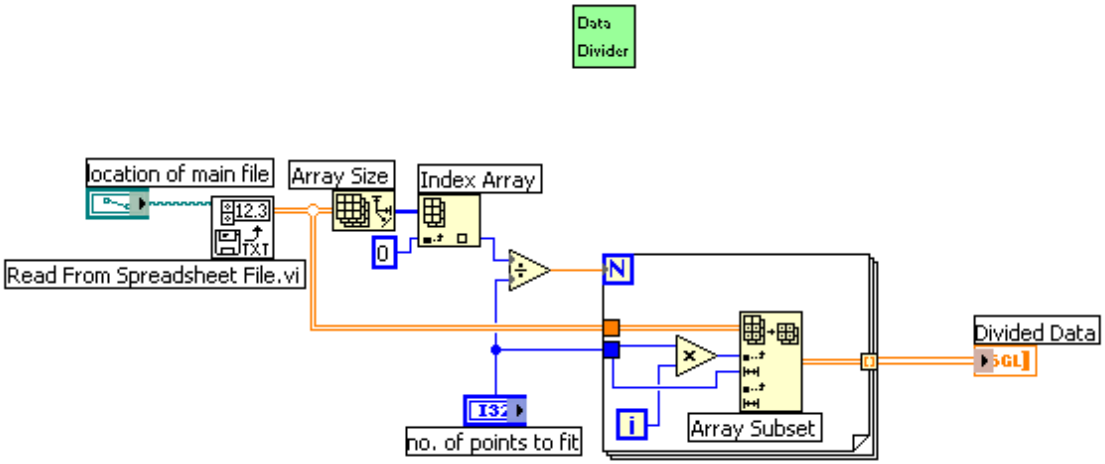
Data Divider
location of main file
Array Size
Index Array
Read From Spreadsheet File.vi
0
N
Divided Data
I32
no. of points to fit
i
Array Subset

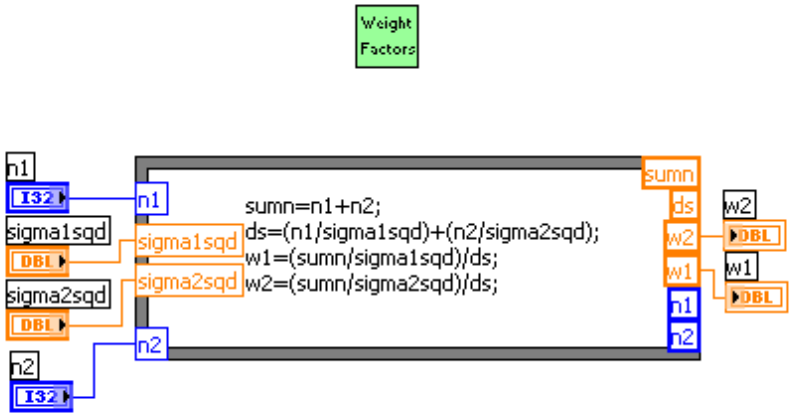
Weight Factors
n1
I32
sigma1sqd
DBL
sigma2sqd
DBL
n2
I32
sumn=n1+n2;
ds=(n1/sigma1sqd)+(n2/sigma2sqd);
w1=(sumn/sigma1sqd)/ds;
w2=(sumn/sigma2sqd)/ds;
sumn
ds
w2
w1
n1
n2
w2
DBL
w1
DBL

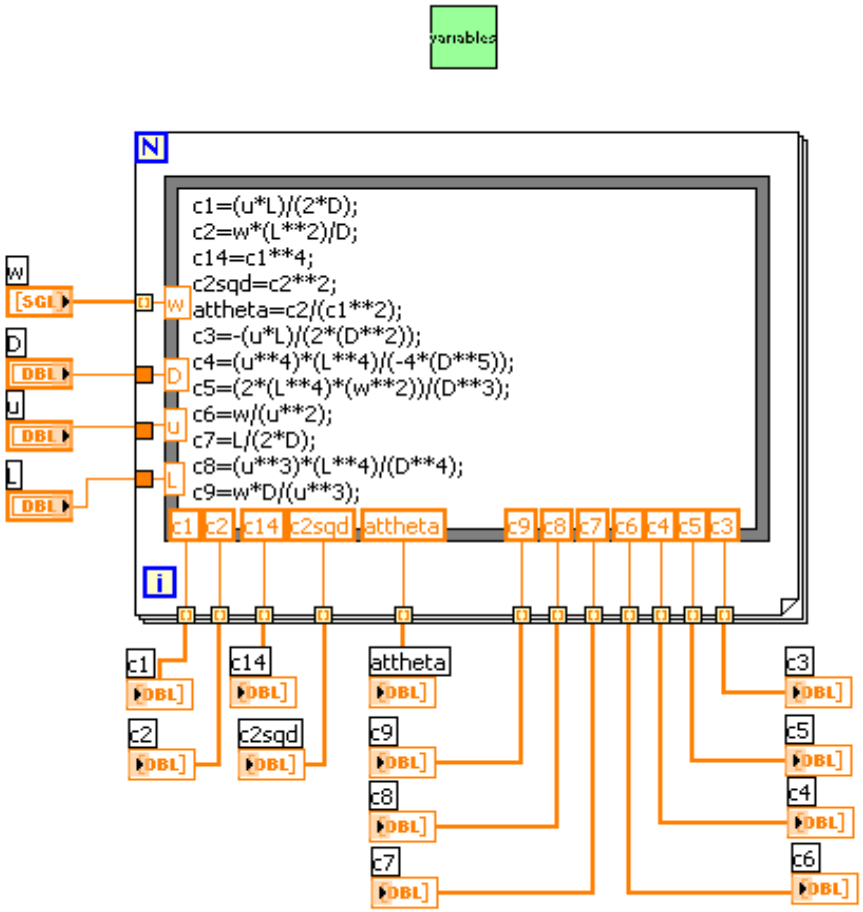
variables
N
c1=(u*L)/(2*D);
c2=w*(L**2)/D;
c14=c1**4;
c2sqd=c2**2;
attheta=c2/(c1**2);
c3=-(u*L)/(2*(D**2));
c4=(u**4)*(L**4)/(-4*(D**5));
c5=(2*(L**4)*(w**2))/(D**3);
c6=w/(u**2);
c7=L/(2*D);
c8=(u**3)*(L**4)/(D**4);
c9=w*D/(u**3);
w
SGL
D
DBL
u
DBL
L
DBL
w
D
u
L
c1
c2
c14
c2sqd
attheta
c9
c8
c7
c6
c4
c5
c3
i
c1
DBL
c2
DBL
c14
DBL
c2sqd
DBL
attheta
DBL
c9
DBL
c8
DBL
c7
DBL
c3
DBL
c5
DBL
c4
DBL
c6
DBL

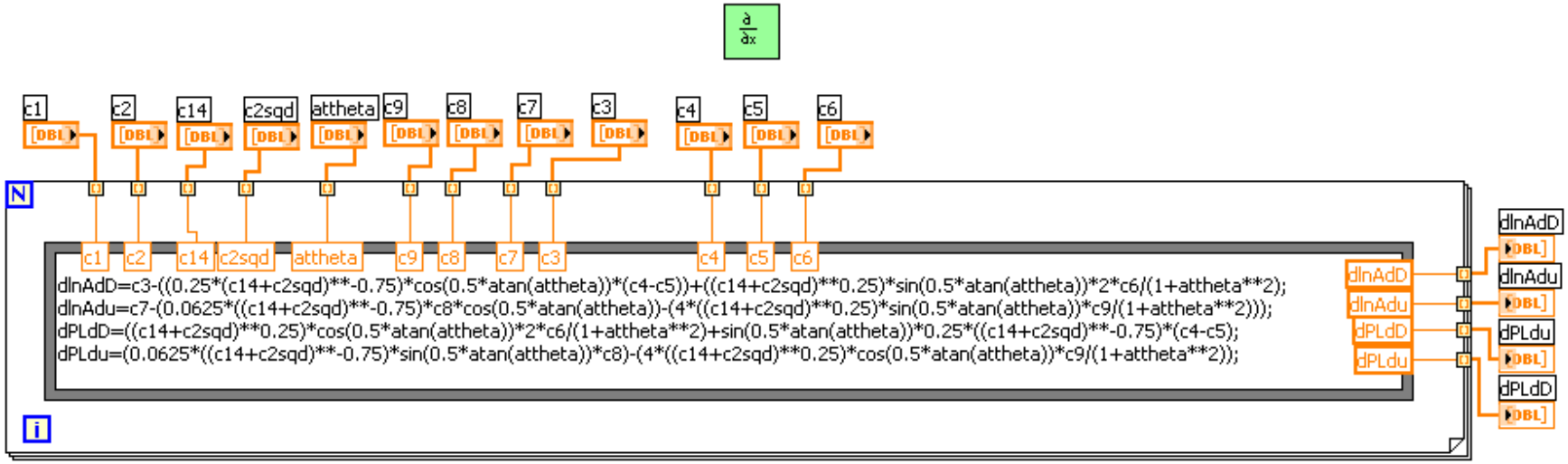
∂/∂x
c1
c2
c14
c2sqd
attheta
c9
c8
c7
c3
c4
c5
c6
N
i
dlnAdD=c3-((0.25*(c14+c2sqd)**-0.75)*cos(0.5*atan(attheta))*(c4-c5))+((c14+c2sqd)**0.25)*sin(0.5*atan(attheta))*2*c6/(1+attheta**2);
dlnAdu=c7-(0.0625*((c14+c2sqd)**-0.75)*c8*cos(0.5*atan(attheta))-(4*((c14+c2sqd)**0.25)*sin(0.5*atan(attheta))*c9/(1+attheta**2)));
dPLdD=((c14+c2sqd)**0.25)*cos(0.5*atan(attheta))*2*c6/(1+attheta**2)+sin(0.5*atan(attheta))*0.25*((c14+c2sqd)**-0.75)*(c4-c5);
dPLdu=(0.0625*((c14+c2sqd)**-0.75)*sin(0.5*atan(attheta))*c8)-(4*((c14+c2sqd)**0.25)*cos(0.5*atan(attheta))*c9/(1+attheta**2));
dlnAdD
dlnAdu
dPLdD
dPLdu

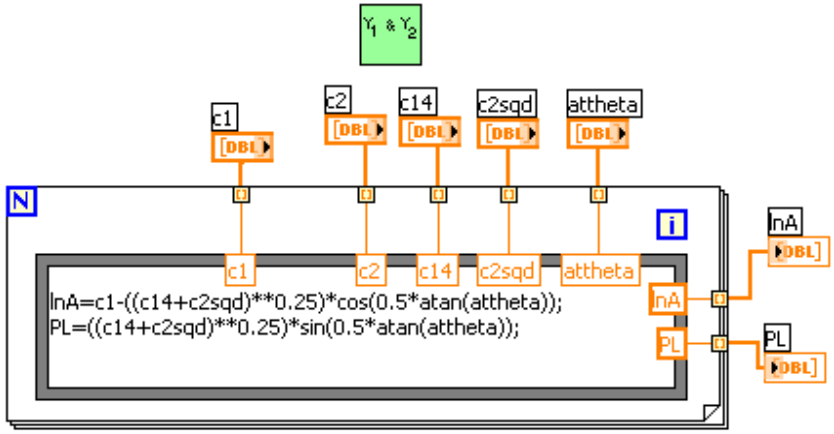
Y1 & Y2
c1
c2
c14
c2sqd
attheta
N
i
lnA=c1-((c14+c2sqd)**0.25)*cos(0.5*atan(attheta));
PL=((c14+c2sqd)**0.25)*sin(0.5*atan(attheta));
lnA
PL

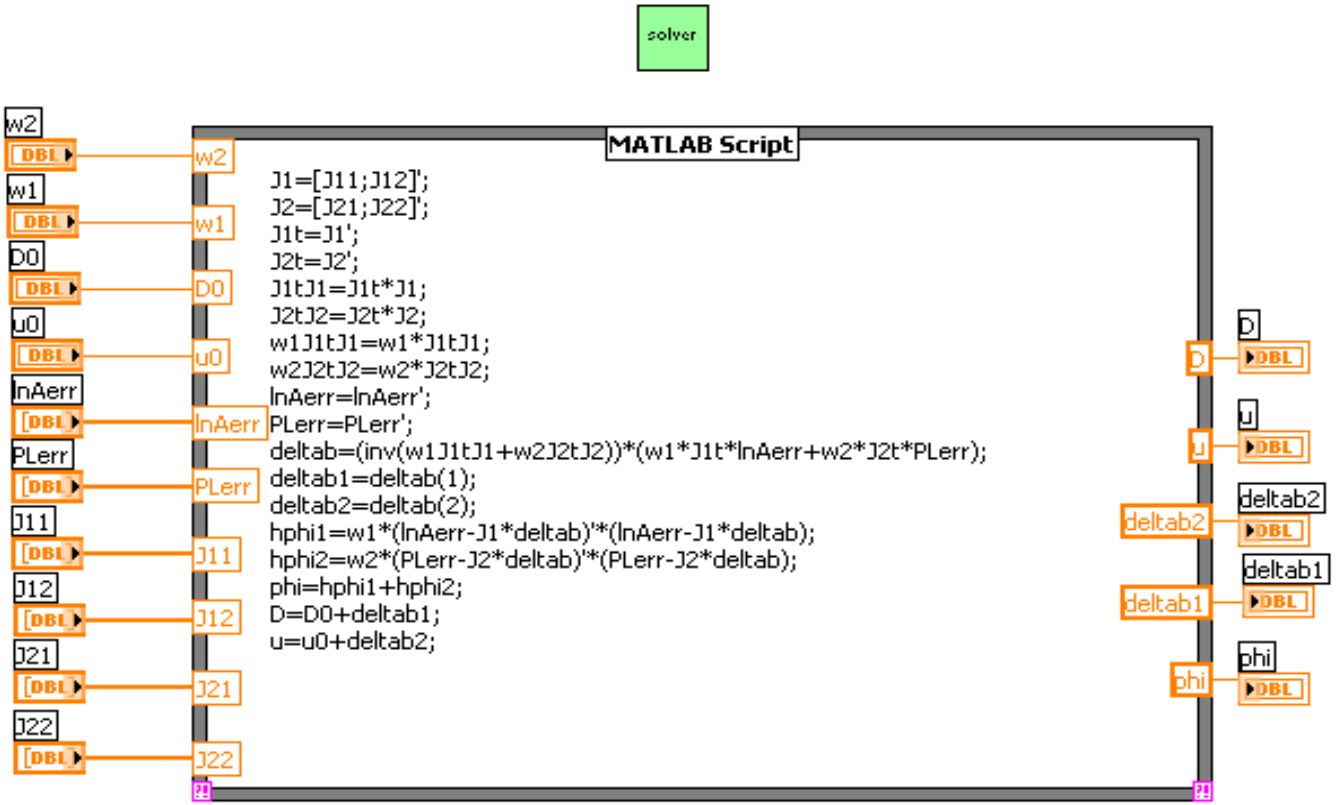
solver
MATLAB Script
w2
w1
D0
u0
lnAerr
PLerr
J11
J12
J21
J22
J1=[J11;J12];
J2=[J21;J22];
J1t=J1';
J2t=J2';
J1tJ1=J1t*J1;
J2tJ2=J2t*J2;
w1J1tJ1=w1*J1tJ1;
w2J2tJ2=w2*J2tJ2;
lnAerr=lnAerr';
PLerr=PLerr';
deltab=(inv(w1J1tJ1+w2J2tJ2))*(w1*J1t*lnAerr+w2*J2t*PLerr);
deltab1=deltab(1);
deltab2=deltab(2);
hphi1=w1*(lnAerr-J1*deltab)'*(lnAerr-J1*deltab);
hphi2=w2*(PLerr-J2*deltab)'*(PLerr-J2*deltab);
phi=hphi1+hphi2;
D=D0+deltab1;
u=u0+deltab2;
D
u
deltab2
deltab1
phi
DBL

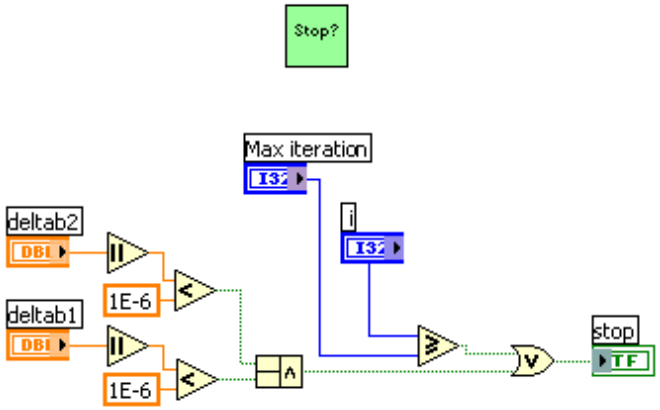
Stop?
Max iteration
I32
i
I32
deltab2
DBL
1E-6
deltab1
DBL
1E-6
stop
TF

H APPENDIX H – PLOTS OF D AND u VS. FREQUENCY

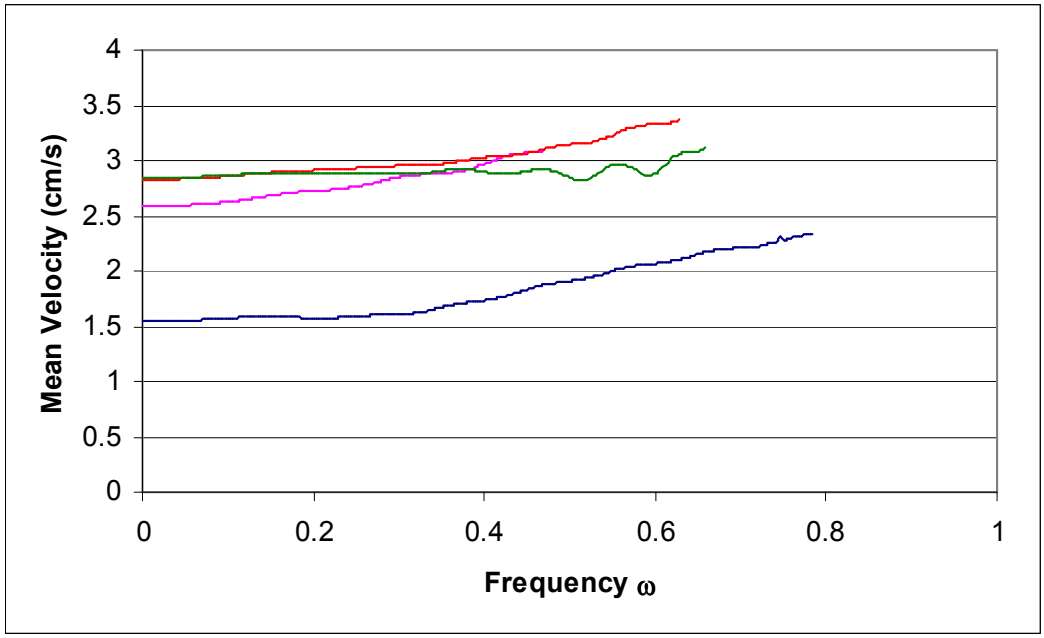

(a)

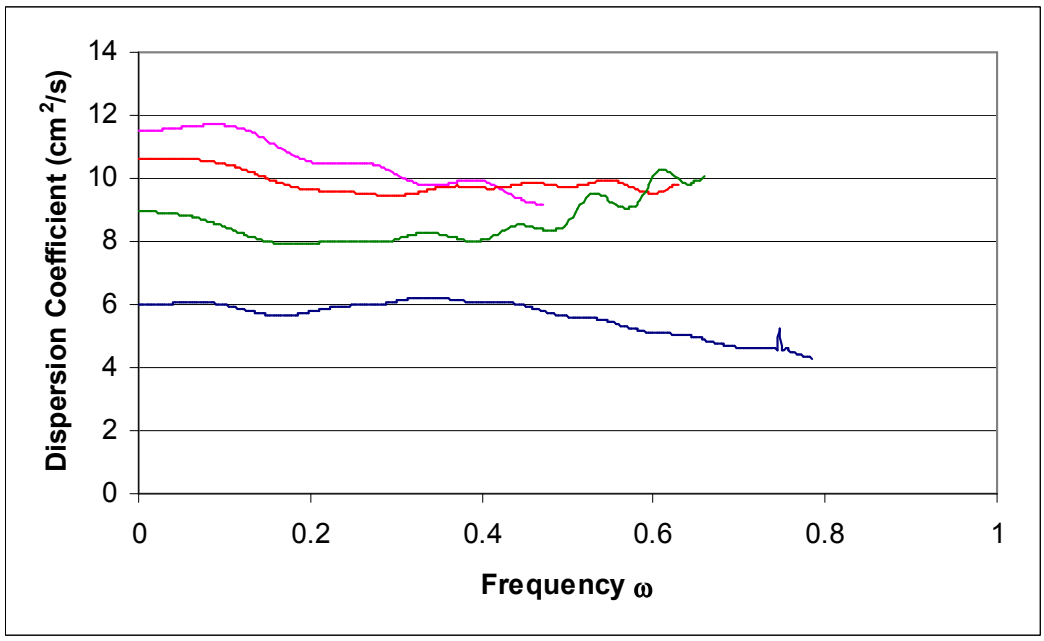

(b)

Figure H.1: Plot of (a) mean velocity and (b) dispersion coefficient vs. frequency for Runs A. The flow rate was 0.5 ml/min. — 0.25 m, — 0.5 m, — 0.8 m and — 1m.

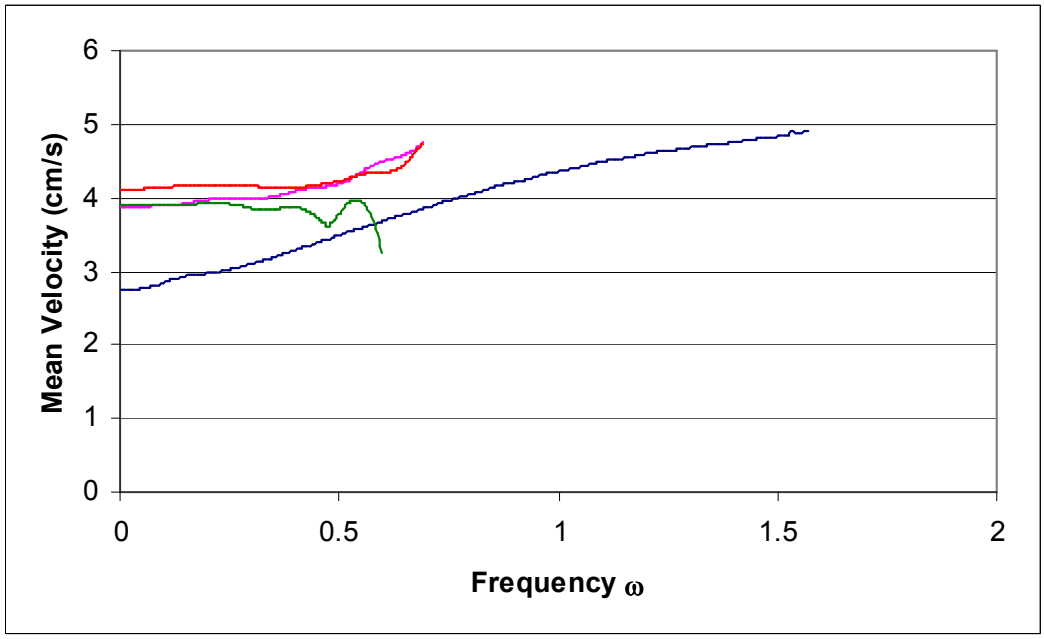

(a)

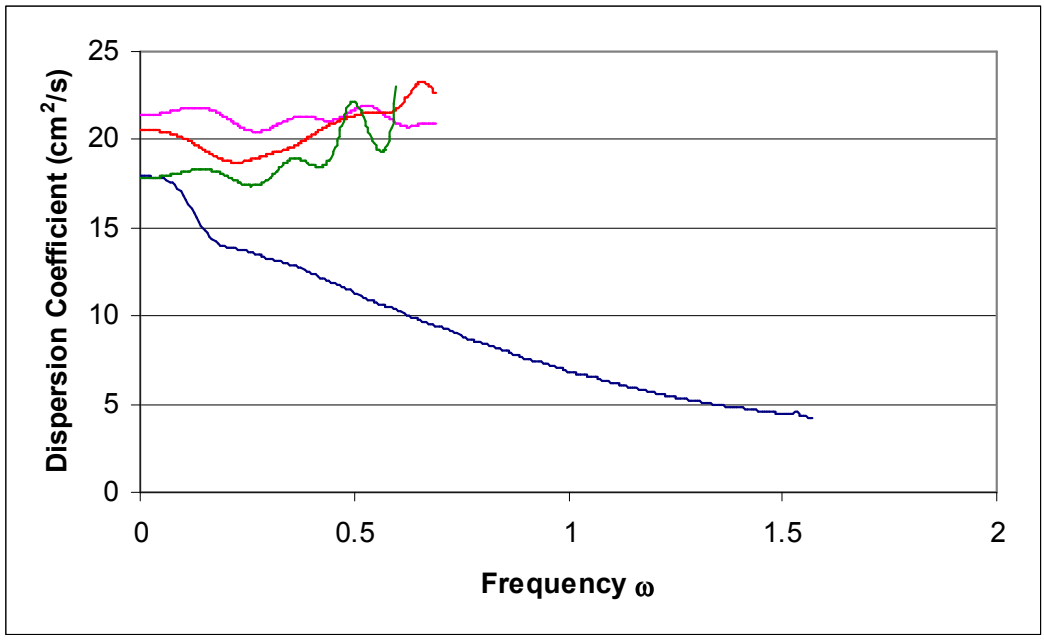

(b)

Figure H.2: Plot of (a) mean velocity and (b) dispersion coefficient vs. frequency for Runs A. The flow rate was 0.75 ml/min. — 0.25 m, — 0.5 m, — 0.8 m and — 1m.

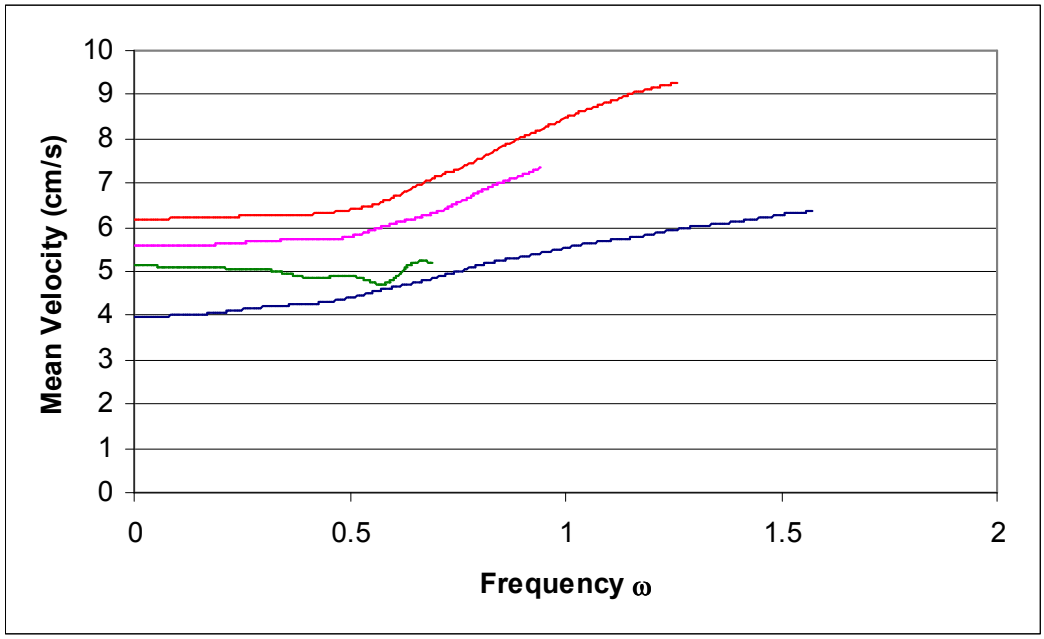

(a)

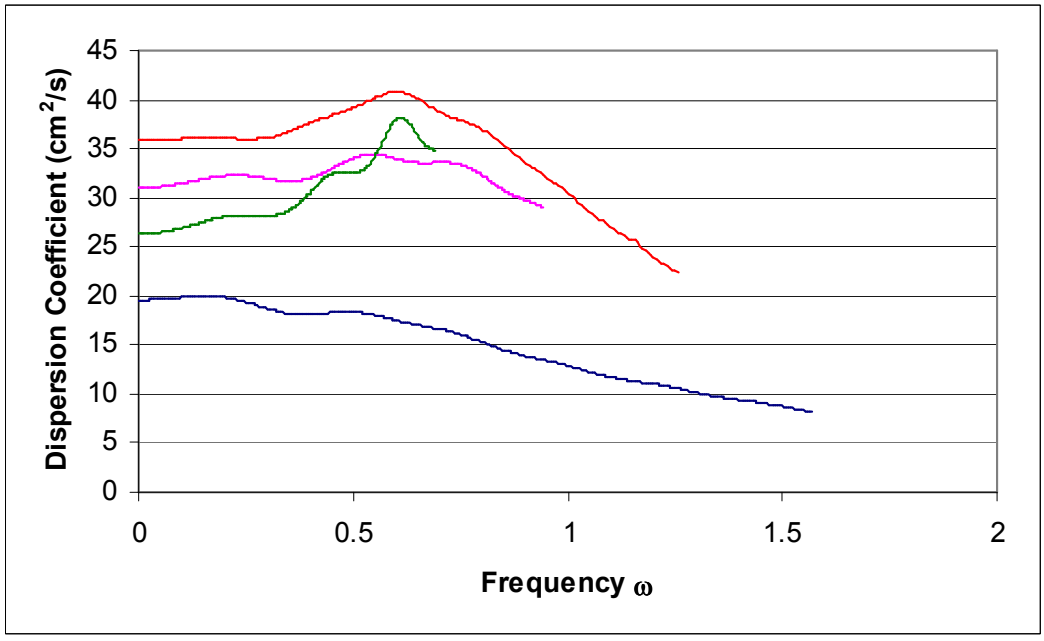

(b)

Figure H.3: Plot of (a) mean velocity and (b) dispersion coefficient vs. frequency for Runs A. The flow rate was 1 ml/min. — 0.25 m, — 0.5 m, — 0.8 m and — 1m.

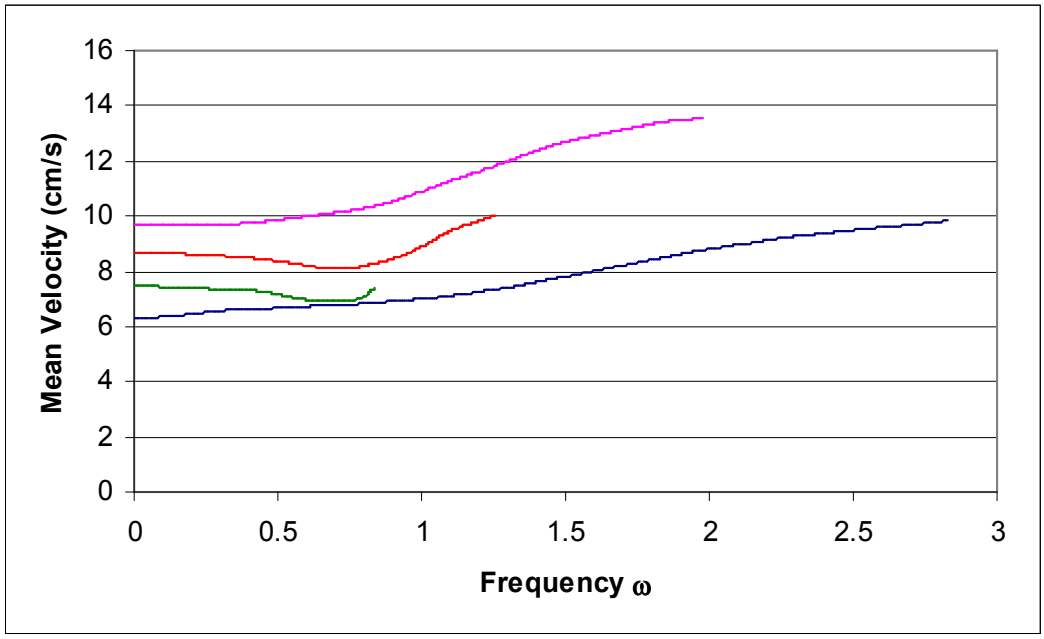

(a)

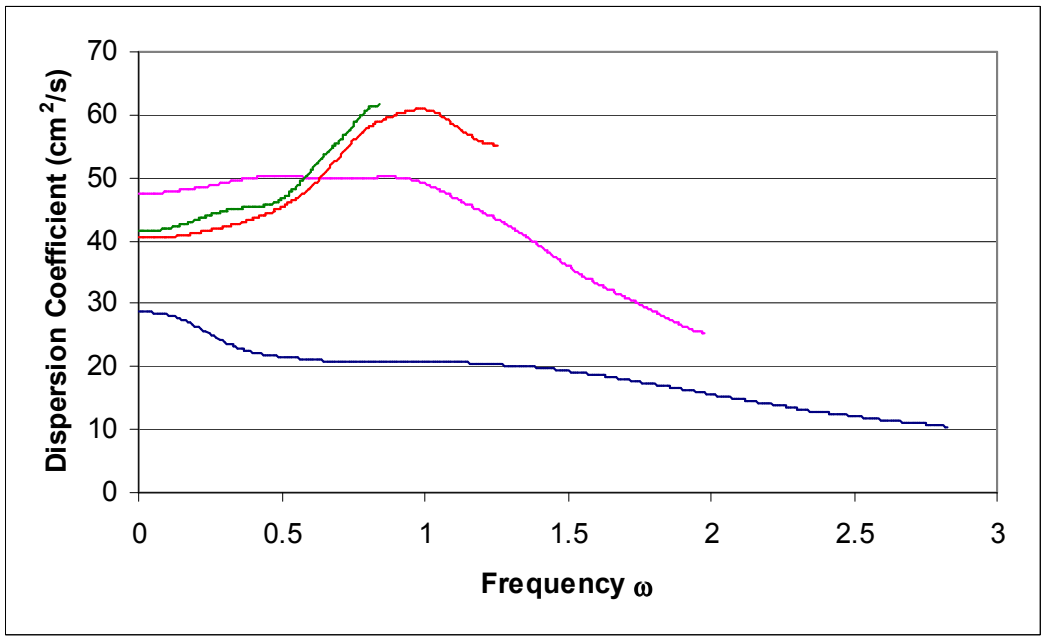

(b)

Figure H.4: Plot of (a) mean velocity and (b) dispersion coefficient vs. frequency for Runs A. The flow rate was 1.5 ml/min. — 0.25 m, — 0.5 m, — 0.8 m and — 1m.

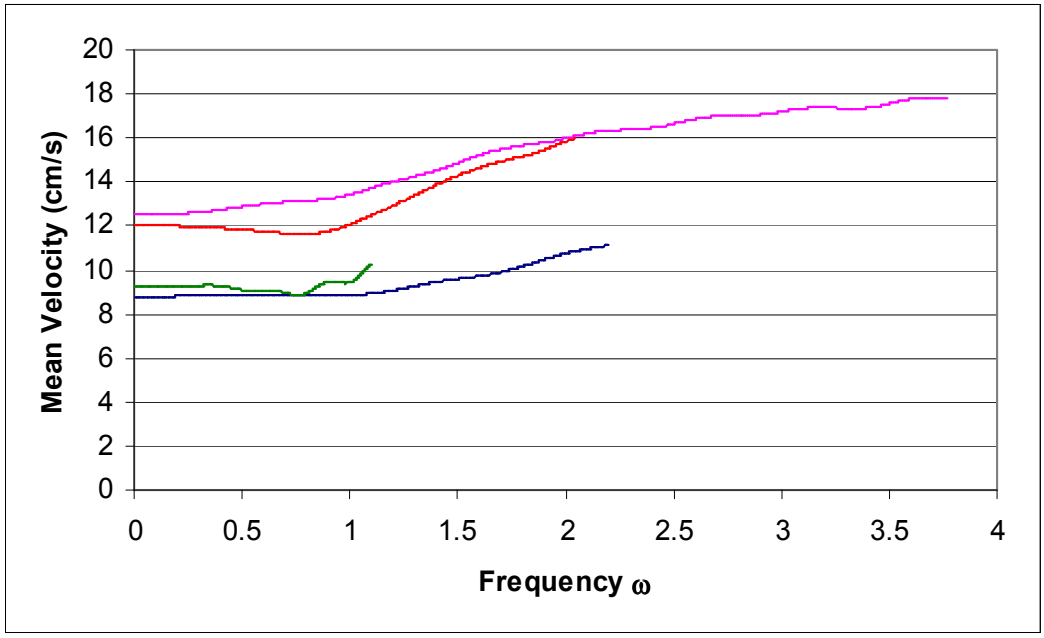

(a)

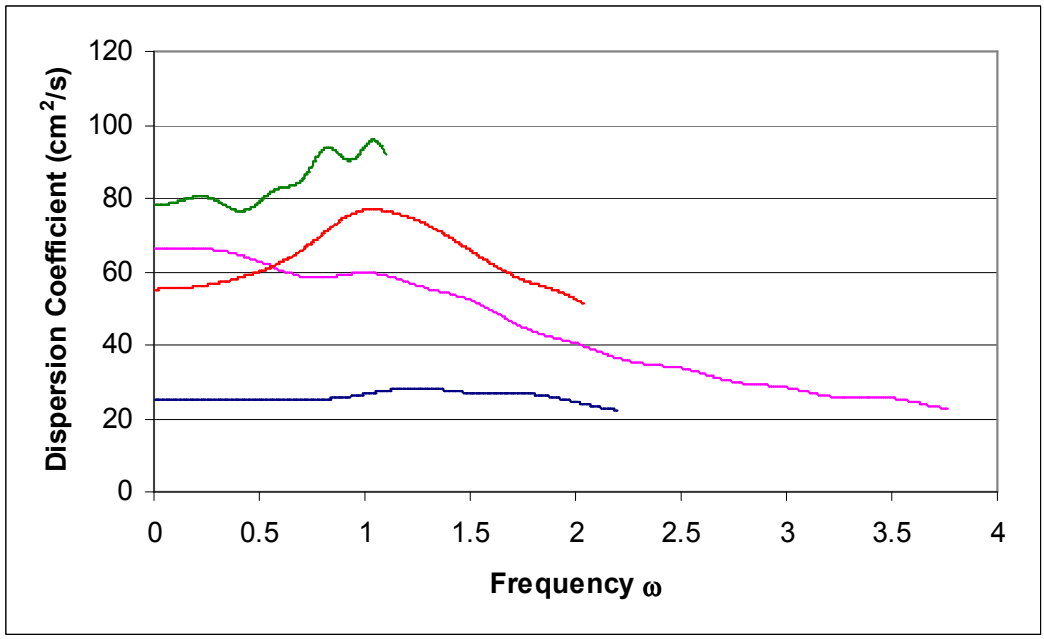

(b)

Figure H.5: Plot of (a) mean velocity and (b) dispersion coefficient vs. frequency for Runs A. The flow rate was 2 ml/min. — 0.25 m, — 0.5 m, — 0.8 m and — 1m.

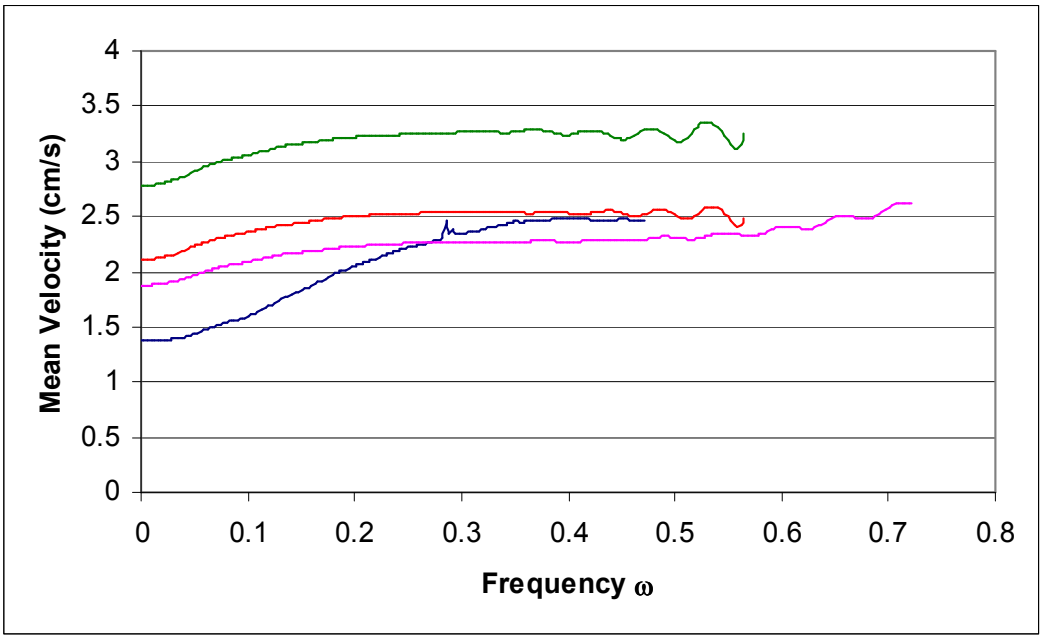

(a)

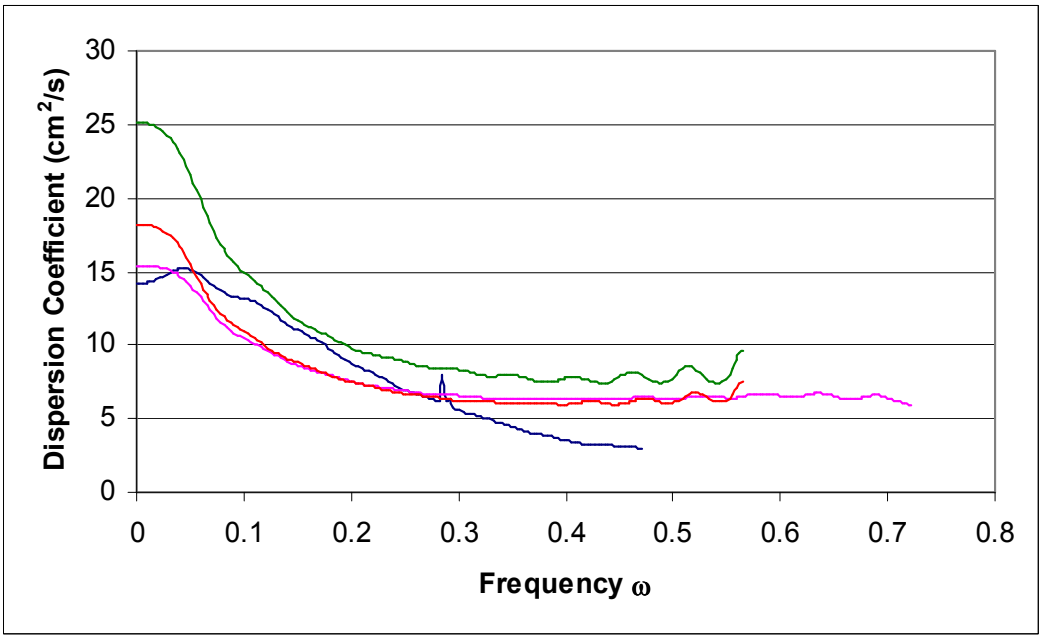

(b)

Figure H.6: Plot of (a) mean velocity and (b) dispersion coefficient vs. frequency for Runs B. The flow rate was 0.5 ml/min. — 0.25 m, — 0.5 m, — 0.8 m and — 1m.

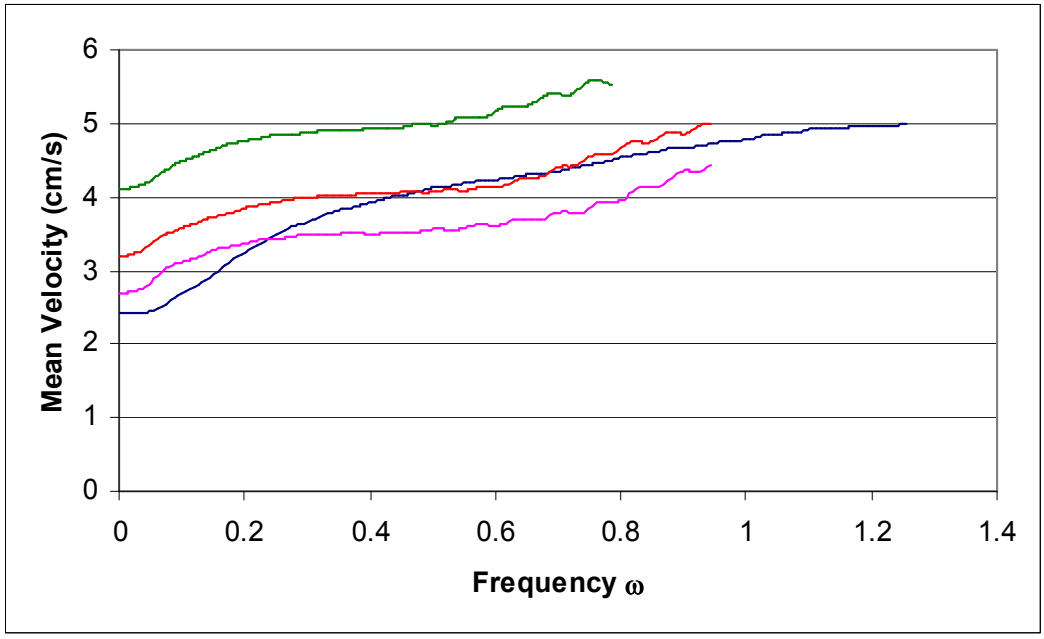

(a)

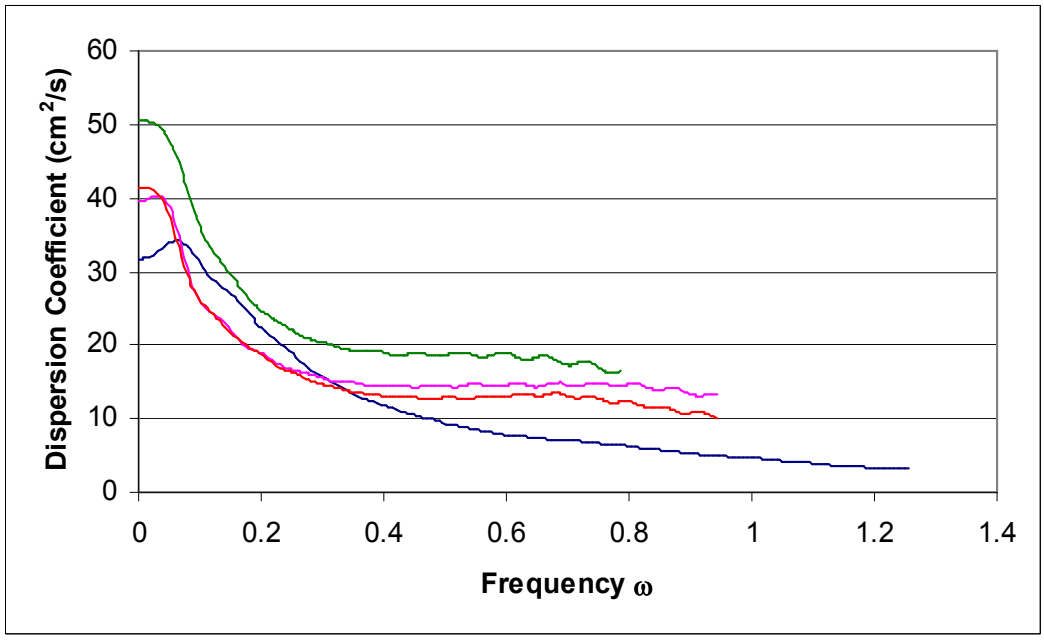

(b)

Figure H.7: Plot of (a) mean velocity and (b) dispersion coefficient vs. frequency for Runs B. The flow rate was 0.75 ml/min. — 0.25 m, — 0.5 m, — 0.8 m and — 1m.

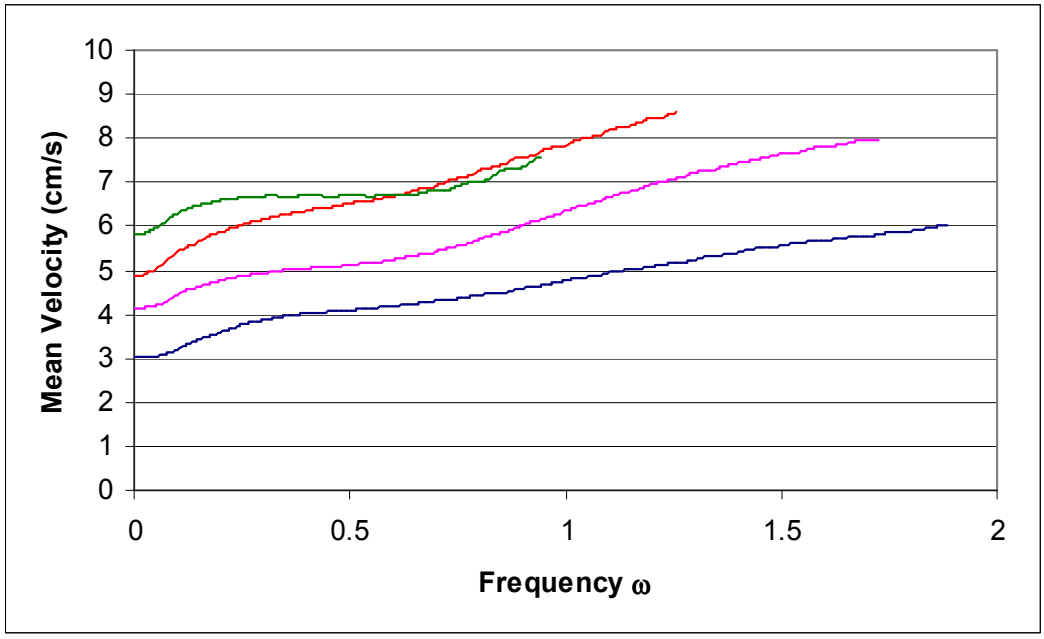

(a)

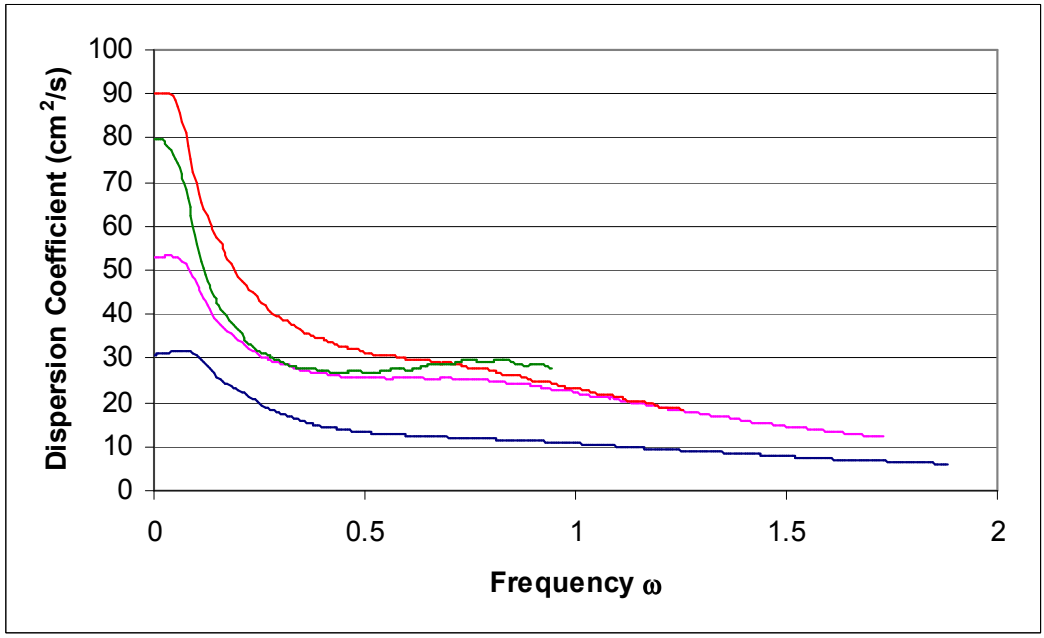

(b)

Figure H.8: Plot of (a) mean velocity and (b) dispersion coefficient vs. frequency for Runs B. The flow rate was 1 ml/min. — 0.25 m, — 0.5 m, — 0.8 m and — 1m.

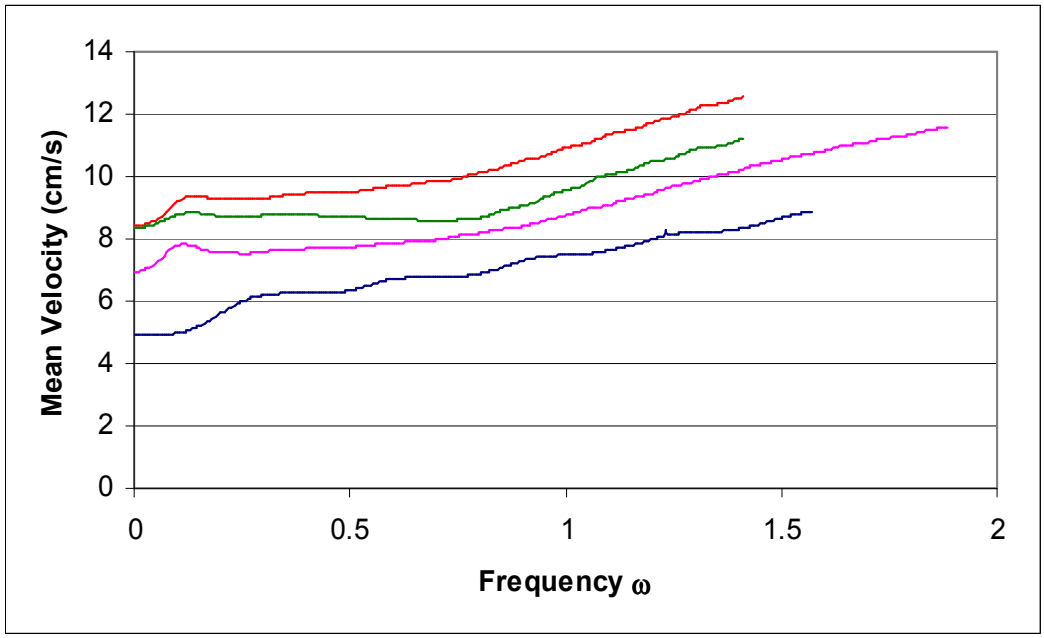

(a)

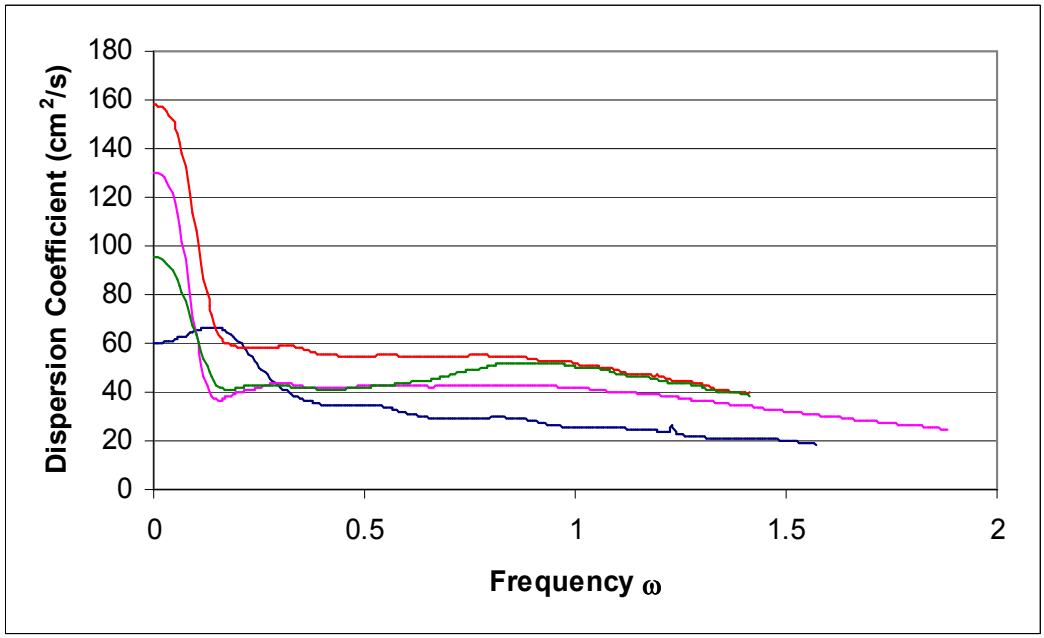

(b)

Figure H.9: Plot of (a) mean velocity and (b) dispersion coefficient vs. frequency for Runs B. The flow rate was 1.5 ml/min. — 0.25 m, — 0.5 m, — 0.8 m and — 1m.

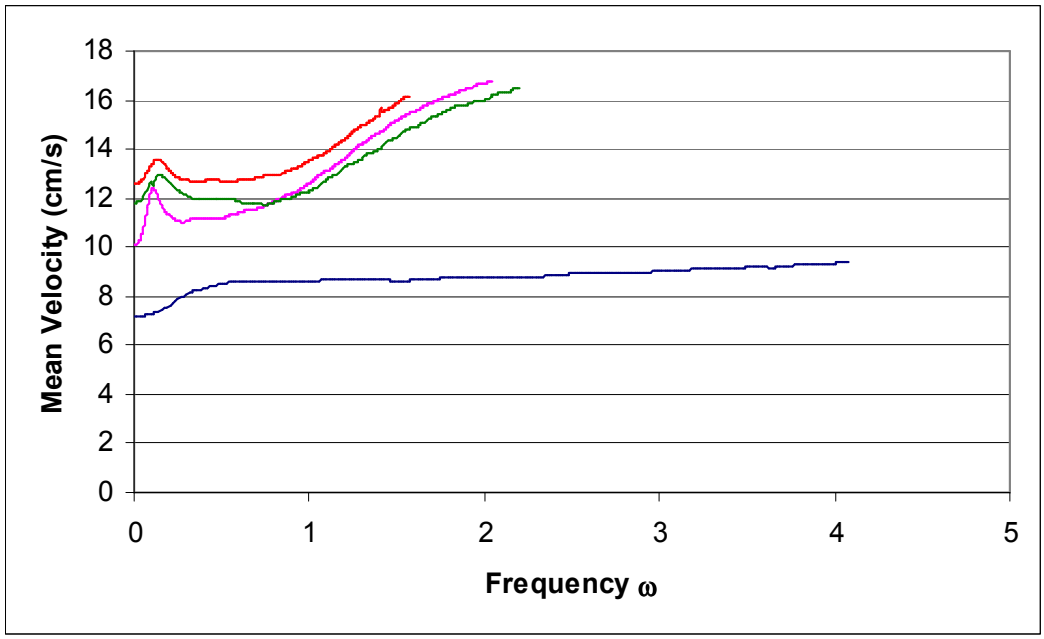

(a)

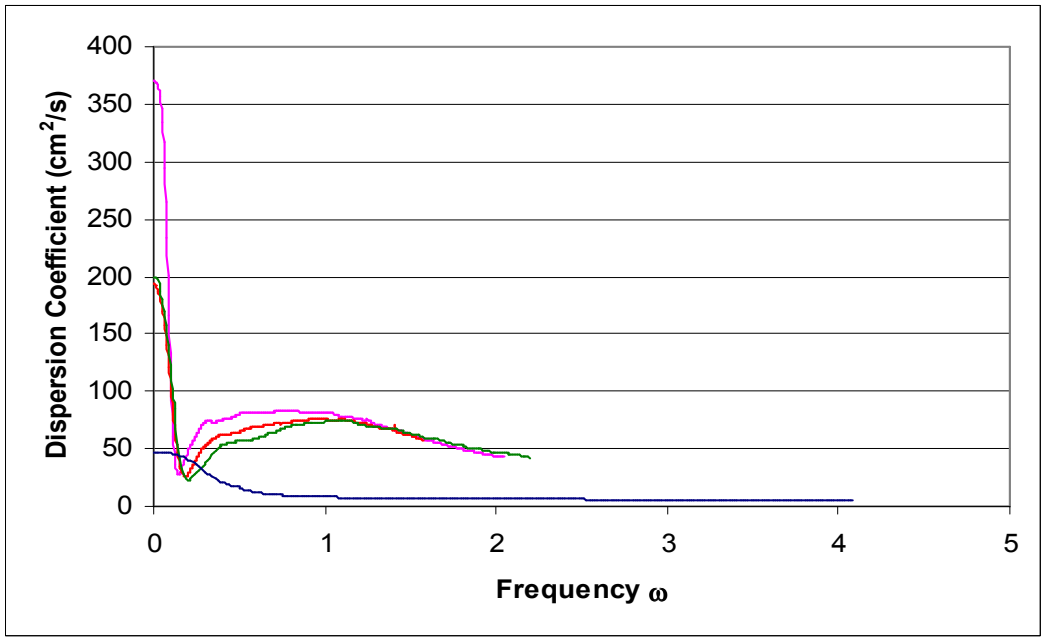

(b)

Figure H.10: Plot of (a) mean velocity and (b) dispersion coefficient vs. frequency for Runs B. The flow rate was 2 ml/min. — 0.25 m, — 0.5 m, — 0.8 m and — 1m.